University of Alberta

Zero offset VSP data processing and attenuation estimates in the Oil Sands

by

Gabriel Ernesto Solano

A thesis submitted to the Faculty of Graduate Studies and Research in partial fulfillment of the requirements for the degree of Master of Science

in

Geophysics

Department of Physics

Edmonton, Alberta

Fall 2004

Your file Votre référence
ISBN: 0-612-95856-6
Our file Notre référence
ISBN: 0-612-95856-6

Acknowledgements

First of all I would like to thank my supervisor Doug for his guidance during this work.

The committee members and Ron Hinds for their revisions and comments on the work.

Natalia for her help with Matlab and Linux at anytime.

Marek for his support with anything to do with my PC at anytime.

Lina for her time and support during this last two years.

My family for their support during my stay in Canada.

Society of Exploration Geophysicists (SEG), Canadian Society of Exploration Geophysicists (CSEG) and the UofA Geophysical Research Institute (IGR) for their financial support.

Canada and its people for being such a nice country.

Contents

List of Figures

Chapter 1

Vertical Seismic Profile Data Processing

1.1 Introduction

A vertical seismic profile (VSP) is the bridge linking surface seismic data in time to borehole data in depth. Along with synthetic seismograms, which are calculated using wellbore knowledge of velocity and density, VSP's have been used as a tool to estimate the depths at which reflections are produced and to discriminate between primary and multiple events. Their advantage over synthetic seismograms is that they use an input signal of a frequency range comparable to the surface seismic which does not experience a large velocity dispersion or shift from sonic log frequencies.

Most of the early development on VSP's were carried out since the early 60's in the USSR by the famous Russian geophysicist Gal'perin and his colleagues [19]. But it was not until the 80's when its usage gained popularity within in the western geophysical industry. Balch *et al.* in 1982 [3] summarize the work done by the US Geological Survey during 8 years on the use of VSP for Earth investigations. The original idea of borehole seismic surveys was called a check shot or velocity survey in which

receivers were spatially clamped to a vertical borehole with a seismic source shot at the surface. This allows for accurate measurements of the time it takes a wave to reach a given depth so that accurate time versus depth plots can be made. VSP's are an extension of those early surveys and they differ in that closely spaced receivers in the borehole record all possible wavemodes: the downgoing pulse, the upgoing reflections and the tubewave. Today it is possible to record three dimensional three component (3D3C) VSP's where the source is moved on the surface around the wellbore on a grid. This allows for high frequency imaging, determination of velocity anisotropy, and amplitude versus offset (AVO) studies for fluid discrimination. Hinds and Kuzmisky in 2001 [24] summarize the last 20 years of VSP development, techniques and future perspective.

The goal of conventional vertical seismic profile imaging is to create, from the borehole observations, a seismic trace that may be directly compared to a surface seismic profile. The trace created serves as a way to calibrate the surface seismic profile with borehole geological observations. This chapter describes the methodology of creating this trace by processing zero offset VSP data. It summarizes the processing of the zero offset VSP data acquired at a borehole in Northeastern Alberta northwest of the city of Fort McMurray. The scope of this chapter is to identify reflection events on the VSP record and relate them to depths in the well. The first section of the chapter gives an overview of the theoretical background and introduces the zero offset VSP technique and the data processing stream. The processing of zero offset VSP includes wavefield separation and corridor stacking. The wavefield separation is done by using a frequency-wavenumber (fk) and median filters and is intended to isolate the VSP data into the upgoing (reflections) and the downgoing wavefields. The second section of the chapter gives the results of the processing of the data and their interpretation. The last section is a summary and conclusions.

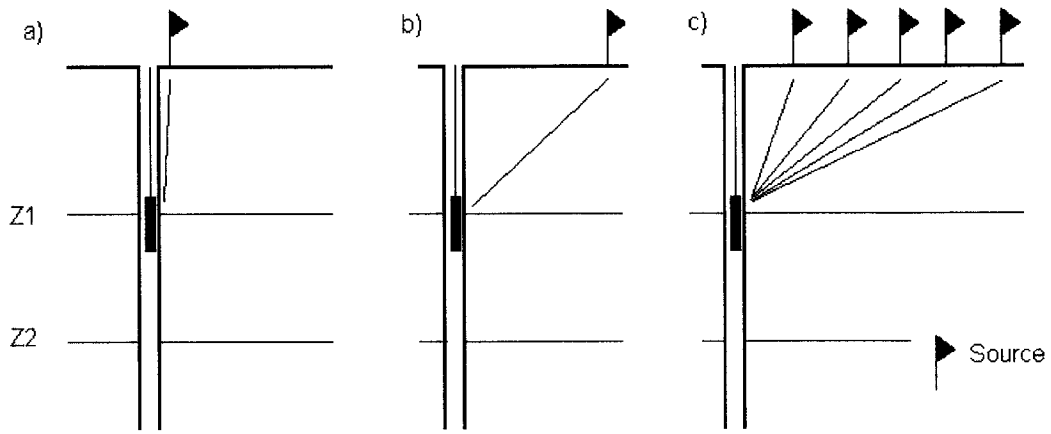

Figure 1.1: Vertical seismic profile geometries. a) Zero offset VSP. b) Offset VSP. c) Walkaway VSP.

1.2 Theoretical Background

1.2.1 The zero offset VSP

This section is not intended to give a detailed description of the vertical seismic profiling technique; for a complete description please refer to Hardage [19] or Hinds *et al.* [23] for more detailed examples. A vertical seismic profile (VSP) is a measurement procedure in which a seismic signal generated at the surface of the earth is recorded by geophones secured at various depths to the wall of a drilled well [19]. In contrast to surface seismic, which records only upgoing reflections, VSP is able to record both the upgoing reflections and the downgoing wavefield as they propagate into the earth. For this reason, VSP's are usually used to assist in the interpretation of surface seismic.

There are different VSP geometries depending of the location of the source relative to the wellbore. Figure 1.1 shows some of these different geometries. If the seismic source is located close to the wellbore, it is called a zero offset VSP (figure 1.1a). An offset VSP is referred to the case in which the offset of the source from the wellbore is comparable to the depth of the objective (figure 1.1b). A walkaway VSP is acquired

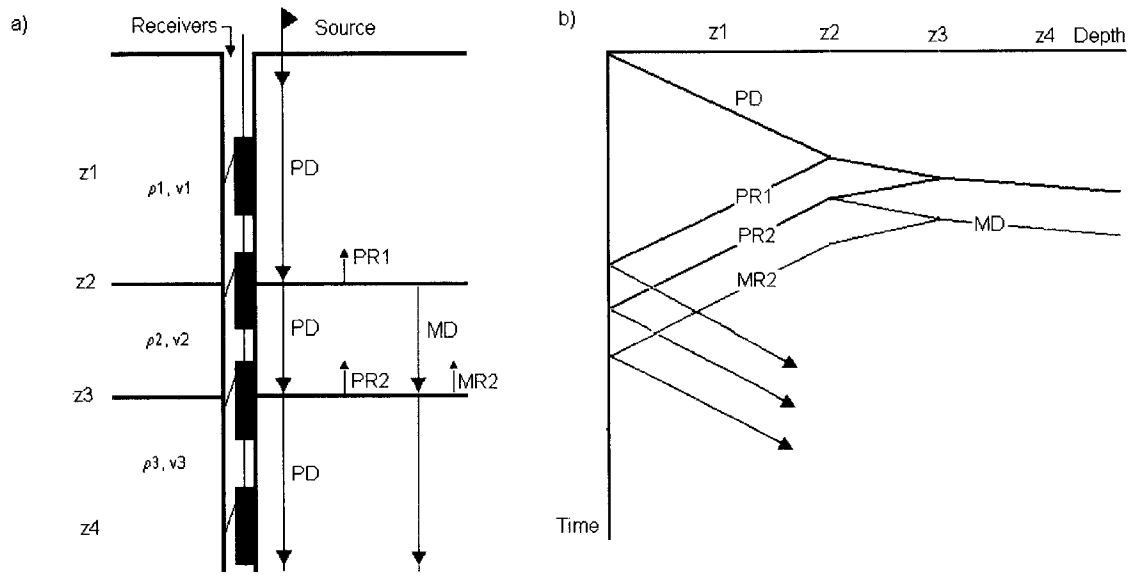

Figure 1.2: Description of the zero offset vertical seismic profile. a) Field geometry. b) VSP record. Black lines denote primary events while red lines denote multiple events. PD: primary downgoing, PR1: primary reflection 1, PR2: primary reflection 2, MD: multiple downgoing, MR2: multiple reflection 2.

when the receivers are fixed at the borehole wall and the source is moved away from the wellbore (figure 1.1c). If the source is moved on a 2D grid on the Earth's surface a 3D VSP is obtained.

Offset and 3D VSP are used for high frequency reservoir imaging, amplitude versus offset (AVO), and anisotropy studies, among others. Zero offset VSP's are used for time-to-depth ties, multiple identification, deconvolution operator estimation, and seismic wave attenuation analysis. The time-to-depth tie is made possible since the time of the reflections can be tracked down to the borehole depth where they were generated and then be identified in the surface seismic in time.

Figure 1.2 illustrates the zero offset VSP geometry. In the borehole, receivers are clamped to the wall and a seismic source is activated at the surface close to the wellhead as shown in figure 1.2a). The receivers are usually orthogonal multicomponent (x, y, z) geophones so that shear waves may be also recorded. The seismic source is usually a gun, dynamite, or a seismic vibrator sweep which gives high signal

repeatability.

The wavefield traveling downward into the Earth is defined as the primary downgoing (PD in figure 1.2). The record of the traveltimes of this downgoing pulse at different depths appears as a linear event (for constant velocity) on the VSP record as in figure 1.2b). When the pulse enters a different velocity layer, the traveltime slope in the VSP record changes. At the same time, primary reflections are produced (PR1 and PR2 in the figure) at those interfaces and travel upward back to the surface. Those reflections together define the upgoing wavefield, they have an opposite apparent velocity in the record than the downgoing wavefield. Note that these reflections cannot be recorded by receivers deeper than the depths at which they were produced. For example PR1 (produced at z2) is recorded by the first receiver (z1) but not by the third one (z3). Multiples (denoted as red lines) are directly recognized as they appear later in time at the same level where are produced. For this reason VSPs may be used to identify multiples which are often problematic in surface seismic data. Once the reflections reach the surface they are reflected back to the subsurface.

1.2.2 Processing of Zero offset VSP data

One of the goals of zero offset VSP surveys is to create a final trace, often called a corridor stack, that can be directly compared to a surface seismic profile. This created trace can be used as a way to calibrate the surface seismic section by identifying the depths at which reflections are produced on the VSP data and relating them to two way traveltime events on the surface seismic record. Note that VSP data show events in one way traveltime and surface seismic is in two way traveltime; if VSP data is to be processed it must be shifted to two way traveltime.

Processing of zero offset VSP's is usually simpler than processing of offset VSP data. Offset VSP data includes p-s wave modes, geometry, and migration among other

complications. Zero offset VSP's involve only the passage of two wavefields traveling in opposite directions. In this section the two main process applied to this data are applied: wavefield separation and corridor stacking.

Wavefield separation

VSP data are useful because one is able to time-to-depth tie two wavefields: the downgoing pulse traveling into the earth and the upgoing reflections to the surface coming from acoustic impedance contrasts. Depending the scope of a particular study, one needs to analyse only one of these. For example, the upgoing wavefield (or reflections) can be used to build corridor stacks that allow recognition of the depth at which reflections are being produced. This is the scope of this first chapter. Conversely, the downgoing wavefield can be used to provide an indicator of the source wavelet. This information is useful in deconvolution procedures that seek to increase the vertical resolution of surface seismic profiles [19]. Less often these downgoing pulses can be used to measure the attenuation that waves suffer when travel through the earth. Attenuation is the focus of the second chapter of this study.
Since the wavefields have different moveouts it is possible isolate them using mathematical filters for separation analysis. The most common filters are the median filter and the fk filter. These are each described below.

Median filters

Median filters were developed as a means of smoothing data in which the signal to be preserved contains abrupt discontinuities [19]. Its initial applications were in the field of speech processing and the enhancement of digital imaging back in the 70's. The central idea is to reject incoherent behavior in a dataset by smoothing it but by

still honoring abrupt boundaries and edges.

Consider a sequence of values $S = s_1, s_2, s_3, s_4, s_5, s_6, s_7$ where each s_i has a different value. Reorder this series ascendantly to yield a new series S^*. For example, this might be $S^* = s_6, s_4, s_1, s_5, s_7, s_2, s_3$. The median value of this new series is given by S_5. In this instance, the median filter operator can be defined as:

$$(s_1, s_2, s_3, s_4, s_5, s_6, s_7) \Rightarrow Median\ Filter \Rightarrow (s_5)$$

Given a series of samples, the median filter yields the median value of that series. This filter has two important properties that make it suitable to filter VSP data:

1. It rejects noise spikes. Any data point having an extreme value within a series will always be put at the end of the rearranged array and consequently can never be the median value. This is crucial when the data have random high amplitude noise due to acquisition problems.

2. It passes a step function without alteration. This is a very important property because different wave modes recorded in VSP may essentially be step functions. For example, upgoing reflections are step functions because they do not exist below the impedance interface at which they are generated.

The procedure to separate upgoing and downgoing wavefields in VSP data is illustrated in figure 1.3:

1. Given a dataset as in figure 1.3a), pick the first arrival time (i.e. first break) at each depth of the downgoing pulse.

2. Flatten the VSP traces to these first break times. This is done by shifting the traces up by the first break time so that the downgoing wavefield is made

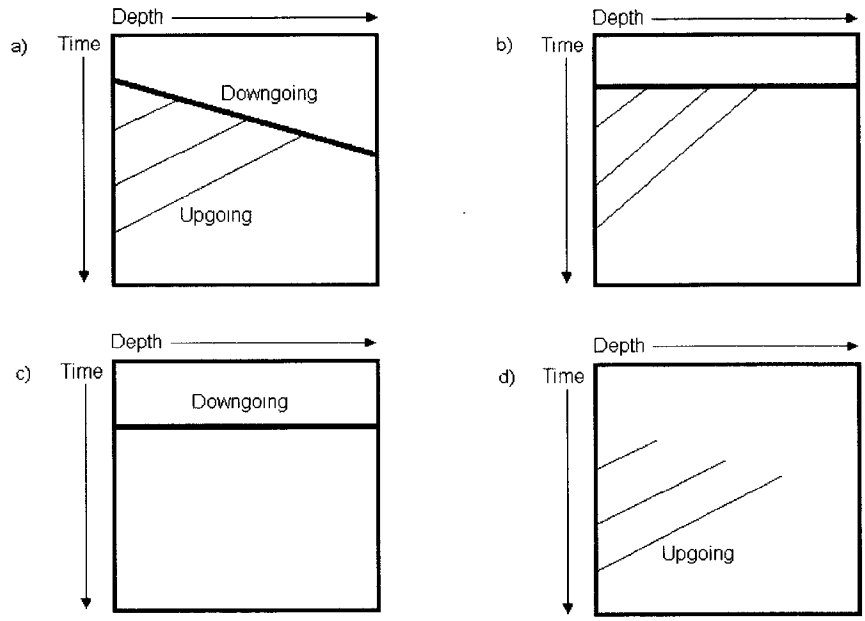

Figure 1.3: Median filtering scheme. a) Raw VSP record. b) VSP record flattened to the first break. c) Enhanced downgoing wavefield by using a median filter. d) Isolated upgoing wavefield.

horizontal. Hinds *et at.* [23] refers to this time shift as (-TT). By doing this the downgoing wavefield becomes a coherent flat event as in figure 1.3b).

3. Equalize the amplitudes. This makes the downgoing event has a constant wave-shape along all traces.

4. Apply a median filter to attenuate all except the horizontal downgoing wavefield. The median filter operates at constant time samples for all depths; when it reaches the aligned downgoing event it smooths and accentuates it because its waveform is relatively constant. When the filter passes the depth at which the upgoing events are present, it rejects them because in this domain (-TT) the upgoing events are not laterally coherent. As a result it attenuates all but coherent flat events so that what is left is primarily the downgoing field as in figure 1.3c). The presumption here is that the median filter provides a good

estimate of the downgoing pulse at each depth.

5. Subtract the filtered data (only the downgoing events in 1.3c) from the raw flattened data (the downgoing and upgoing events in 1.3b) to obtain the residual upgoing wavefield.

6. Unflatten the residual data (reverse step 2) so that reflections are left at the field VSP time as in figure 1.3d).

7. Conversely, if the downgoing wavefield is to be obtained in real time, unflatten the data obtained in 3.

There are two concerns that will influence the utility of the median filter: the accuracy of the first break times and window length (i.e. the number of traces over which filter is applied). The uncertainty on where to pick the first break times due to noise levels leads to incoherency in the flattered downgoing events that can reduce the accuracy of the median filter. If the first break times are not properly picked the phases will not be properly horizontally aligned (figure 1.3b). This problem can be ameliorated by, for example, centering all peaks to a same time to increase the horizontal coherency under the assumption that these represent the same phase.

The window length is the number of traces over which the median filter is applied. It can be an odd or even number of samples in depth. The samples within this window are arranged and an appropriate median selected. If the window is an odd number of samples the median is the value in the center of the series. If the window is an even number of samples the output is the mean of the two centre samples. This operator works at each time sample on the number of traces within the window then it iteratively moves to the next time sample until it covers the complete VSP dataset. Each of the two end-points are padded with N additional points to accommodate the

centre location of the window [23]. Usually window lengths are from 6 to 11 samples in practice.

fk Filtering

Seismic data in the time-depth domain can be transformed to the frequency-wavenumber domain by a 2D Fourier Transform. Yilmaz [59] provides a complete illustration of this technique. The computation of the 2D transform can be achieved, for example, by first a Fourier Transform to the frequency-depth (i.e. $f - z$) domain followed by a second Fourier Transform to the frequency-wavenumber (i.e. $f - k$) domain. Mathematically it is illustrated as follows:

$$\text{input data} \Rightarrow VSP\,(z,t)$$

$$\text{1D Fourier transform in the time direction} \Rightarrow VSP\,(z,\omega) = \int VSP\,(z,t)\; e^{(-i\omega t)}dt$$

$$\text{1D Fourier transform in the space direction} \Rightarrow VSP\,(k,\omega) = \int VSP\,(z,\omega)\; e^{(-ikz)}dz$$

Both domains are exchangeable by transforming and back transforming the data. Computationally the transforms are done digitally by a Fast Fourier Transform (FFT) and its inverse.

Figure 1.4 illustrates fk filtering. In the time-depth domain a VSP record looks like that on figure 1.4a). The velocity of each event is defined as the slope of the arrival times $v = \frac{z}{t}$ so that the upgoing and downgoing wavefields exhibit opposite apparent velocity. The downgoing wavefield is defined as traveling with a positive velocity, while upgoing wavefield is defined as having a negative velocity. The corresponding 2D Fourier transform of the VSP record is shown on figure 1.4b). On this $f - k$ domain the events with different slopes are plotted, in principle, in different quadrants and their velocities are also defined as the slope $v = \frac{\omega}{k}$. Although the upgoing and

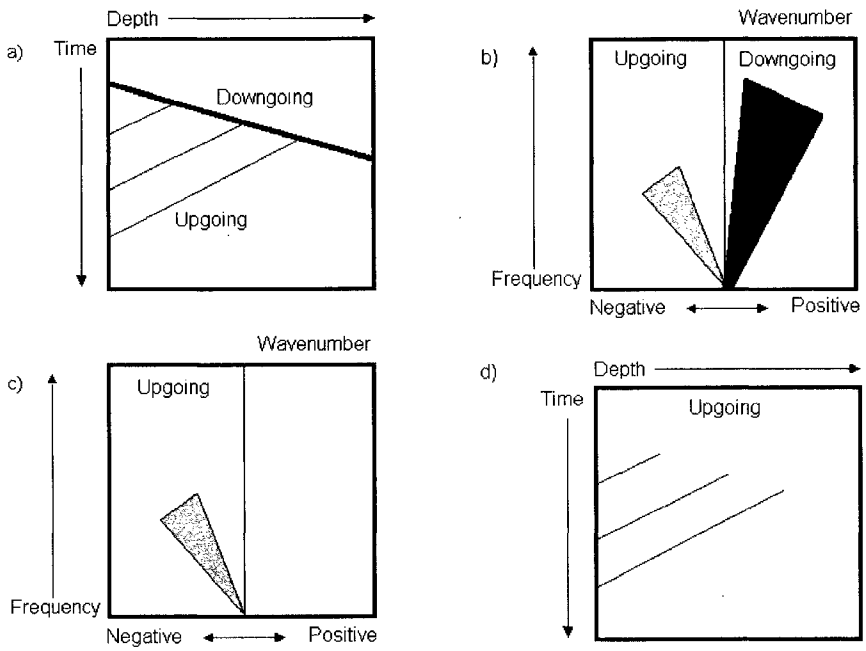

Figure 1.4: *fk* filtering scheme. a) VSP record. b) *fk* domain. c) Muting of the downgoing wavefield in the *fk* domain. d) Isolated upgoing wavefield.

downgoing wavefields overlap in the time-depth domain, in principal they do not overlap in the $f-k$ domain. This fact permits the application of a filter in the $f-k$ domain to attenuate one of them. Figure 1.4 shows schematically the process of wavefield separation using this filter and can be summarized as follows:

1. Given a VSP dataset as in figure 1.4a), apply a two dimensional FFT. In this new fk domain (1.4b), the downgoing wavefield falls in the positive k half space while the upgoing wavefield is in the negative k half space as they have opposite apparent velocities. Note the larger amplitude of the downgoing events in comparison with the upgoing ones.

2. In the fk domain, mute the downgoing wavefield by multiplying the positive half space by 0 as in figure 1.4c). The downgoing wavefield is not altered.

3. Invert the two-dimensional FFT. By doing this, the back transformation returns

only the upgoing wavefield to the time-depth domain as in Figure 1.4d).

4. If the downgoing wavefield is to be computed, the obtained upgoing wavefield has to be subtracted from the raw VSP data or attenuate the negative fk half space in step 2.

A small function in one Fourier domain represents a wide function in the other Fourier domain; the same way as a delta function has a flat or "white" frequency spectrum. This fact leads to a smearing problem called the Rieber mixing effect caused by fk filtering [19]. For example a function which spans a narrow range of wavenumbers transforms into a function that is wide in the distance space so that if a narrow pie slice is used to attenuate one wavefield it will cause severe spatial mixing in the time-depth domain data. This causes misplacement and averaging of the events. In structural imaging this problem is not critical; but if relative amplitudes are to be kept this problem can be minimized by muting large areas of the fk panel.

Corridor stacking

A corridor stack is a summation of portions of the traces in an upgoing vertical seismic profile that have been shifted to their two way arrival time at the surface [48]. It can be summed as an *outside* corridor which is meant to contain only primary events or an *inside* corridor that contains both primary and multiple events. Hinds *et al.* [23] provide a detailed explanation on this technique.

As mentioned before, a corridor stack trace can be obtained to identify primary and multiple events. Once the upgoing wavefield is separated using any of the techniques discussed above, it is possible to window a part of this record to obtain its portion containing only primary reflections as well as a second section contaminated by multiple reverberations.

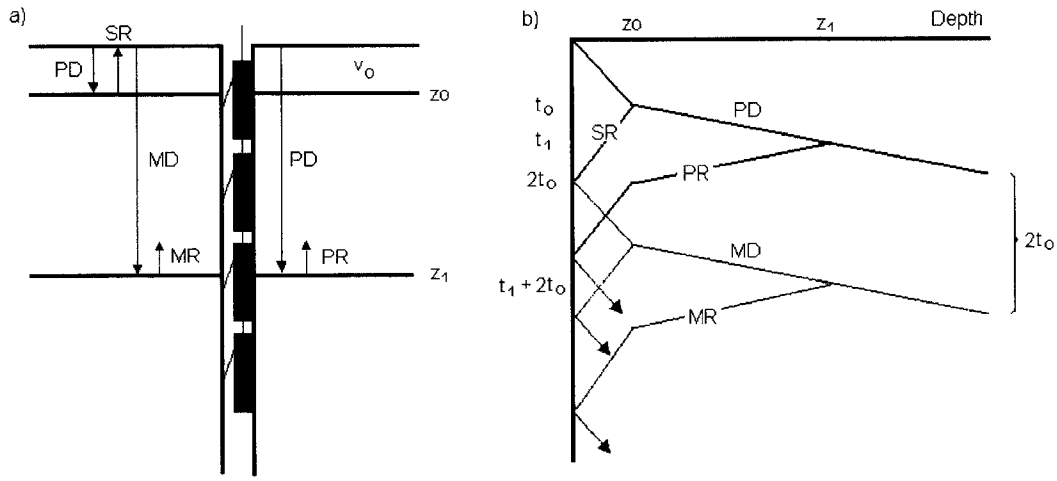

Figure 1.5: The vertical seismic profile record. a) Ilustration of the raypaths. Black lines: primary events, red lines: multiple events, PD: primary downgoing, MD: multiple downgoing, PR: primary reflection, MR: multiple reflection, SR: shallow reflection. b) Actual VSP record.

The time delay between the arrival of a primary reflection event and its associated multiple is key to discriminating them on a VSP record. Figure 1.5 illustrates how this is accomplished. In a zero offset VSP, the downgoing primary event (PD in the figure) reaches the geophone at level z_1 at a time t_1 . A primary reflection (PR) at this interface z_1 is also produced at the same time t_1 and continues its way up to the surface. However, the intrabed multiple (MD) and its associated reflection at depth z_1 (MR) will reach the geophone at z_1 at a time $\delta t = 2\,\frac{z_0}{v_0}$ after the primary reflection (i.e. $t_1 + \delta t$) and will not be recorded close to the primary downgoing. This time delay δt separates all possible multiples from primary events. As a result all the reflection events recorded close to the first break (within a time window ofδt) will represent primary reflections while later portions of the traces record both primary and multiple events. This time difference δt is crucial for the discrimination of primary and multiple events.

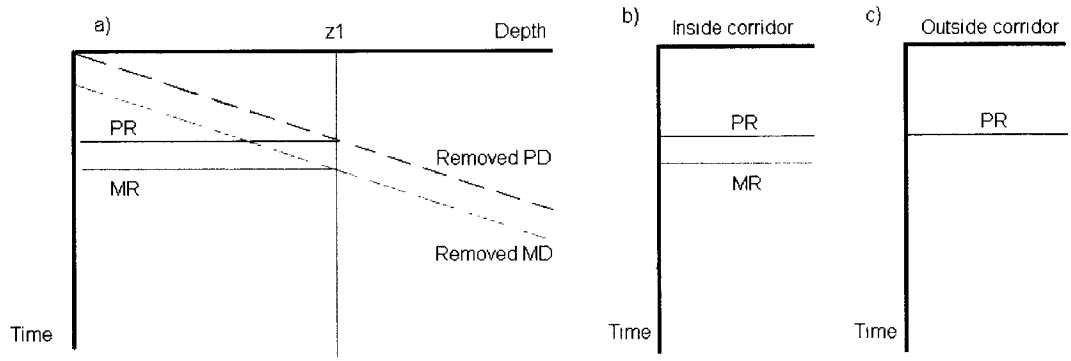

Figure 1.6: Multiple identification on a VSP record. a) Flattened upgoing wavefield. Dashed lines show where the downgoing events were before wavefield separation. b) Outside corridor stack. c) Inside corridor stack.

To illustrate the concept of corridor stacking, suppose that the downgoing wavefield of the VSP data in figure 1.5 was removed so that the residual data consists of only upgoing reflections (PR and MR). The shallow events have been also removed. Suppose also that the first break times are added to the traces to mimic two way travel time as depicted in figure 1.6a) (+TT time Hinds *et al.* [23]). There, the traces have been flattened simulating two way traveltime as that in surface seismic. The primary reflection is denoted by PR (in black) and its associated multiple by MR (in red). The dashed lines show where the downgoing wavefield was (primary pulse in black and its associate multiple in red dashed line). If the inner part of the dataset down from the removed multiple downgoing (Removed MD) were stacked in time, one would obtain a zero offset trace containing both the primary and multiple events. This trace is defined as the inside corridor as illustrated in Figure 1.6b). Alternately, if the outer part of this record is stacked, i.e, the area enclosed by the removed primary downgoing (Removed PD) and the removed multiple downgoing (Removed MD) , one would obtain a zero offset trace that contains only the primary

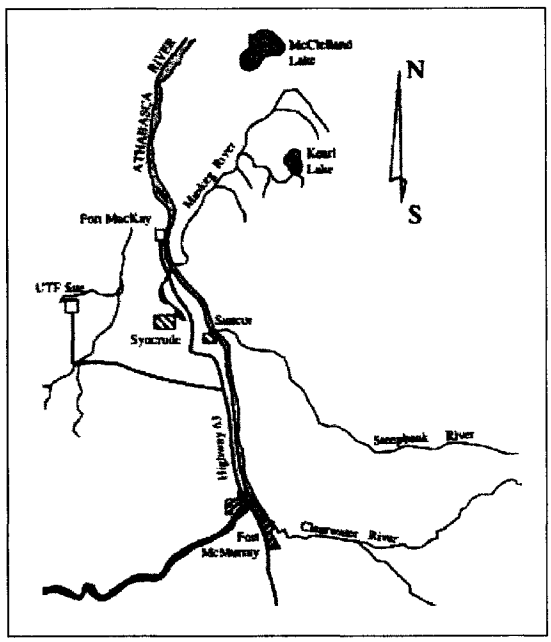

Figure 1.7: Location of borehole BC06 in study. Currenlty the place is called the Dover SAGD site. After Chalaturnik, 1996.

reflection. This last trace is defined as the outer corridor stack and is shown in figure 1.6c).

The fact that inside and outside corridor stacks are in two way traveltime and represent a zero offset trace makes them suitable to be used with surface seismic to tie depths with travel times. They can also be used identify multiples in surface seismic so that they can be removed during early processing.

1.3 Data processing of BC06 VSP data

1.3.1 Area of study

The VSP data were acquired at the borehole BC06 (01-18-93-12W) located in the Underground Test Facility (UTF) in Northeastern Alberta close to the Suncor and Syncrude mines. Several wells have been drilled in this facility where the Athabasca bituminous reservoir is exploited from the McMurray Formation. The estimated

amount of oil in situ in the Athabasca Reservoir is estimated in 1.3 trillion barrels [9] and is currently produced in this facility using the "Steam Assisted Gravity Drainage" (SAGD) approach. Figure 1.7 shows a map of the location of the area. This site is currently called the Dover SAGD site.

1.3.2 Geology

The geological column at borehole BC06 is characterized by the regional Paleozoic-Cretaceous unconformity at 160 meters depth. A simplified stratigraphic column, next to a sonic velocity and a density logs sampled at 10 cm, is shown in figure 1.8. From top to bottom, it consists of:

- Grand Rapids Formation(Albian): Consists of approximately 30 meter of Sandy shales.
- Clearwater Formation (Albian- 110Ma): Constitute approximately 75 meter of a series of upward coarsening, dominantly shale and siltstone cycles. Its lithology indicates that during its formation, the area was subject to a number of transgressive-regressive pulses[58].
- Wabiskaw Member(Early Albian-112 Ma): Represents the bottom member of the Clearwater Formation and consists of a 2 meter thick water and gas saturated sandstone. This is considered as a regional seismic marker because of the strong impedance contrast with the McMurray and Clearwater Formation. This formation is distinguishable in the logs by a low sonic velocity of approximately 1500 m/s.
- McMurray Formation (Aptian- 119 Ma): Rests unconformably on the Devonian Waterways Formation. Consists of 40 meter of massive heavy oil satu-

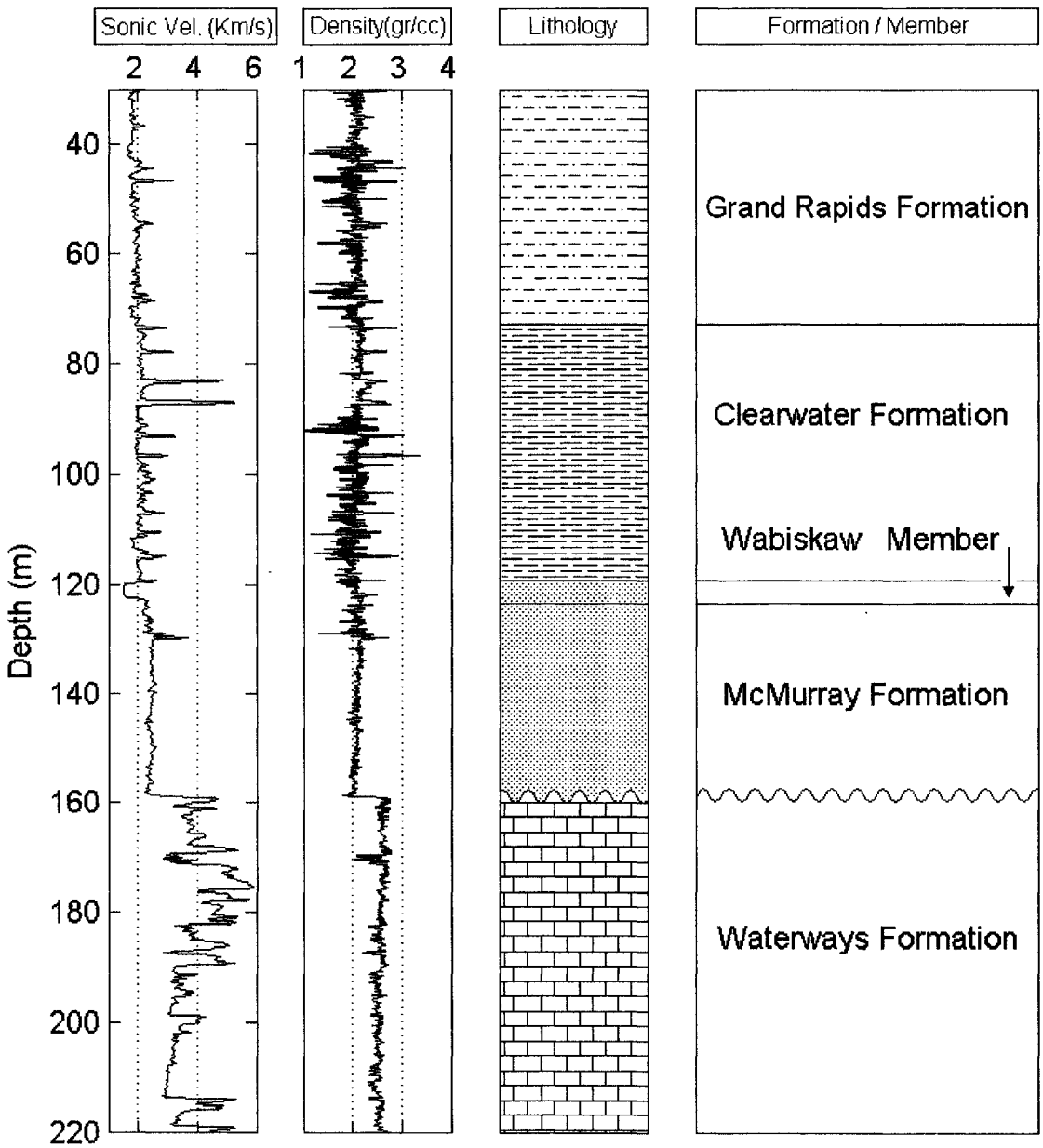

Figure 1.8: Stratighaphyc Column at borehole BC06. From left to right: sonic velocity log, density log, lithology and formation name.

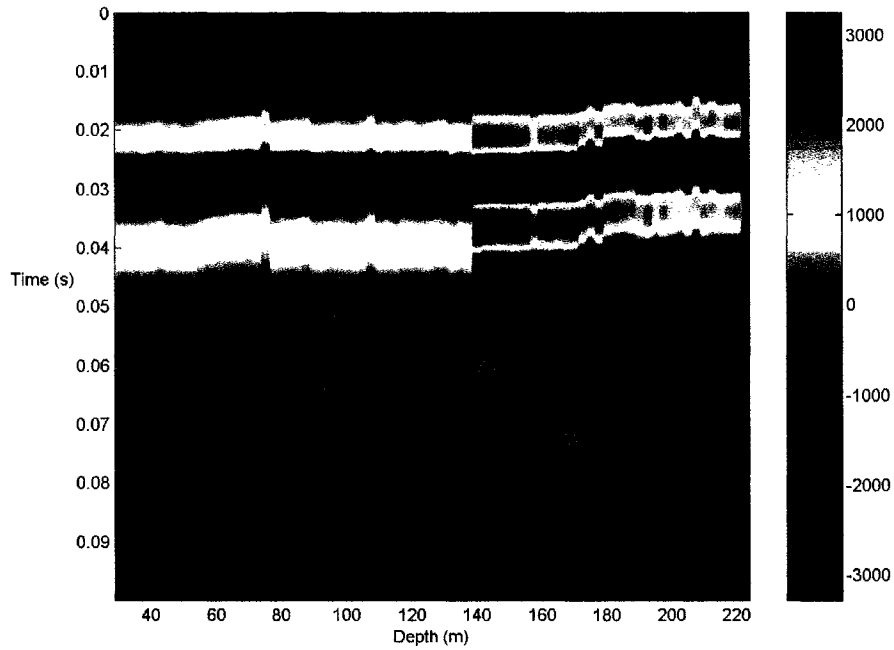

Figure 1.9: Monitor geophone signal. A geophone close to the source was placed to monitor the input signal. This had to be replaced when the borehole sonde was recording at 137.5 m and at 167.5 m depth since it was decoupled with the ground. Up to 8 records were stacked at each level.

rated sandstone interrupted by shale stringers. There are four main lithofacies associated with the formation [10]: fluvial channels, estuarine channels, tidal creeks and bay fills. This formation is characterized by an uniform velocity of approximately 2400 m/s.

- Waterways Formation (Devonian- 380 Ma): Consists of 30 meter of alternating argillaceous, nodular and massive limestone units. Is characterized by interbedded thin clay layers with high velocity.

1.3.3 The VSP Data

The VSP data were acquired by the University of Alberta in 1991 [18] under the supervision of Dr. Schmitt. The wellbore was steel cased to the bottom and water filled. This was a specially drilled observation wellbore and, as such, was not perforated or under pressure. The data were acquired prior to the start of the steam injection into the reservoir.

The seismic source consisted of a Betsy Gun fired into a mud pit. This provided a source that was highly repeatable in term of both its seismic signature and its energy. A surface geophone was planted close to the source for quality control. Figure 1.9 shows the signal recorded by the monitor geophone. The proximity of the geophone to the source made it susceptible to being decoupled from the ground when the source was shot and as a consequence it had to be replanted when the tool was at depths of 137.5 m and 167.5 m. A change in amplitude and character is seen after the monitor was replaced. However, the shape of the wavelet is consistent between the times at which the geophone was moved. As a side note, the difference in the character points out the difficulty in using a surface geophone signature for deconvolution. The weaker amplitude in comparison with the adjacent traces observed at 157.5 m is due to an improper stacking. This artifact is also observed in the VSP record.

The detector in figure 1.10 consisted of a 3 component SIE wall locking geophone package. The vertical seismic profile consists of 77 particle velocity traces at a 2.5 m spacing from 30 m to 220 m depth. Each trace is 500 ms long at a sampling rate of 0.1 ms per sample. At each level, up to 8 shots were stacked to improve the signal to noise ratio.

Figure 1.11 shows the raw VSP traces. The McMurray Formation is sampled by the 13 traces from 125 m to 155 m depth. The VSP record is characterized by:

Figure 1.10: The detector consisted of a 3 component SIE wall locking geophone package.

- A high amplitude first break event with a roughly constant slope from top of the borehole down to the unconformity at 160m. Below this point, a large change in amplitude and slope is observed. At this point, the amplitude decreases relative to that in the overlying Clearwater Formation in response to the increased acoustic impedance of the carbonate Waterways Formation. This also causes a decrease in the slope due to the higher velocity of the formation.

- Two strong reflections originating at the Wabiskaw Member and the regional unconformity at 160 m and indicated by R1 and R2 on the record. These reflections are very small in amplitude in comparison with the first break and sometimes are difficult to track. Other reflections do not show in the record because of their small amplitude in comparison with the overwhelming downgoing event.

- Tube wave. This noise is caused by surface waves that find their way down to the earth through the borehole [19]. Once the downgoing tubewave (indicated by TW1) reaches the bottom of the borehole, it gets reflected back to the surface (indicated by TW2) due to the acoustic impedance at the bottom of the

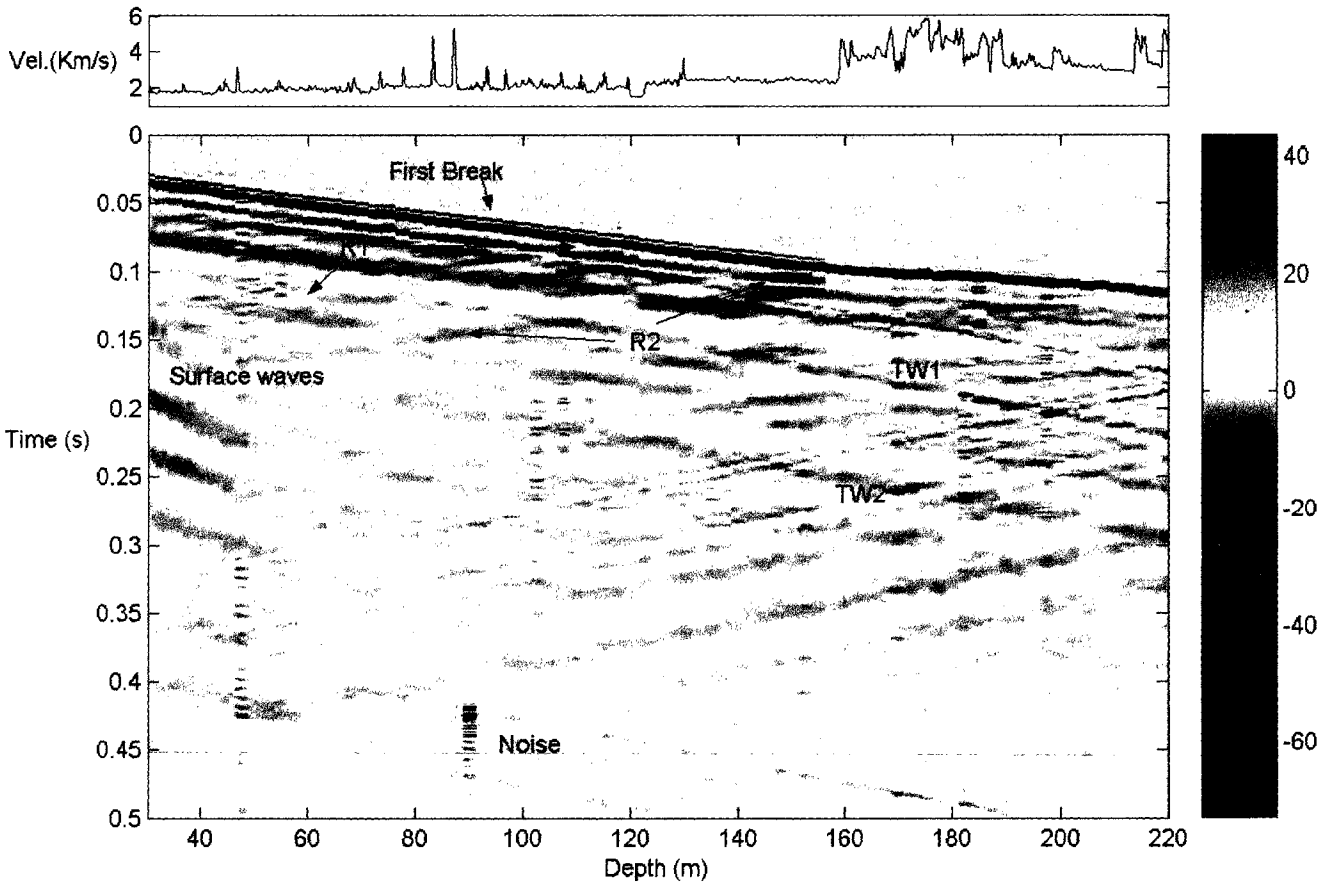

Figure 1.11: The VSP data. Top: sonic velocity log. Bottom: VSP data.

borehole.

- High frequency noise at late time recorded by the trace at 90m. This is electronic random noise caused by the acquisition equipment that can be easily attenuated by a bandpass filter.

1.3.4 Data Processing

Wavefield separation

Before wavefield separation, the first step was to resample the data to from 0.1 ms to 1 ms to decrease statistical fluctuations. The wavefield separation was carried out using different techniques as discussed before. Next, the details of the wavefield separation are shown.

fk filtering

In the fk domain, it is possible to see if the events are aliased. Aliasing is a consequence of insufficient sampling applied to the to the wavefield which is a function of time and distance. When there are fewer than two samples per cycle, an input signal at one frequency yields the same sample values (an hence appears to be) as another frequency [48]. Aliasing applies to both time and space coordinates. In the time domain the sampling theory yields a maximum unaliased frequency or Nyquist frequency. If events with higher than this frequency are contained in the signal they alias as lower frequencies. The same happens in the depth domain where the spatial sampling rate yields a Nyquist wavenumber. For this dataset that has a sampling rate of 1ms in time, the Nyquist frequency at which events alias is given by:

$$f_{nyq} = \frac{1}{2\,\Delta t} = \frac{1}{2\,(0.001s)} = 500\,Hz$$

The sampling rate in distance ($\triangle z = 2.5m$) yields the wavenumber at which events alias; this is given by:

$$k_{nyq} = \frac{1}{2\,\Delta z} = \frac{1}{2\,(2.5m)} = 0.2\,cycle/sec = 1.25\,rad/m$$

Figure 1.12 shows the fk transform of the VSP data in decibel scale. It is characterized by:

- Linearity of the events due to their linear moveouts in the $t - z$ domain. The downgoing wavefield has positive wavenumber as defined before with positive apparent velocity. On the other side, the upgoing wavefield plots in the negative wavenumber axis since it has a negative apparent velocity.

- Neither the upgoing reflections nor downgoing pulses are aliased. This is due to the small sampling rate in both time and depth which yields a Nyquist frequency of 500 Hz and a Nyquist wavenumber of 1.25 rad/m .

- The tubewave, which travels approximately at 1250m/s, plots in the fk domain as a strong linear event that alias at frequencies higher than 260 Hz for both the upgoing and downgoing tubewave events. The downgoing tubewave alias to the negative wavenumber panel while the upgoing tubewave alias to the positive wavenumber axis. Note that the apparent velocity of the downgoing tubewave and the downgoing wavefield are comparable and as a consequence at small wavenumber (~0.25rad/m) the tubewave overlaps the downgoing events. The same effect happens with the upgoing wavefield and the upgoing tubewave on the other side of the plot.

The fact that signal and noise overlap in the fk domain is critical because if the noise is to be muted in the fk domain one would have to design a filter that does not

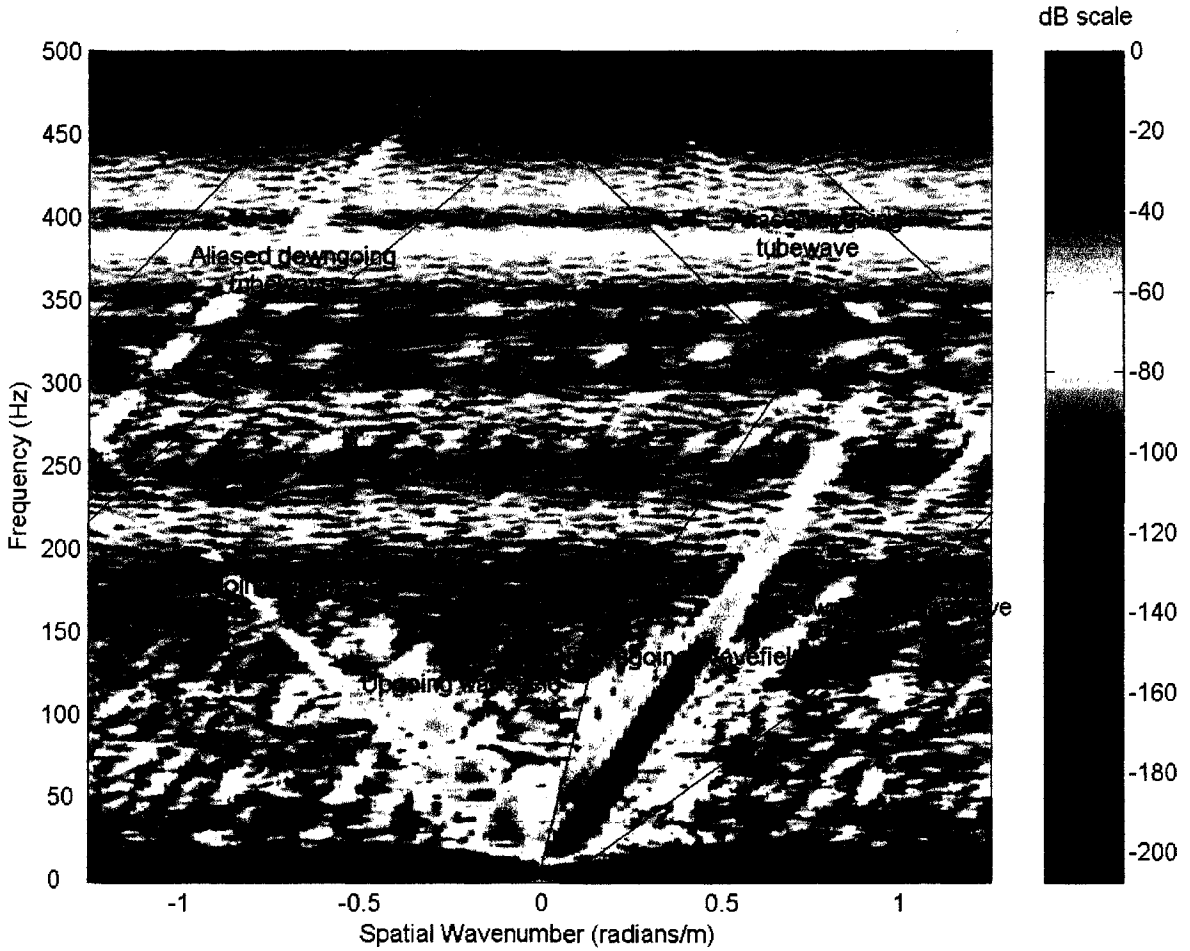

Figure 1.12: *fk* transform of the VSP data. The thin black lines define the fk window filter. It attenuates the downgoing wavefield, the aliased upgoing tubewave and the downgoing tubewave.

approach the signal to avoid distort it. As a consequence the total removal of this noise cannot be achieved.

The fk wavefield separation method isolates upgoing and downgoing events in the $f-k$ domain. The thin black lines in figure 1.12 delineate the fk window filter designed to isolate the upgoing wavefield. A polygon-type window is designed such that the downgoing wavefield, the aliased upgoing tubewave and the downgoing tubewave are attenuated in the fk domain. The back transformation of this filtered fk data yields only the upgoing events in the $t-z$ domain.

In order to avoid adversely affecting the upgoing signal with the taper of the polygon filter; the upgoing tubewave is left in the data. This has little effects in the interpretation since this wavemode can be attenuated later in processing using a median filter. After the reflected upgoing wavefield is obtained, the downgoing wavefield is obtained by subtracting the calculated upgoing wavefield from the raw VSP data.

Figure 1.13 summarizes the fk filtering process. Figure 1.13a) shows the raw VSP data, figure 1.13b) shows the upgoing wavefield obtained using the fk filter and figure 1.13c) shows the downgoing wavefield obtained by subtraction. All panels have been equalized for better visualization. In the raw VSP data (figure 1.13a) the data is primarily characterized by a strong downgoing event (first break) and the tubewave. In this data some weak upgoing reflections can be seen after equalization. Alternatively, the enhanced upgoing wavefield (figure 1.13b) is characterized by two strong reflections produced at depths of approximately 120m and 160m. The upgoing tubewave which was not muted is also observed since it overlaps the upgoing reflection in the fk domain. Figure 1.13c) shows the isolated downgoing wavefield so obtained.

Median filtering

Figure 1.14 shows each step applied to the VSP data for wavefield separation using

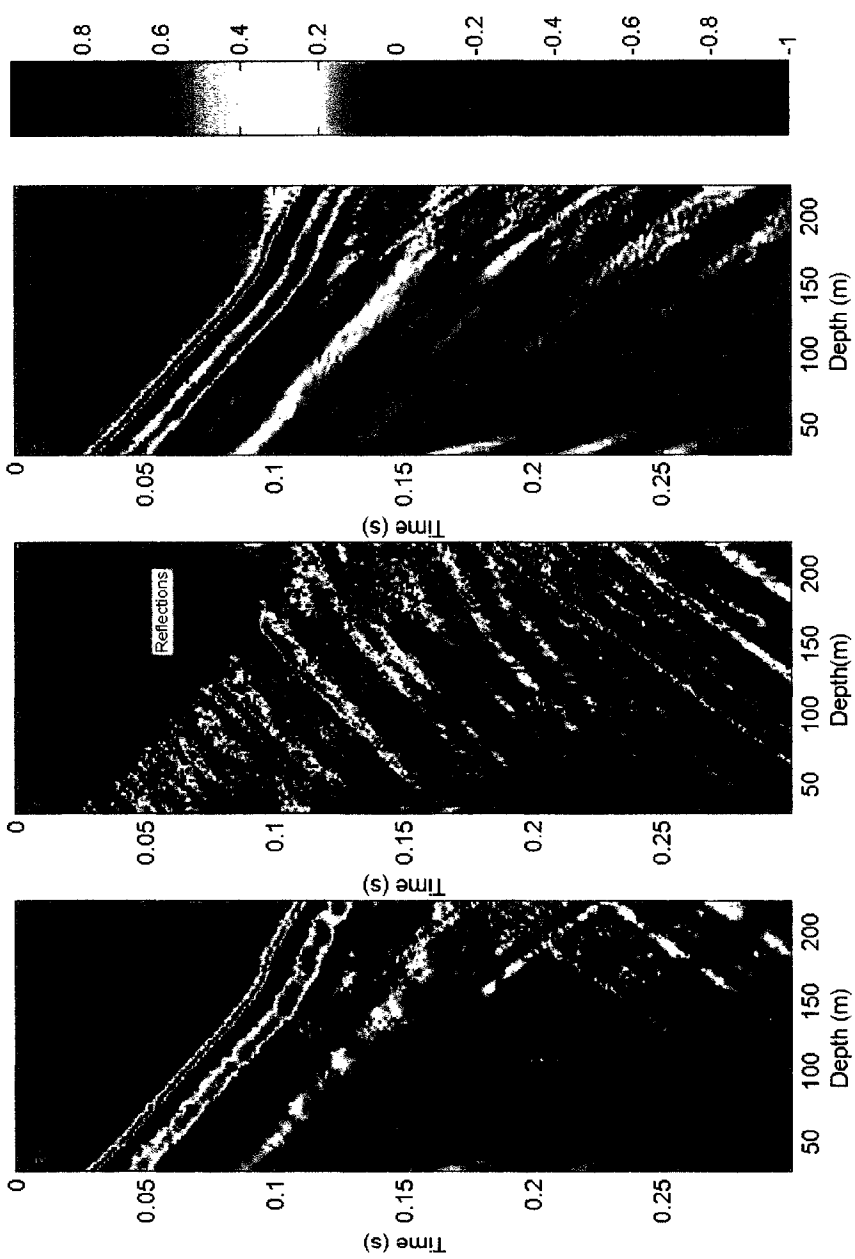

Figure 1.13: fk filtering panel. a) Raw VSP data .b) Upgoing wavefield. c) Downgoing wavefield.

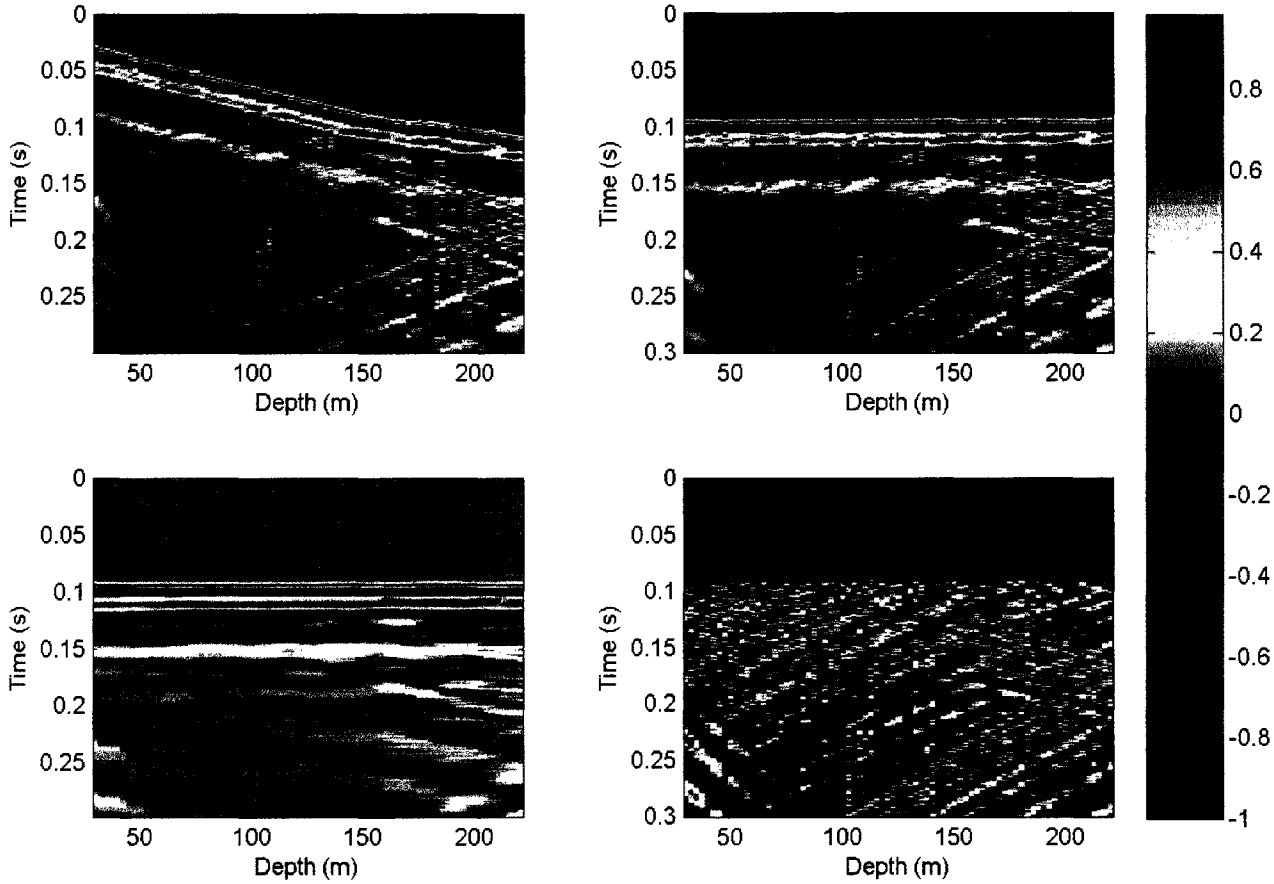

Figure 1.14: Median filtering panel. a) Equalized VSP data. b) VSP data flattened at 100ms. c) Downgoing events flattened at 100ms. d) Upgoing residual wavefield produced by subtracting image c) from b).

the median filtering method.

- Figure 1.14a). The traces are equalized and the first break times are picked. The first peak time is picked for each trace.

- Figure 1.14b). The VSP data is flattened at an arbitrary but convenient time of 100 ms. This is done by subtracting the first break times from the traces and then statically shifting by 100ms. Observe the alignment and continuity of the downgoing wavefield in the figure.

- Figure 1.14c). A median filter is applied to enhance laterally coherent events in the flattened dataset and in order to attenuate the upgoing wavefield. The median filter is applied to samples at the same time over a 7 trace interval. This figure is the result of that process.

- Figure 1.14d). The upgoing wavefield is obtained by subtracting the enhanced downgoing wavefield from flattened VSP data.

The upgoing wavefield is characterized by those reflections resolved by the fk filter at 120m and 160m. Other deeper reflections from below the bottom of the wellbore are also seen but their depths cannot be identified. As with the fk filter, the median filter does not attenuate the upgoing tubewave. This is, however, of no importance since it can be attenuated afterward in processing applying a frequency filter, for example. Figure 1.15 shows a comparison of the upgoing wavefields obtained using the fk (figure 1.15a) and the median filters (figure 1.15b). The traces have been shifted in time to two way traveltime as they would look as recorded by geophones on the surface (+TT time of Hinds *et al.* [23]). This is done by adding the first break time to the traces . Both panels are filtered using a 10-15-80-90 trapezoidal frequency filter and equalized afterwards to enhance event display. Observe how the tubewave is attenuated by the frequency filter. The two upgoing wavefields are similar and as noted are characterized

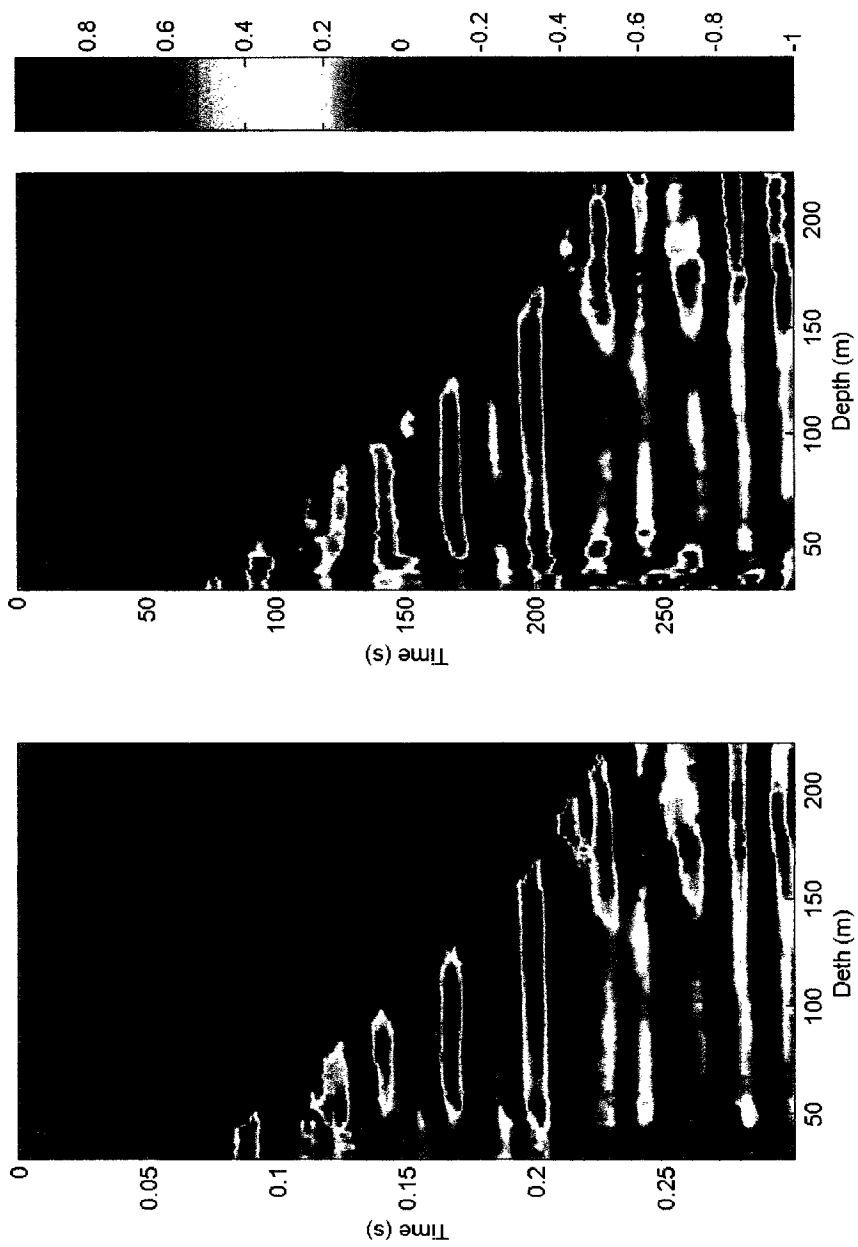

Figure 1.15: Comparison between fk and median filtered results. a) fk filtered dataset. b) Median filtered dataset.

by two strong reflection at 200 ms and 165 ms approximately coming from depths of 160 m and 120 m, respectively. Those events display strong amplitudes up to shallow levels as expected due to the roughly constant impedance of the layers. The reflections produced at depths below the unconformity at 160 m change in amplitude once they reach the unconformity at 160 meters due to the considerable change in acoustic impedance of the layers. Briefly, for a given constant wavefield intensity, the particle velocity due to the wave motion are inversely dependent on the impedance (i.e. the product of velocity and density).

Corridor stacking

Figures 1.16 and 1.17 illustrate corridor stacking using the fk filtered data and median filtered data, respectively. Panel (a) shows the upgoing wavefield in two way travel time. This dataset is equalized by dividing each trace by its minimum amplitude. Observe the dipping events in both datasets denoted by TW in the figure. This corresponds to the upgoing tubewave that was not filtered. This mode does not interfere with the reflections and gets attenuated after the vertical stacking. Panel (b) shows the outside corridor mute, panel (c) shows the outside corridor trace and panel (d) the inside corridor trace. The corridor traces are plotted repeatedly 5 times for better display.

In panel (b), a 25 ms pass window from the first break time is applied to isolate the outside corridor. For the 20 deepest traces no window is applied as there is no well control there. The resultant stacked outside corridor traces are shown in panel (c). The inside corridor in panel (d) corresponds to the data muted from the outside corridor. This inside corridor contains both primary reflections and multiples.

The outside and inside corridor panels for both datasets essentially are the same over the depth of interest (from the surface to 160m or channel 60); this means that no

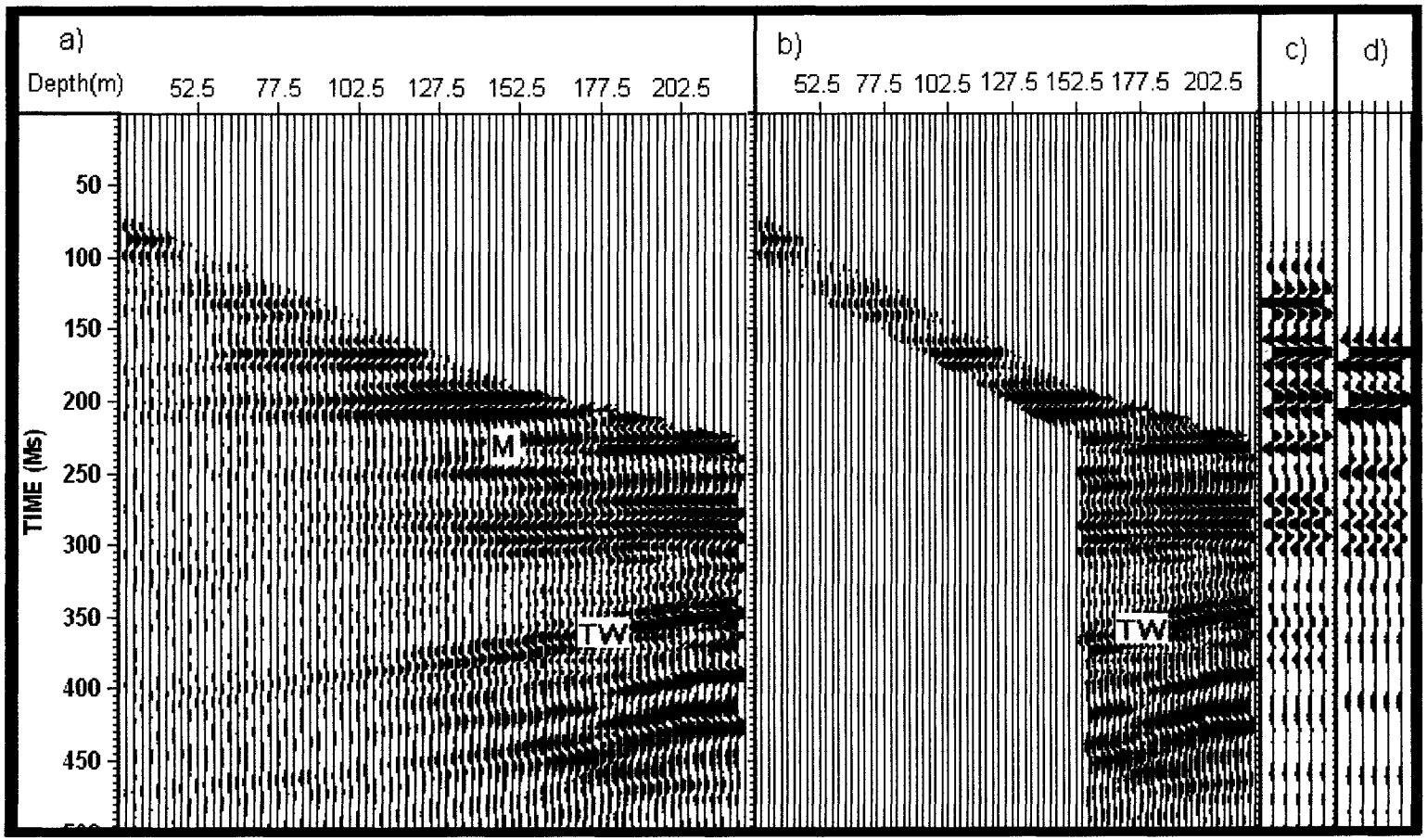

Figure 1.16: Corridor stack panels of *fk* filtered dataset. a) Flattened reflections to two way travel time. b) Outside corridor mute. c) Stacked outside corridor. d) Stacked inside corridor. TW: tubewave, M: multiple event.

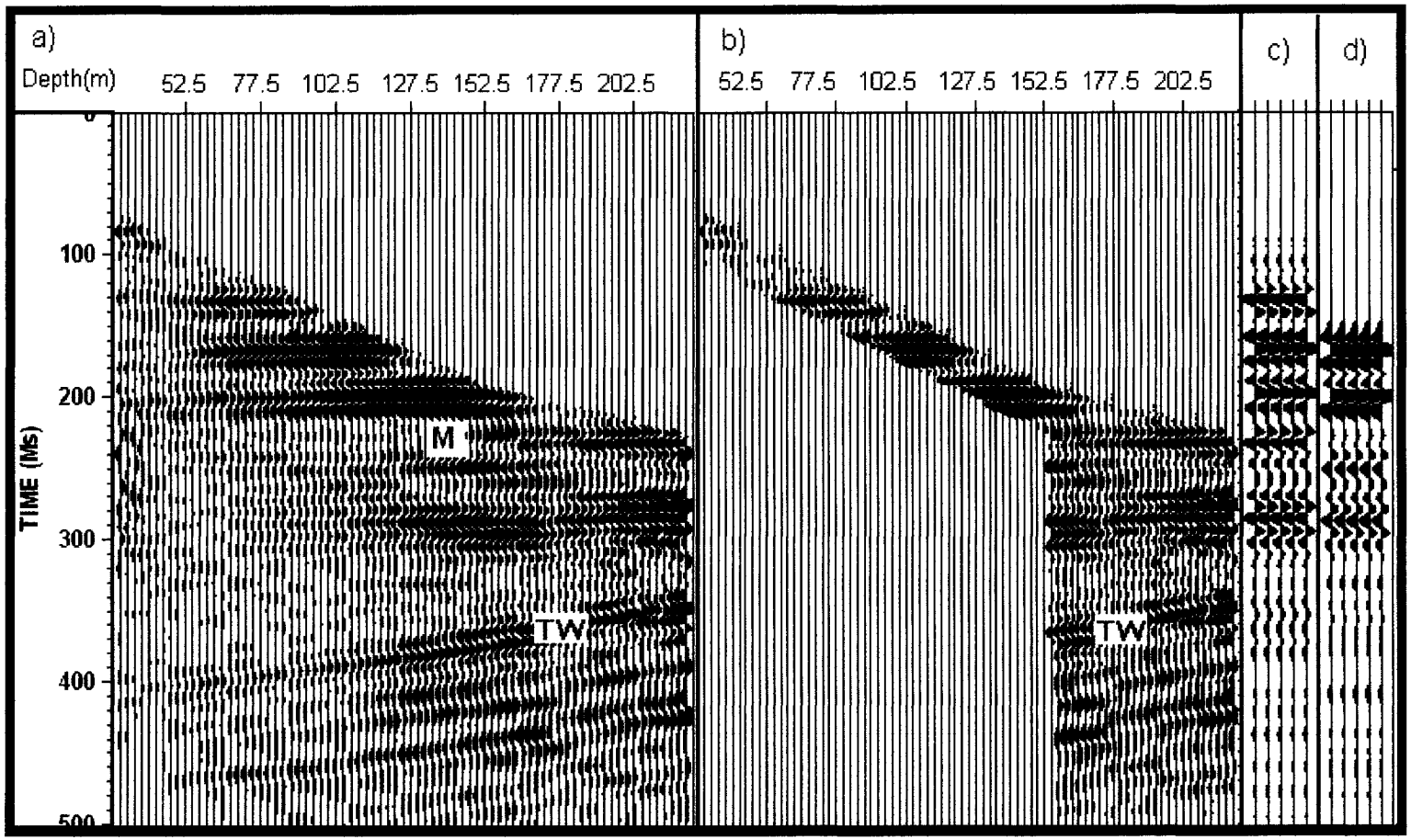

Figure 1.17: Corridor stack panels of median filtered dataset. a) Flattened reflections to two way travel time. b) Outside corridor mute. c) Stacked outside corridor. d) Stacked inside corridor. TW: tubewave, M:multiple event.

strong multiples are present in the data. The event denoted by "w" in the panel may represent a weak multiple from the regional unconformity at 200ms. For later times below the area of interest no conclusion can be drawn about the presence of multiples because the events do not intercept the first break pulse.

Synthetic Seismogram generation

In addition to corridor stacks from VSP's, it is also possible to recognize and tie events in the seismic by using synthetic seismograms based on borehole log measurements. Synthetic modeling of seismograms is critical when VSP information is not available due to economic or logistic limitations. They make use of a simplified optical ray theory (i.e. $f \longrightarrow \infty$) of wave propagation in a layered media to mimic the earth response to the passage of a wavefield.

For the zero offset case, the Earth response $e(t)$ to the passage of a wavefield can be modeled as the convolution of the reflectivity $r(t)$ series with the input signal $w(t)$to the Earth. This is:

$$e(t) = r(t) * w(t)$$

The reflectivity series $r(t)$ is constructed by computing the normal incidence reflection coefficient using the density (ρ) and velocity (v) logs. At each log sample the reflection coefficient is given by:

$$r = \frac{\rho_2 v_2 - \rho_1 v_1}{\rho_2 v_2 + \rho_1 v_1}$$

where 2 is assigned to the deeper sample. Once the reflectivity is calculated in depth it is referred to two way traveltime by using the sonic velocity. This reflectivity series in time is then convolved with an input source wavelet $w(t)$ to obtain a model seismogram that represents a zero offset seismic trace.

In order to transform the logs into time; it is necessary to use interval velocities as measured from the sonic log. For depths shallower than 30 m where no log was acquired the velocity is computed from the first break time of the first VSP trace at

30 m to be 840 m/s.

The input wavelet $w(t)$, can be either a theoretical synthetic wavelet such as a Ricker wavelet or the estimated downgoing signal from the actual VSP data. A Ricker wavelet has a zero phase signature, and is given by [48]:

$$f(t) = (1 - 2\pi^2 f_M^2 t^2)\, e^{-\pi^2 f_M^2 t^2}$$

where f_M represents the peak frequency of the wavelet. The peak frequency is chosen close to the peak frequency of the actual seismic data which is approximately 50 Hz. The estimate of the downgoing input signal from the actual VSP data is obtained by averaging the downgoing pulse over all the receiver levels and windowing it with a 60 ms cosine bell type window. Figure 1.18 (a) and (b) show a comparison of a 50 Hz Ricker wavelet and the average estimated downgoing wavelet extracted from the VSP data. Both traces are sampled at 0.1 ms. Observe that the extracted wavelet has a broader frequency bandwidth, particularly at early times which makes it spikier at the onset of the energy.

Figure 1.19 (d) and (f) illustrates the two synthetic traces made using the Ricker wavelet and the estimated downgoing signal, respectively. Figure 1.19a) and 1.19b) are the sonic velocity and density logs, respectively. Figure 1.19c) is the resultant reflectivity. All of the logs are in two way traveltime. The figure 1.19d) shows the synthetic seismogram obtained using the 50Hz Ricker wavelet multiple free while figure 1.19e) is contaminated by multiples. The seismogram using the average downgoing pulse is shown in figure 1.19f).

The strong amplitude event at the onset of the synthetic traces is an artifact due to the lack of knowledge of the well logs at depths shallower than 30m. This creates an important change in the acoustic properties. This event does not represent any earth response and must not be misinterpreted as a real reflection. It could be eliminated by windowing the seismic trace.

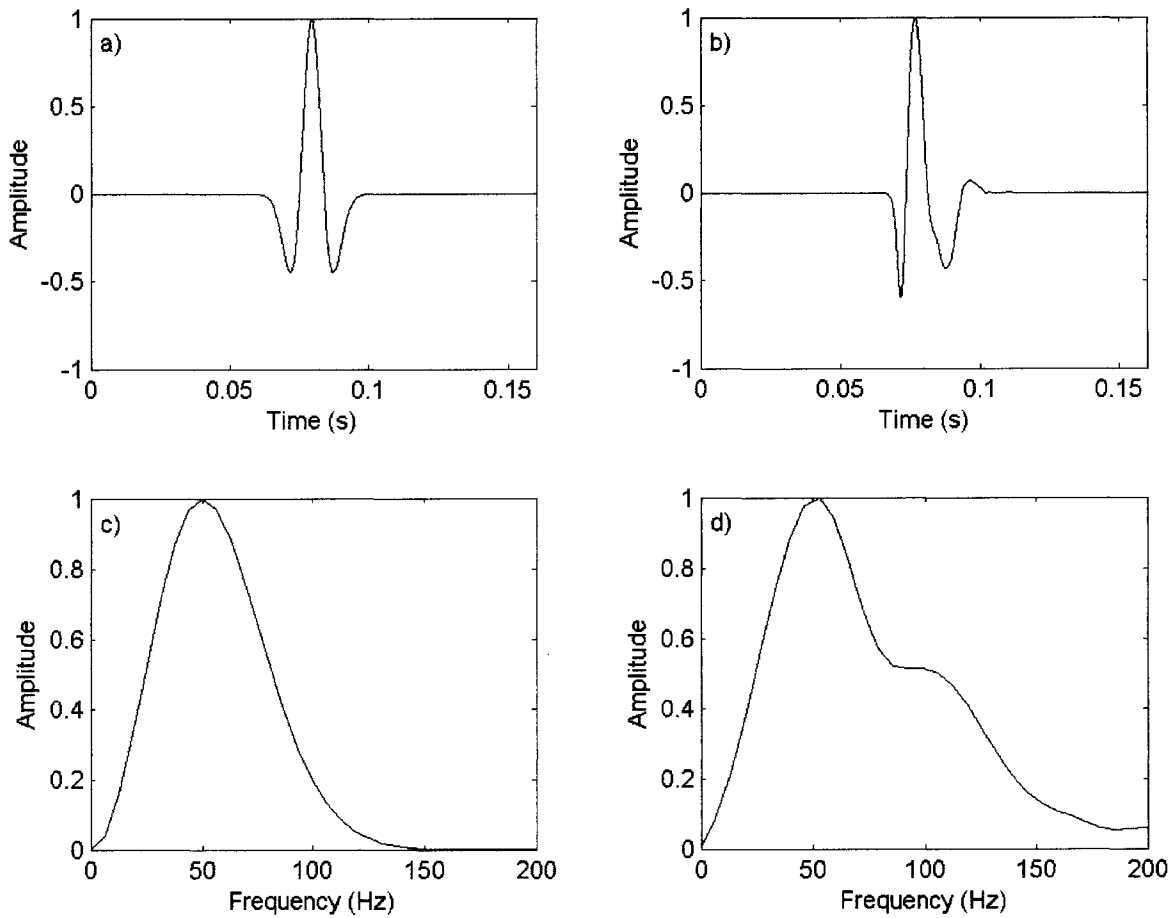

Figure 1.18: Comparison beween Ricker wavelet and average downgoing pulse from the VSP data. a) 50Hz Ricker wavelet. b) Average downgoing pulse from the VSP data. c) Amplitude espectra of (a). d) Amplitude spectra of (b).

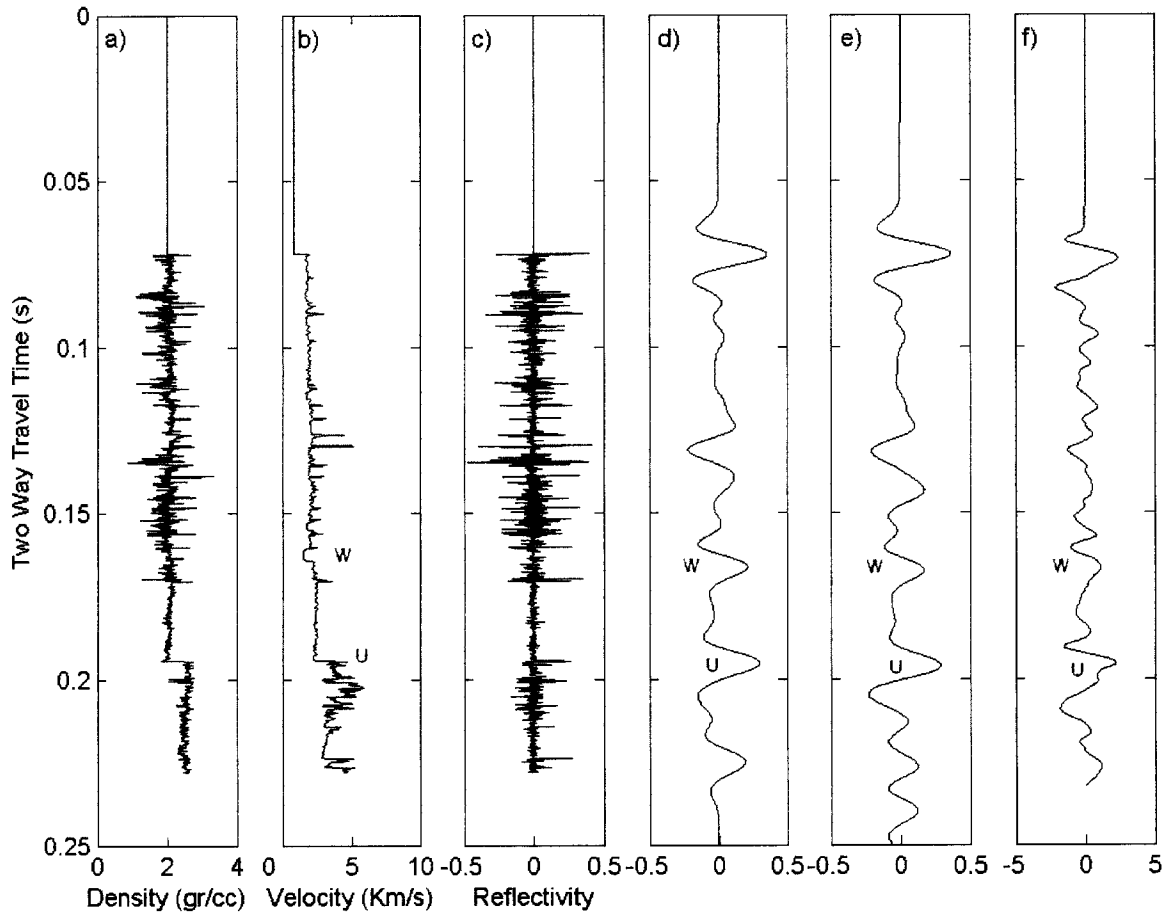

Figure 1.19: Synthetic seismograms. a) Sonic velocity log. b) Density log. c) Reflectivity series. d) Synthetic seismogram using the 50Hz Ricker wavelet multiple free. e) Synthetic seismogram using the 50Hz Ricker wavelet contaminated by multiples. f) Synthetic seismogram using the average downgoing pulse from the VSP data. w: Wabiskaw member, u: regional unconformity.

The synthetic trace using the estimated wavelet displays a higher frequency content as is expected from the convolved input wavelet. However, overall both show the same features characterized by:

- A strong positive peak associated with the regional unconformity (160m) at approximately at 0.20 seconds. This represents a strong first order reflection.
- A strong peak event associated with the Wabiskaw member (120m) at approximately 0.165 seconds. The Wabiskaw Member itself is too thin to produce a strong reflection all by itself and this event represents the tuning of the wavelet.
- Two small peak events at 0.14 seconds and 0.12 seconds associated with intrabed contrasts within the Clearwater Formation.

1.3.5 Analysis of results

Figure 1.20 shows a comparison between the corridor stacks and the synthetic traces. Panels a) and b) show the outside corridors for the fk and median filtered data, respectively. Panel c) and d) show the synthetic seismograms obtained using the 50 Hz Ricker wavelet and the average downgoing pulse from the data. Panel e) shows the sonic log in two way travel time. All traces have been filtered using a 10-15-90-110 trapezoidal frequency filter. Note that the synthetic traces end at the greatest depth of the sonic log.

All the events recognized before on the synthetic traces are recognized on the corridor stacks and align without any major mismatching in time. The following features may be identified:

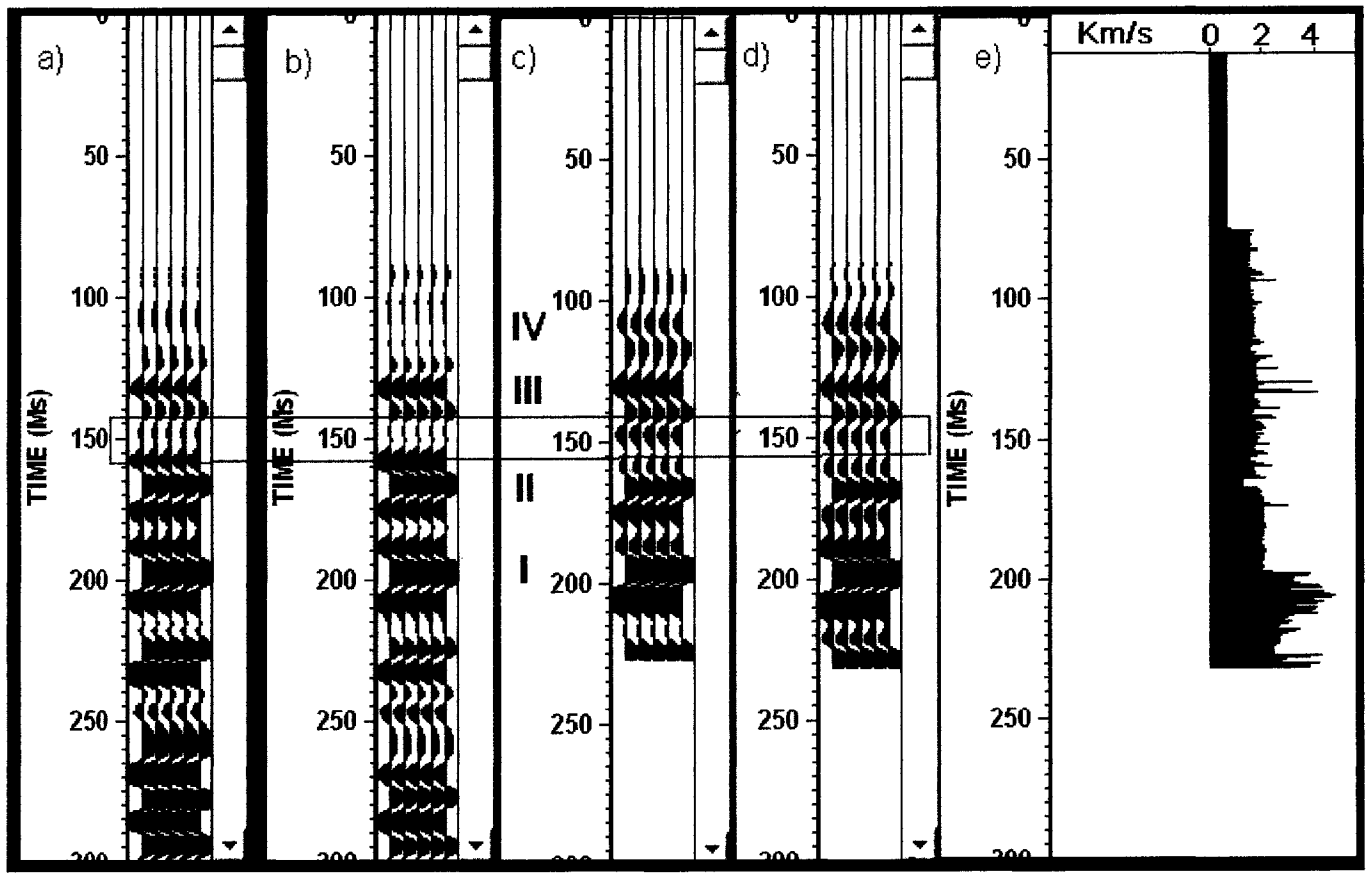

Figure 1.20: Corridor and synthetic seismismogran comparison. a) Outside corridor from fk filtered data. b) Outside corridors from median filtered data. c) Synthetic seismogram using the Ricker wavelt. d) Synthetic seismogram using the average downgoing wavelet from the VSP data. e) Sonic velocity log in two way travel time.

- A major positive peak event at approximately 200 ms (denoted by I on the figure) corresponding to the regional unconformity at 160m.
- A second major peak event, smaller in amplitude, at approximately at 165 ms (denoted by II on the figure) associated with the Wabiskaw gas Member at 120 m.
- A strong trough event at 130 ms (denoted by III) produced within the Clearwater Formation.
- A minor shallower peak event at 120 ms (denoted by IV) is observed in the synthetic traces. However, this event is resolved poorly on the seismic traces due to the high noise levels of the shallow traces as shown before. As such it may not exist in reality.
- A difference in amplitudes from the synthetic to the corridor traces from approximately 140 ms to 160 ms. These events are enclosed by the red square on the figure.
- A small difference in shape at late time after 210 ms. This may be due to the phase difference from the different source wavelets used, together with the lack of reflectivity series information at later times. These act all together to produce such difference.

Overall, the synthetic seismograms and corridor stacks match well both in amplitude and time. No time shift has to be applied to the synthetic data to match the VSP events. Figure 1.21 shows a comparison of the average VSP and sonic average velocities. The average VSP velocity (denoted by a the red line) is related to the actual velocity of the events while the average sonic velocity (denoted by the green

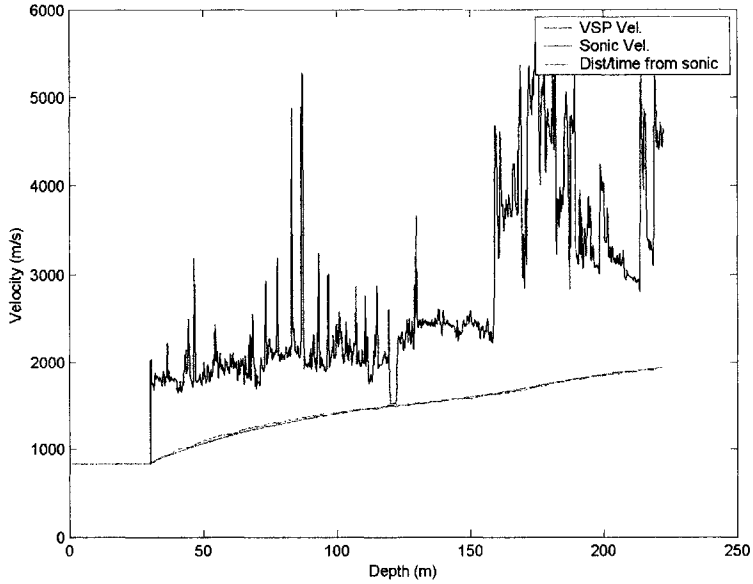

Figure 1.21: Sonic and VSP average velocity comparison. Blue line: sonic velocity log, red line: VSP average velocity, green line: sonic average velocity. The average VSP and sonic average velocities overlap.

line) gives the velocity of the modeled events. Note that both average velocities are close and as a result both the real VSP and synthetic datasets match in time.

1.4 Summary and conclusions

In contrast to surface seismic which records only upgoing reflections, VSP surveys record both the downgoing and the upgoing wavefields. The downgoing wavefield corresponds to the source wavelet traveling into the earth while the upgoing wavefield represents the reflections. Depending on the scope of a particular study, one would be interested in processing only one wavefield. In this chapter the fk and median filters were used to separate the upgoing wavefield from the zero offset VSP data acquired at the borehole BC06 at the Underground Test Facility in Northeastern Alberta drilled through the Athabasca reservoir. Once the reflections are separated they are shifted

to two way traveltime and stacked into corridor traces.

A comparison of the outside and inside corridors as in figure 1.16 (panels c and d) or 1.17 (panels c and d) shows no strong presence of multiple events. Multiples are expected to show in the inside corridor but not in the outside corridor because of their time delay, but in this case both corridors show essentially the same character. This is in concordance with surface seismic observations [2] acquired years later nearby where no multiples were found. It can be also shown by looking at the flattened upgoing wavefield (panel a) where multiple events are also not seen. In this case multiples are expected to show later in time at the same levels of the primary reflection.

The outside corridor traces are then compared to synthetic seismograms obtained using density and velocity logs. Seismic events are recognized in both time and depth in the synthetic traces. Two synthetic traces were made to compare with the corridor stacks: one by convolving the reflectivity series with a synthetic 50Hz Ricker wavelet and other by convolving an extracted downgoing signal wavelet from the filtered downgoing wavefield. No major differences between the two synthetic traces are seen. The corridor stack traces for both the fk and median filtered datasets are compared to synthetic traces and shown in figure 1.20. The following conclusions are made:

- The fk and median separation methods yield similar corridor stacks. Panel a) and b) of figure 1.20 show the two outside corridors after applying a 10-15-90-110 trapezoidal frequency filter. Besides minor differences both traces show the same features.

- The synthetic seismograms made using the 50 Hz Ricker wavelet and the estimated downgoing pulse do not show important differences. In the range 10-110 Hz both show the same features and are mostly similar in shape to the corridor stacks.

- The major events are associated with the regional unconformity at 160 m and the Wabiskaw gas Member at 120 m. The unconformity is associated with a peak event a 200 ms while the gas sand is associated with a smaller peak event at 165 ms. Both events are very well recognized at the corridor and synthetic traces.

- Good alignment of the events is observed over the depth of interest. No shifting in time was necessary to align the VSP and synthetic data due to the fact that the velocity of the VSP data is very close to that estimated for the synthetic using the sonic log velocities.

- The corridor traces have shown that, within the current economical area of interest, no strong multiples are recognized. A weak multiple event of the regional unconformity may be present. This conclusion can be used as an aid in processing of future surface seismic surveys that could be carried in this area.

Chapter 2

Attenuation in Oil Sands

2.1 Introduction

Seismic attenuation has a considerable impact on the amplitude and frequency content of a signal. As a wave propagates through the Earth; its energy decreases due to different factors such a spherical divergence, transmission coefficients, non ballistic scattering, wave mode conversion, and internal friction. Intrinsic attenuation, or absorption, is related to the loss of energy due to those irreversible internal processes that cause a transfer of the wave energy into heat. These processes are linked in part to the matrix-fluid interaction leading to dissipation of the wave's energy.

Attenuation is described in terms of the quality factor Q or the absorption coefficient α. The larger the quality Q factor the lower the attenuation and *vice versa*. Values of Q for sedimentary rocks range from as low as 20 to as high as 150 [47].

Although attenuation has for the most part been ignored in geophysical studies, understanding and quantifying it is key in geophysical prospecting for two reasons. First, attenuation is linked to other petrophysical characteristics such as fluid saturations, degree of consolidation, permeability, fluid viscosity, and porosity, to name a few. This knowledge can be used as a tool in exploration. On this line of research, for

example, Rapoport and Ryjkov [44] found a strong correlation between attenuation and the presence of oil pools using VSP data from Russia and Asia. Martin *et al.* [29] found a strong correlation of attenuation and the presence of oil using 3D seismic data in the complex Eastern Venezuela. Mitchell [31] used surface seismic data from Texas to link the presence of gas with high values of attenuation. Dila and Eastwood [14] studied time-lapse 3D of a steam injected reservoir and found a pronounced loss of high frequencies during the oil production attributed to the interaction of the gas with other pore fluids; although they did not consider the influence of tuning in their study.

The second reason why the study of attenuation is important arises from the desire to increase the vertical resolution in surface seismic profiles by broadening and increasing the frequency content. This can be done by, for example, using deconvolution operators based on the actual downgoing wavefield [19]. If the attenuation can be better quantified, this knowledge could be used in developing an inverse Q filter to amplify the high frequencies that are most attenuated during propagation. Different "inverse Q filter" methods have been developed in the last two decades to remove the effect of attenuation on surface data to increase the resolution with satisfactory results. Bickel [4] proposed the use of an inverse Q filter by reversing the propagation of the plane wave. This propagation reversal is done by a time reversal with Q replaced by $-Q$. Hargreaves and Calvert [20] combined a cascade phase compensation with a windowed approach to build a Q inverse algorithm for prestack data processing. Wang [57, 56] used a method based on the theory of wavefield downward continuation to build an improved image in amplitude, bandwidth and S/N ratio.

Attenuation remains one of the most challenging physical properties to measure in geophysics. There are a number of different techniques to measure attenuation in the laboratory or the field. Each technique has its own limitations. In the laboratory measurement techniques may be placed in 4 categories [52]:

- Free vibration. In this technique the attenuation is found by the amplitude decay of successive cycles of free vibrations. See Peselnick and Outerbridge [37] for example.

- Forced vibration. It is based on the phenomenon of standing waves. The more common methods are the forced longitudinal, flexural, or torsional vibration of long bars. See Tittmann [51] for example.

- Wave propagation. Designed for low ultrasonic frequencies. They involve pulse shape modeling, predictive wavefront, and spectral ratios. See Peselnick and Zietz [38] for example.

- Observation of stress-strain curves. Make uses of the measurement of hysteresis in stress-strain curves obtained from loading-unloading cycles well off the resonance frequency of the sample. See Gordon and Davis [17] for example.

The choice of the method depends on the physical conditions under which the sample is being studied, the actual value of the attenuation, and the objective frequency range.

In the field, attenuation is primarily measured from borehole seismic data (VSP); although surface seismic can also be used. Tonn [53] summarizes different techniques in time and frequency to compute attenuation form VSP data. These methods include: amplitude decay, analytical signal method, modeling, risetime method, and amplitude method; in the frequency domain the methods include: matching technique, spectral modeling, spectral ratios. Each technique is introduced later in the chapter. From all the techniques, the spectral ratio has been the most accepted and used in the industry.

The present chapter is a summary of the estimation of attenuation values (Q) of the McMurray Formation in Northeastern Alberta from vertical seismic profile data using

the spectral ratio technique. The first section is a theoretical background that includes wave propagation and attenuation, the spectral ratio technique and the processing stream of VSP data for attenuation estimation. The second section describes the details of the pre-processing of the VSP data and the application of the spectral ratio method. The last section describes the results of the measurements and speculate on what produces this attenuation.

2.2 Theoretical Background

2.2.1 Wave Propagation and Attenuation

Intrinsic attenuation

As waves propagate into a perfectly elastic Earth, geometrical spreading, scattering, specular reflections, local impedance, and the transmission coefficients control the amplitude decay. Geometrical spreading decay is due to the fact that the initial energy E input by a source is distributed over a shell as $E/4\pi r^2$; and as the radius r of the shell increases the energy density will decrease. As a result, the amplitude is reduced proportionally to the square root of the energy. For the layered case where rays are refracted with focusing and defocusing , this decay can be approximated using different techniques [33, 35]. Further, the additional amplitude decreases due to reflections at the interfaces between layers of different elastic impedances can be estimated using the Zoepprits equations as a function of the incidence angles [47]. Correcting for these two effects amplifies the amplitudes to correct for differences in amplitude with respect to the distance traveled.

In the real layered earth, however, waves are additionally attenuated due to the fact that the layers behave anelastically, that is the energy is dissipated irreversibly as the wave travels. This type of attenuation is an intrinsic property of the media and depends on the nature of the rock and the conditions to which it is subjected.

Intrinsic attenuation processes are understood in terms of the physical process not being completely reversible. In the earth, the particles are displaced as waves pass them and acquire a particle velocity that varies with time.

At the microscopic level the actual intrinsic attenuation processes are complex and still not always understood. Many mechanisms have been proposed to explain the dissipation of the wave energy to heat at the microscopic level. Such phenomena include [52, 7]:

- Dissipation in a fully saturated rock because of relative motion of the frame with respect to fluid inclusions [5, 6].
- Local flow or "squirting" phenomena [30].
- Matrix anelasticity including frictional dissipation owing to relative motion at grain boundaries and across crack surfaces[54].
- Attenuation attributable to fluid flow, including relaxation owing to shear motion at pore-fluid boundaries [55].
- Grain boundary sliding, among others.

Conceptually, a measure of the anelastic damping of seismic waves is given by the quality factor Q. This is defined in terms of the fractional loss of energy per cycle of oscillation. Mathematically it is described as follows [43]:

$$\frac{1}{Q} = -\frac{\triangle E}{2\pi\, E} \tag{2.1}$$

where $\triangle E$ is the adsorbed elastic energy per cycle and E is the total energy. In differential form, equation 2.1 is written as

$$\frac{1}{Q} = -\frac{T}{2\pi\, E}\frac{dE}{dt} \tag{2.2}$$

where T is the period of the vibration. Integrating equation 2.2, we get

$$E = E_0\, e^{-\frac{2\pi\, t}{T\, Q}} = E_0\, e^{-\frac{2\pi\, f\, x}{Q v}}$$

where f is the frequency of the seismic wave (inversely proportional to the period T) and $t = \frac{x}{v}$. Since the amplitude of a seismic wave is proportional to the square

root of the energy, it means that the amplitude decay exponentially at a rate of Q^{-1}. Then the seismic amplitude can be written as

$$A(f,x) = A_0\, e^{\frac{-\pi f}{Qv}x} \tag{2.3}$$

From equation 2.3, it is observed that for a given constant Q model, higher frequencies are attenuated more rapidly than low frequencies over the same distance traveled due to the fact that higher frequencies go trough more oscillations and hence lose energy at a higher rate.

The factors describing attenuation are numerous and may be put in many forms. Often, the exponential coefficient within the equation 2.3 is called the absorption coefficient α with units of dB/λ , this is:

$$\alpha = \frac{\pi f}{Qv} = \frac{\pi}{Q}\frac{1}{\lambda}$$

or

$$Q = \frac{\pi}{\alpha\lambda}$$

where $\lambda$is the wavelength.

Attenuation estimates are usually presented as absorption coefficients (α) or quality factors (Q). For purposes of reference, for a high quality fused-quartz used in a variety of technological applications the value of Q can varies from 10^5 to 10^7 [34](or equivalently α from 0.03x10^{-3} to 0.3x$10^{-6} dB/\lambda$). In sedimentary rocks, Q has been reported to vary from as low as 20 to as high as 150 (α from 0.16 to 0.02 dB/λ) [47] ; whereas for unconsolidated sediments it is expected to be even lower. Values of 200 or more are typical for strong crystalline rocks. Q is estimated to be 8000 for the the outer core of the Earth [27].

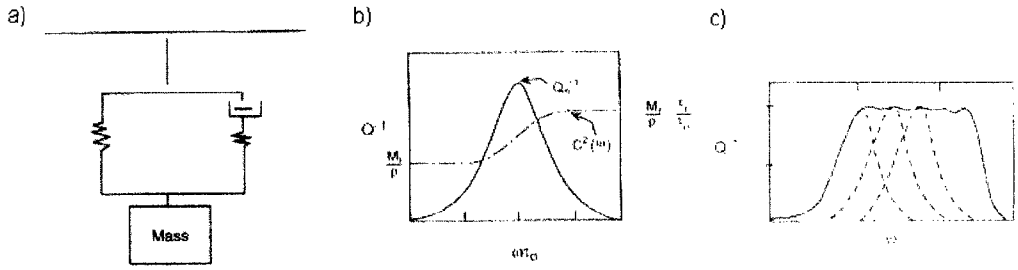

Figure 2.1: Standard linear solid. a) Phenomenological model. b) Attenuation function. c) Superposition of many standard linear models. After Lay and Wallace, 1995.

For purposes of illustration, suppose two pulses of frequencies 10 Hz and 100 Hz traveling through a formation of velocity 2K m/s and absorption coefficient α =0.5 dB/λ or Q=6.2. The 100 Hz pulse, which has a wavelength of 20 m, will be attenuated 5dB over a distance of 200 m, whereas the 10 Hz pulse (λ=200 m) will be attenuated only 0.5 dB over the same distance. This illustrates the fact that the Earth acts as a low pass filter, i.e. it highly attenuates the high frequencies.

Phenomenologically, attenuation can be described using different viscoelastic models such a the one shown in figure 2.1a) called the standard linear solid [27]. The springs represent elastic behavior, and the dashpot represents anelastic or viscous looses. If the mass is deflected, it reaches a point L where it is acted on by a restoring force F. However, if the mass is is held at L, the force F will diminish with time as the dashpot relaxes. This reduction in restoring force is not recoverable and hence the system behaves anelastically in this case. As a consequence of all this, the behavior of the system depends on the frequency applied which implies that if a wave travel through such a solid it will be dispersed, i.e. the different frequencies in a seismic wavelet will travel with different velocities.

For a standard linear solid, the phase velocity and attenuation are a function of frequency and are given by:

$$v_p(\omega) = \sqrt{\frac{M_r}{\rho}}\left(1 + \frac{1}{2}\frac{\delta M}{M_r}\frac{\omega^2\tau_\sigma^2}{(1+\omega^2\tau_\sigma^2)}\right)$$

$$\frac{1}{Q(\omega)} = \frac{\delta M}{M_r}\frac{\omega\tau_\sigma}{1+\omega^2\tau_\sigma^2}$$

where $\delta M = M_u - M_r$, M_u is the unrelaxed elastic modulus (for high frequencies), M_r is the relaxed modulus (for low frequencies) and τ_σ is the stress relaxation time. This mechanism is characterized by a peak of attenuation defined the Debye peak as that shown in figure 2.1b).

It is observed, however, that in some cases the quality factor Q is not dependent on the frequency **(author?)** [27, 52]. This independence of Q may be the result of the superposition of different mechanisms at different scales due to the fact that not just one viscoelastic mechanism dominates. However, it is the superposition of different viscoelastic mechanisms acting at different scales which give the response of the Earth to the passage of a seismic wave. Figure 2.1c) illustrates the Q response in the case of the superposition of many standard linear solid elements. Observe that the seismic response is independent of the frequency in this dependence case. Another reason for this Independence comes from the fact that the attenuation measurements are done at limited frequency bandwidth that we are not able to observe those changes which would only be observable at large scales. Sams *et al.***(author?)** [45] observed the dependence of Q after gathering seismic, sonic and ultrasonic attenuation measurements in sediments in the Imperial College Test site.

The effect of scattering.

In a real layered Earth intrabed multiples play an important role in the propagation of a downgoing pulse [39]. As it travels downward into the Earth it is typically distorted by intrabed multiples and as a result a boost of the low frequencies and

attenuation of the high frequencies is observed. Due to this distortion an apparent attenuation, which is not due to intrinsic absorptive properties, is observed [46, 36]. This attenuation is defined as scattering attenuation and is due to i) stratigraphic filtering due to the layering in the Earth and, ii) the deviation of the wavefront due to single and multiple reflections.

In some cases a large part of the total attenuation on seismograms can be attributed to intrabed multiples rather than the intrinsic attenuation [36]. The proportion of the scattering attenuation depends on the amount of scattering present in the medium.

Effective attenuation

The effective attenuation, Att_{eff}, that is observed on the recorded seismic traces is defined as:

$$Att_{eff} = Att_{int} + Att_{scatt}$$

where A_{int} is the attenuation due to internal frictional processes and A_{scatt} is the attenuation due to scattering. Intrinsic attenuation is related with the physical properties of the rocks while scattering attenuation is due to the distortion caused by intrabed multiples as noted above. In order to perfectly measure the intrinsic attenuation of a rock, it is necessary to isolate from the effective attenuation the scattering part. This is not so easily accomplished and is often attempted by modeling[39, 40].

2.2.2 The Spectral Ratio Method

As described earlier, there are many different techniques to measure attenuation (quality factor Q) from VSP data. Tonn [53] describes different methods to measure Q on both the time and frequency domain. In the time domain it includes:

- Amplitude decay technique based on computing Q from amplitudes recorded at different depths. It requires true amplitude measurements.
- Analytical signal method based on complex trace analysis.
- Waveform matching based on the forward modeling of a recorded signal by varying the attenuation.
- Phase modeling based on a forward modeling of the instantaneous phase.
- Frequency modeling which is the derivative of the instantaneous phase.
- Risetime method based on the dispersion of the traveling wave.
- Pulse amplitude method which is based on analysing the maximum amplitude of the first arrival as it is proportional to attenuation.

In the frequency domain the methods include:

- Matching technique. It is based on the transfer function that matches the signal at a depth 1 to the signal at depth 2.
- Spectral modeling. Is similar to wavelet modeling but it models the amplitude spectra of a recorded pulse.
- Spectral ratio technique. It compares the amplitude spectra of two traces recorded at different depths.

Attenuation remains a difficult parameter to measure in the Earth. No single method is superior; however in case of a dataset with high S/N ratio the performance of the spectral ratio method is optimal since it yields more reliability over others [53].

Author	Date	Rock type	Method	Attenuation
Ganley and Kanasewich	1980	Sediments	fixed depth	549-1193m: Q=43+2 945-1311m: Q=67+6
Hauge	1981	Sediments	fixed depth	α = 0.1-0.9 dB/wavelenth
Stainsby and Worthington	1985	Sediments	fixed depth	4900-5600m: Q=25+3
Pujol and Smithson	1991	Basalts	fixed freq	1.1×10^{-4} dB.s/m at peak freq.
Pujol *et al.*	1998	Metamorphic rocks	fixed freq	at 7.8 Hz: Q=14 at 46.9 Hz: Q=32
Pujol *et al.*	2002	Unconsolidated sediments	fixed depth	1.5-44.2m: Q_s=34-44
Maresh *et al.*	2003	Basalts	fixed depth	2000-3000m: Q:15-35

Table 2.1: Reference papers on spectral ratio using VSP data

The spectral ratio method has been the technique most used in the industry and many references can be found on it. Table 2.1 shows some of the studies where the spectral ratio technique is applied to VSP data. The work done by Ganley and Kanasewich in 1980 [16] is one of the first references found in the literature. They used the spectral ratio technique in 2 trace pairs to find attenuation values from the Beaufort Sedimentary Basin to be 43 ± 2 for the interval 549-1193 m and 67 ± 6 in the interval 945-1311 m. Hauge in 1981 [22] used borehole data from Texas to measure α in different sediments ranging from 0.1 to 0.9 dB/wavelength (i.e. Q from 31 to 4). Stainsby and Wothington [49] found Q for the depth interval 4900-5600 m to average to 25 ± 3 in the North Sea. All this studies were done in sedimentary rocks for a fixed depth and fitting a straight line to the logarithm of the amplitude for different frequencies. Pujol has proved the technique in different environments. In the work done in the German continental deep borehole (KTB) [42] it was found Q to range from 14 to 32 in the depth interval from 3.5 to 4.5 Km dominated by amphibolite and metagabbro. For the unconsolidated sediments of the Mississippi it was measured Q_s to range from 34 to 44 for the depth interval 1.5-44.2m. In his work in the Columbia

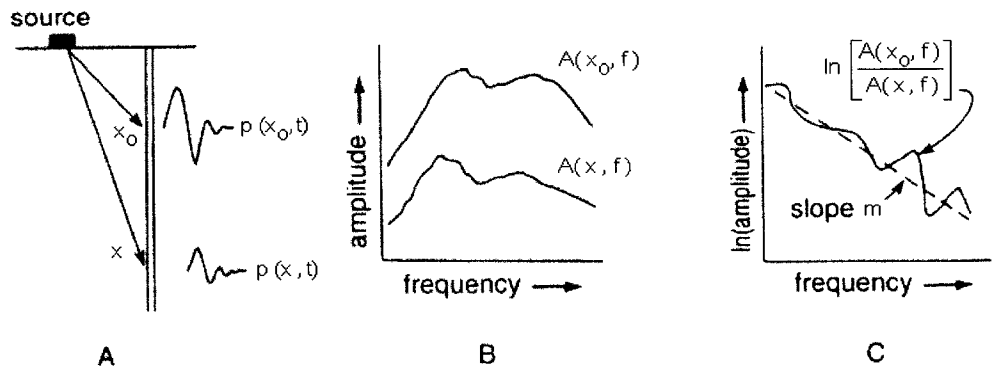

Figure 2.2: Spectral ratio method. a) Pulses P(xo,t) and p(x,t) acquired at different levels in the borehole. b) Amplitude spectra of the two pulses A(xo,f) and A(x,f). c) Spectral ratio plot. After Hardage, 2000.

Plateau Basalts [40] it was found that most of the dissipation seen in the basalts is attributed to scattering. Maresh *et al.* [28] found Q to range from 15 to 35 in Atlantic basalts.

The spectral ratio method

From equation 2.3, the seismic wave amplitude of a monochromatic plane wave of frequency f can be modelled as the solution for a damped oscillating system as:

$$A(x\ ,\ f) = G\ A(x_0\ ,\ f)\ e^{-\frac{\pi f}{Q v}(x - x_0)} \tag{2.4}$$

where $A\,(x_0\ ,\ f)$ is the amplitude at some depth x_0 closer to the source. The term v represents the wave velocity. In an attenuating medium v must be frequency dependent [1] but we have assumed in the current analysis that over the bandwidth of the signal employed the attenuation, and hence the velocity, remains constant. Further, it is shown later that the phase velocity may be assumed frequency inde-

pendent. The term G is a frequency independent factor that has been introduced to account for changes in the pulse amplitude with depth and to consider spherical divergence, dependence of the pulse magnitude on local impedance, source directivity, and scattering losses [19, 22].

Equation 2.4 can be used to resolve Q given a set of pulses $p(x_0, t)$ and $p(x, t)$ recorded at different depths x_0 and x in a borehole as in figure 2.2a). Their amplitude spectra are given by $A(x_0, f)$ and $A(x, f)$, respectively. Taking the logarithm and rearranging equation 2.4 becomes:

$$ln\frac{A(x,f)}{A(x_0,f)} = -\frac{\pi\,\Delta x}{Q\,v}\,f + ln\,G \tag{2.5}$$

where $\Delta x = x - x_0$. Equation 2.5 describes a line of slope $-\frac{\pi\,\Delta x}{Q\,v}$ and intercept $ln\,G$ within a given frequency range from which the quality factor Q can be isolated. This equation can also be written as:

$$ln\frac{A(x,f)}{A(x_0,f)} = -\frac{\pi}{Q\,\Delta t}\,f + C \tag{2.6}$$

where Δt is the time arrival difference between the two pulses.

The geometry of a VSP experiment is ideal for acquiring seismic information from which attenuation can be obtained because the amplitude traces are sampled at various depths and are hence amenable to analysis via equations 2.5 or 2.6. Figure 2.2 illustrates the technique. In a zero offset VSP experiment a source is activated at the surface close to the wellbore and receivers sample the downgoing wavefront at different depths. Suppose that the wavefront has been sampled at two different depths as

those shown in figure 2.2a). Given two such pulses $p(x_0, t)$ and $p(x, t)$, Q may be obtained using the spectral ratio method by:

1. Computing the amplitude spectra $A(x_0, f)$ and $A(x, f)$, respectively via an FFT. The pulse recorded at depth x has a lower amplitude than the first pulse at x_0 as shown in figure 2.2b) due to the attenuation of the frequencies it experienced as it traveled through more layers. Note that the traces will require appropriate pre-processing to account for distortion caused by upgoing reflections, for example.

2. At each frequency, calculate the simple ratio. Divide the second amplitude by the first amplitude for each frequency sample.

3. Take the natural logarithm of this ratio for each frequency sample (i.e. take the logarithm of the ratio).

4. Plot the logarithm as a function of frequency. The data will be aligned as in figure 2.2c).

5. Determine the linear slope of this plot from the best fitting line.

6. Calculate Q from the slope of equation 2.5 or 2.6 depending of what variables were plotted.

The greatest advantage of this technique that all of the factors influencing the overall amplitude such as geometrical wavefield spreading, loss of transmission and local impedance effects are all contained within in the intersect $ln\, G$ of the line plotted in step 4 above and may be ignored if a value of indicative of the absorption only is to be found. This considerably simplifies the determination of Q to other methods in which

these factors are all deterministically corrected for, and which can add substantial error.

With several VSP traces, the trace closer to the source is selected as a reference and then compared against all the deeper traces via the spectral ratio. In this way "near" and "far" Q estimates can be obtained. As well, with such a method the reference trace is easily changed within a same lithology for alternative comparisons.

There are a number of issues that need to be considered when attempting to measure Q in a real field experiment with the spectral ratio technique. The most important of these issues is uniformity of the source and/or receiver. An ideal VSP survey would be that where all levers can be recorded with one shot using perfectly matched receivers; this would ensure the same input signal to the earth and a consistent earth response at all the levels. However, as the number of geophones in a VSP downhole tool is limited (1 to 6 typically), the source must be repeatedly activated several times while the receivers are moved to different depth levels. For this reason source repeatability is crucial to minimize error.

2.3 Data processing

A monitor geophone was placed close to the source to reject inconsistent input signals. Figure 1.9 shows the signal recorded by a monitor geophone planted close to the mud pit. The proximity of the geophone to the source made it susceptible to be inadvertently moved when the source was shot and as a consequence it had to be replanted when the VSP tool was at depths of 137.5 m and at 167.5 m, a change in amplitude and character is seem. Despite this experimental problem, the results of figure 1.9 show that the Betsy gun source provides a repeatable signature; the shape of the wavelet is very consistent over the range from 125 m to 155 m where the

spectral ratio is to be applied. The trace 157.5 m, however, shows a weaker amplitude which may due to an improper stacking of the traces since the same weak amplitude is observed on the actual VSP record at that level.

VSP traces record both the downgoing pulse and the upgoing reflections and their associated upgoing and downgoing multiples. Reflections interfere with the downgoing pulse. Depending of the reflection coefficient, they superpose either constructively or destructively with the downgoing pulse and consequently the downgoing pulse is distorted. This effect is even more critical at late times when the downgoing pulse has been broadened due to the lose of high frequencies. This stratigraphic filtering leads to erroneous attenuation estimates because the first break pulse is contaminated by this interference with other upgoing pulses. For this reason it is necessary to process the VSP traces so that the downgoing pulse to be analyzed is minimally distorted by reflections. It is necessary to carry out a wavefield separation to clean the downgoing pulse. Wavefield separation was carried in chapter 1 but focused in obtaining the upgoing path of the wavefield towards a geological analysis. In this chapter we use only the stronger downgoing component and hope that the upgoing reflections have been removed as much as possible.

The wavefield separation is carried through all the 77 traces recorded at the borehole using the different techniques described last chapter. Then the 13 traces that sample the McMurray Formation from 125 m to 155 m are used in an application of the spectral ratio technique.

2.3.1 Wavefield Separation

Wavefield separation was carried out using an fk and a median filter as described in the last chapter. Figure 2.3 shows the results obtained after applying the techniques. The datasets have been flattered to the first break and centered at 100 ms. A spherical divergency gain as that computed by Grech [18] is applied for better display.

Figure 2.3a) shows the flattened raw VSP data. The first break pulse corresponds to

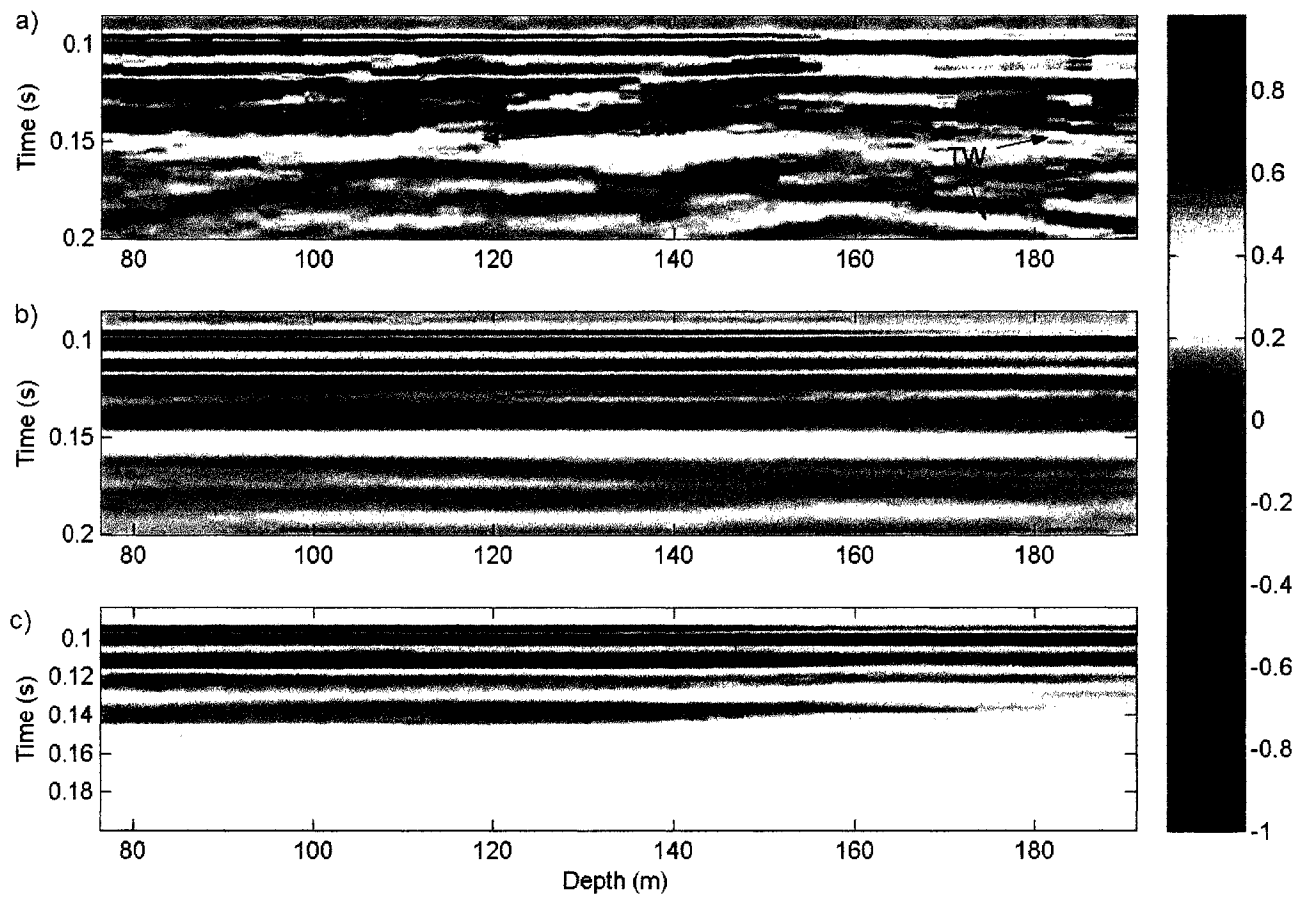

Figure 2.3: Time flattened isolated downgoing wavefield. a) Raw VSP Data: Upgoing reflections distort the shape of the downgoing pulse. TR: top reflection, BR: bottom reflection of the McMurray Formation. b) *fk* filtered dataset downgoing pulse. c) Median filtered downgoing pulse.

the energy from 95 ms to 120 ms approximately. Note the sharp change in amplitude from the bottom of the McMurray Formation at 160 m due to the abrupt change in the elastic impedance as discussed in the last chapter. Two important reflections are observed in the data: bottom at 160 m (BR in the figure) and top at 120 m (TR in the figure). The tube wave (TW) also causes distortion of the first break at shallower levels. As discussed before, the downgoing pulse (within 95 ms-120 ms) is distorted by those reflections. The bottom reflection distortion reaches 8 traces up from the bottom of McMurray Formation as the downgoing pulse is wide enough to be reached by this upgoing event.

Figure 2.3b) shows the downgoing wavefield obtained after applying the fk filter while figure 2.3c) shows the downgoing field obtained after applying a 7-point median filter. The median filter retains the sharp change in amplitude at the bottom of the McMurray Formation (160 m). The median filter was tested for window lengths of 11, 9, 7 and 5 traces. The shortest window length that yielded satisfactory results was the 7-point. Longer filters also yielded reasonable results but increased the smoothness of the amplitudes as they where not able to retain the sharp change in amplitude at the unconformity. The 5-trace filter results are poor as the upgoing wavefield is not attenuated.

2.3.2 Windowing.

Once the downgoing wavefield is separated, it is necessary to isolate the first break from later downgoing multiples. This is achieved by appropriately modulating the signal with a cosine type window. Adverse side effects of isolating the signal with a window is a broadening of the signal spectra. Pujol and Smithson [40] proposed the use of a Blackman-Harris type window to decrease this effect. The shape of this window is described by [21]:

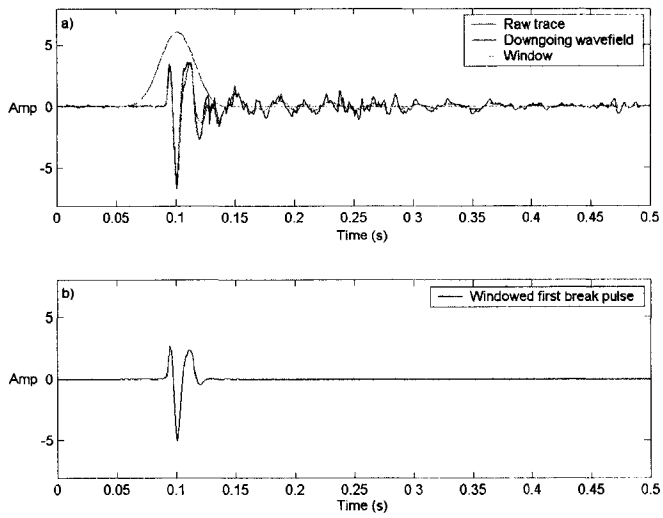

Figure 2.4: Windowing of the first break pulse at 125 m. a) Raw trace in blue, downgoing wavefield in green and 80 ms-window in red. b) Isolated first break pulse.

$$w(k+1) = a_1 - a_2 \cos\left(2\pi \frac{k}{n-1}\right) + a_3 \cos\left(4\pi \frac{k}{n-1}\right) + a_4 \cos\left(4\pi \frac{k}{n-1}\right) \quad (2.7)$$

where,

$k = sample\ position$

$n = window\ length\ in\ samples$

$a_1 = 0.35875$

$a_2 = 0.48829$

$a_3 = 0.14128$

$a_4 = 0.01168$

Figure 2.4a) shows the windowing at trace 1 (125 m). The raw trace is in blue, the downgoing wavefield obtained from median filtering is green and the corresponding 80 ms window is in red. Upgoing events are highly attenuated in the downgoing wavefield. The resultant first break pulse after windowing is shown in figure 2.4b).Figure 2.5a) shows the downgoing wavefield after fk filtering while figure 2.5b) the shows

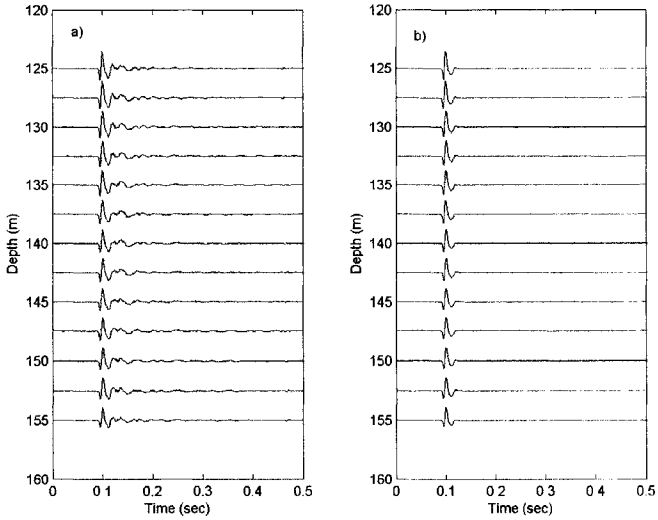

Figure 2.5: Windowing of the first break pulse at all levels. a) Downgoing wavefield. b) Windowed first break pulse.

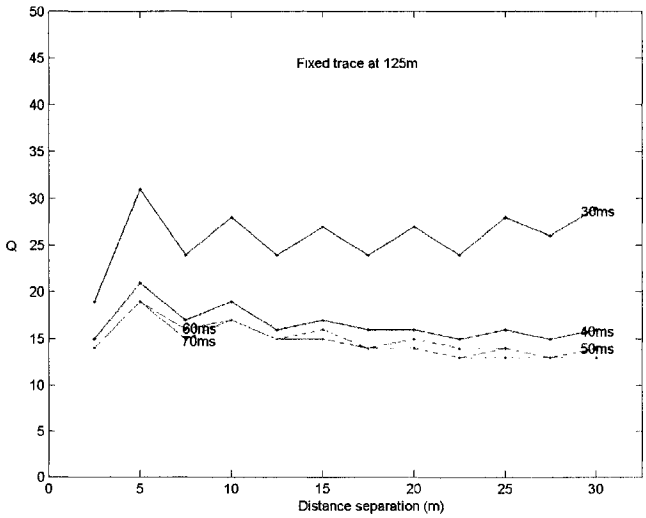

Figure 2.6: Window length verus Q for fixed trace at 125m.

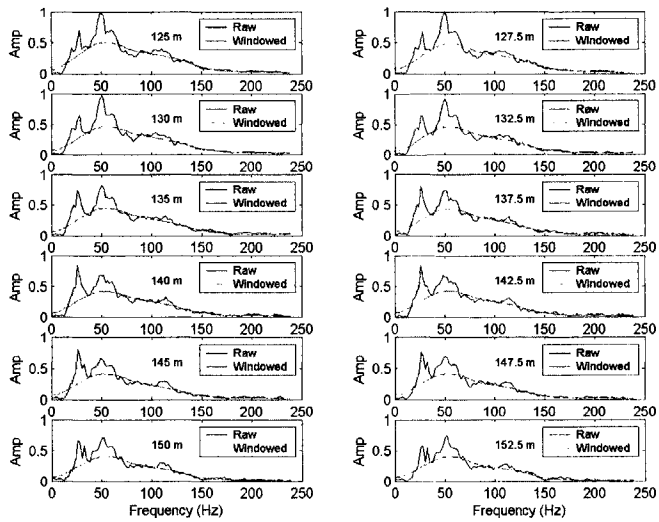

Figure 2.7: Amplitude spectra comparison before (blue line) and after windowing (red line)for the 13 traces sampling the McMurray Formation.

windowed downgoing first break pulse using a 80ms window.

Figure 2.6 shows the effect of using different window lengths on the Q estimates for a reference trace at 125 m. For 30 ms length, the estimates are relatively high (average to 25). As the window length is increased, the estimates decrease and stabilize approximately to the same values. Varying the window to more than 60 ms does not change Q the estimates. For this reason a 60 ms window is chosen to isolate the the first break pulse.

After the downgoing pulses have been isolated from upgoing reflections and isolated from later multiples they are ready to be applied to equation 2.5 or 2.6. The amplitude spectra of the windowed pulses is computed through a Fast Fourier Transform. Figure 2.7 shows the 13 amplitude spectra for the downgoing wavefield (blue line) and the windowed first break pulse (red line), respectively. The downgoing wavefield amplitude spectra show two frequency peaks at 25 Hz and 55 Hz. The predominant energy in the signal comes from 25 Hz to 120 Hz with peak amplitude at 50 Hz. The amplitude spectra of the windowed first break pulse is a broadened version of the

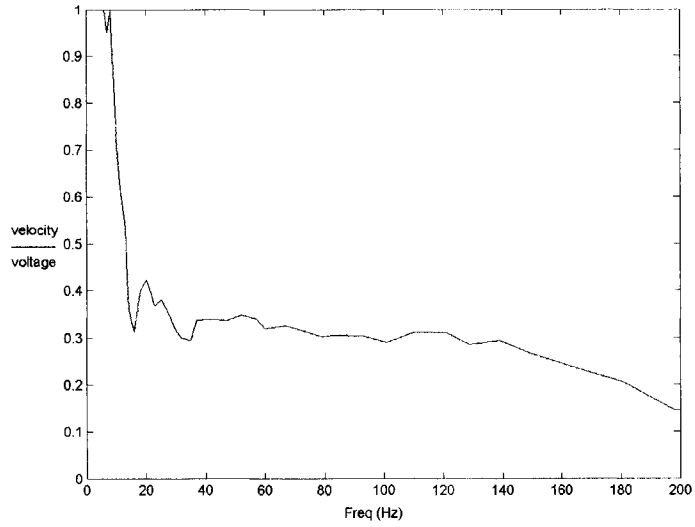

Figure 2.8: Receiver response. The ratio of particle to geophone output velocity to voltage is plotted to see the type of response of the receiver.

original before windowing and shows the same peak frequency.

Figure 2.8 shows the calibration curve for the VSP tool. The equipment's response is observed in this plot of particle velocity normalized by measured peak voltage versus vibration frequency. This measurement was obtained by shaking the tool at constant frequency in a vertical direction on a calibrated shake table in the Department of Mechanical Engineering. For frequencies lower than 25 Hz the response is not constant as seen in the plot. From 25 Hz the response is more uniform with a linear trend up to 140Hz. Based on this observations it can be concluded that all frequencies lower than 25 Hz recorded by the tool are noisy as the response is not linear. As a result the frequency of the signal in this dataset will be limited between 25Hz and 120Hz.

2.3.3 Spectral Ratio

As discussed before, the spectral ratio method used in this study assumes that Q is constant or nearly so over the band of interest. To compute the quality factor Q, the logarithms of the amplitudes can be plotted using different approaches as a test of

consistency:

1. $\frac{1}{\Delta t} \ln \frac{A(x\,,f)}{A(x_0\,,f)}\ Vs\ f$; which yields a slope equals to $-\frac{\pi}{Q}$ or

2. $\frac{v}{\Delta x} \ln \frac{A(x\,,f)}{A(x_0\,,f)}\ Vs\ f$; which also yields a slope equals to $-\frac{\pi}{Q}$.

The first uses the first break time differences $\triangle t$ while the second employ both the velocity of wave propagation v and the distance separation between the traces $\triangle x$. The first break times are picked from the raw data, however the velocity of wave propagation can be approached using the furthest VSP first break times, an average velocity from the sonic log, or the phase velocities derived from the FFT. Next sections describe the velocity computation using the VSP first breaks and the phase velocity.

Average velocity from VSP first breaks.

From the VSP first break times, an average VSP velocity is computed from the local slope of the $t - x$ curve. This is:

$$v_{average} = \frac{\triangle x}{\triangle t} \tag{2.8}$$

where $\triangle x$ is the trace separation and $\triangle t$ is the time difference between arrival times. The first breaks are picked from the raw VSP data at the first energy maximum to avoid uncertainty in where to pick the arrival of the energy due to noise levels. This is a very good approach since what is important in the velocity calculation is the time difference between pulses.

Figure 2.9 shows a comparison of the velocities obtained using the first break times and the sonic velocity for the borehole from 30m to 220m. Figure 2.9a) shows the first

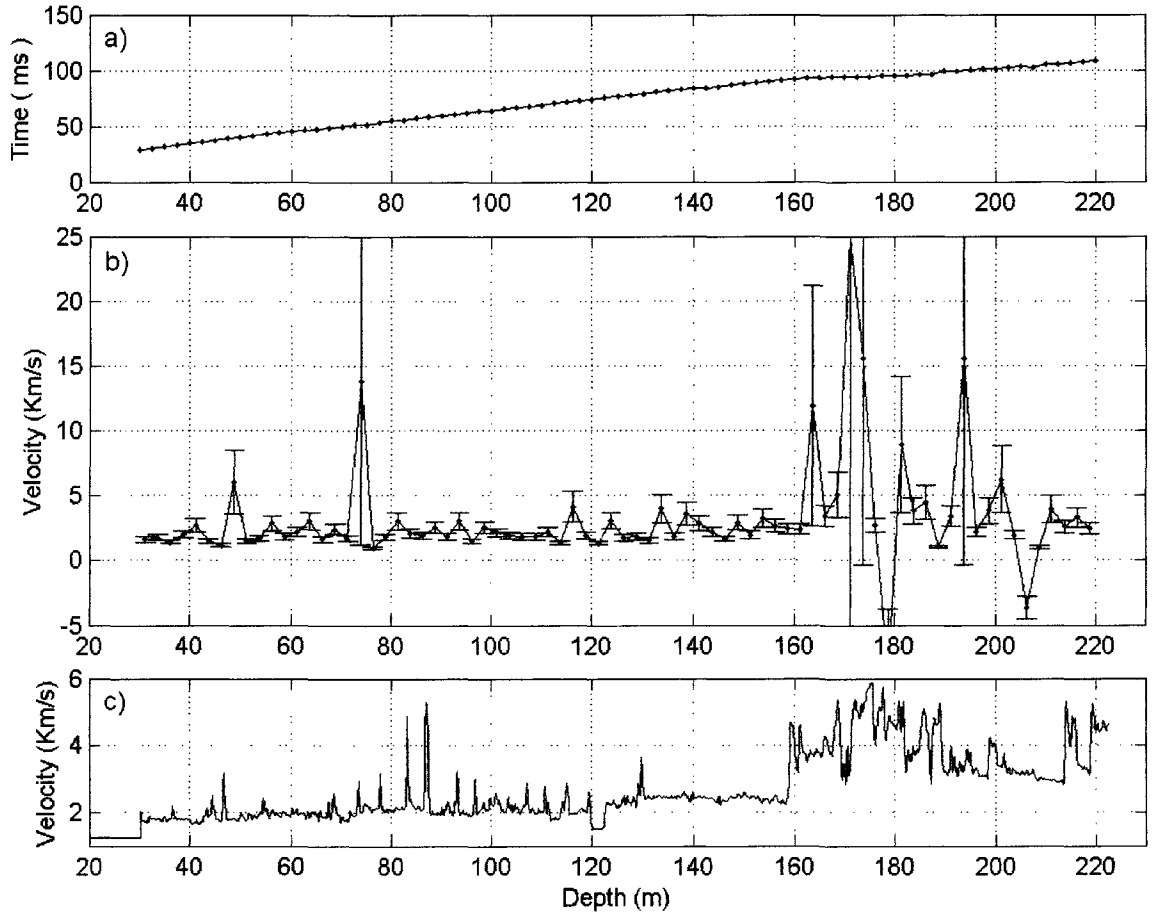

Figure 2.9: VSP and sonic velocity comparison. a) First break times from VSP. b) Interval VSP velocity using the slope of adjacent traces. c) Sonic velocity log.

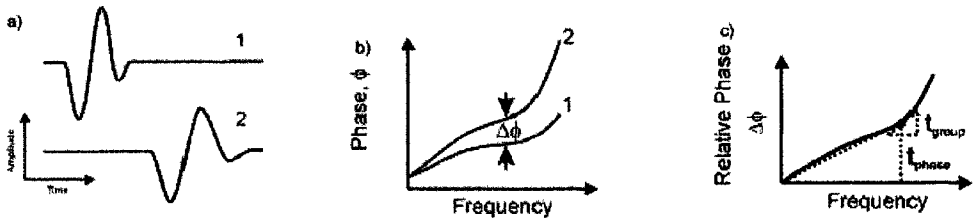

Figure 2.10: Phase velocity calculation.a) Two pulses recorded at different depths. b) Their unwrapped phases.c) The phase difference. From Molyneux and Schmitt, 2000

break times, figure 2.9b) shows the interval velocity from the slope of the adjacent traces, and figure 2.9c) is the sonic velocity log.

In figure 2.9b) the VSP interval velocities for the McMurray Formation (120 m to 155 m) varies from 2000 m/s to 5000 m/s. This behavior of the velocity is not physical. This is the product of the close spacing between the receivers. The small separation between the receivers makes the time difference to be comparable to the sampling rate and as a consequence large uncertainty in the velocity estimates, especially when the velocity is higher (i.e. carbonates below 160 m). This causes anomalous traveltimes and as a consequence erroneous velocity within a given geological layer. This effect is not be evident in conventional VSP practice where the depth sampling rate is farther. A more reliable average velocity from the VSP data is found by smoothing the data by a 5 point filter. Using this approach the average velocity over the McMurray Formation is 2280 ± 280 m/s. Using the first and last time samples within the formation yields an average velocity of 2260 ± 290 m/s. The average sonic velocity (2.9c) within this formation is 2420 ± 140 m/s.

Phase velocity computed from VSP traces

The frequency dependent phase velocity is computed as described in Molyneux and

Schmitt[32] using phase differences. For a pair of pulses separated a distance Δx, the phase velocity is given by

$$V_{phase}(\omega) = \frac{\Delta x}{\Delta t_{lag}} \tag{2.9}$$

where $\Delta t_{lag}$is the time lag difference between pulses given by

$$\Delta t_{lag} = \frac{\Delta\varphi(\omega)}{\omega} \tag{2.10}$$

and $\Delta\varphi$ is the unwrapped phase difference given by

$$\Delta\varphi(\omega) = \varphi_2(\omega) - \varphi_1(\omega)$$

The calculation of the phase velocity is illustrated in figure 2.10. Given two pulses recorded at different depths x_1 and x_2 (Fig. 2.10a), their unwrapped phase (Fig. 2.10b) at a given frequency can be computed via a Fast Fourier Transform. The phase difference (Fig. 2.10c) between those yields the time phase delay used to compute the phase velocity using the equation 2.9. The slope of this $\Delta\varphi - f$ curve can also be used to compute the group velocity.

Figure 2.11 shows the amplitude and the unwrapped phase spectra for both the raw VSP data and the windowed first break pulse up to 500 Hz. Figure 2.11a) shows the raw VSP data, its amplitude spectra in decibel scale is shown in figure 2.11b) and its unwrapped phase spectra is shown in figure 2.11c). The windowed first break pulse is shown in figure 2.11d), e) and f). As discussed before, most of the energy lies from 20 Hz to 120 Hz. The McMurray Formation corresponds to depths from 125 m to 155 m sampled by 13 traces. For those depths (arrow in panel f), the phase spectra does not have important change from 20 Hz to 120 Hz which suggests a roughly constant phase velocity velocity over this range.

With the available 13 traces in the formation, the phase velocity can be computed for all possible trace pairs. Figure 2.12 shows the phase velocity from 125m (trace 1) to all other 12 trace distances (down each 2.5 m up to 150 m) for frequencies up to 500 Hz. Overall, the phase velocities are constant over the frequency bandwidth in this

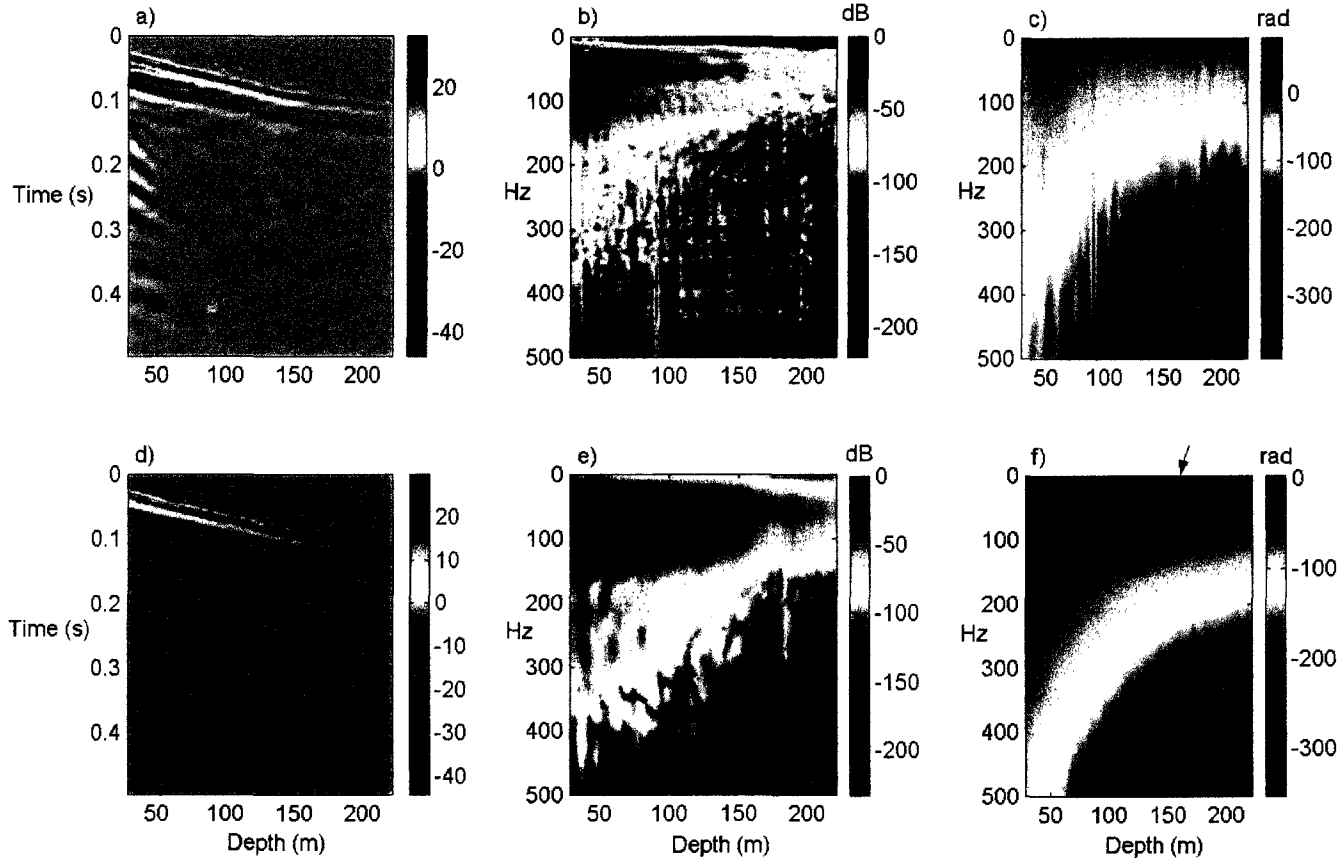

Figure 2.11: Amplitude and phase spectra of raw VSP data and windowed downgoing pulse. a) Raw VSP. b) Amplitude spectra in decibel scale. c) Unwrapped phase change. d) First break pulse. e) Amplitude spectra in decibel scale. f) Unwrapped phase change.

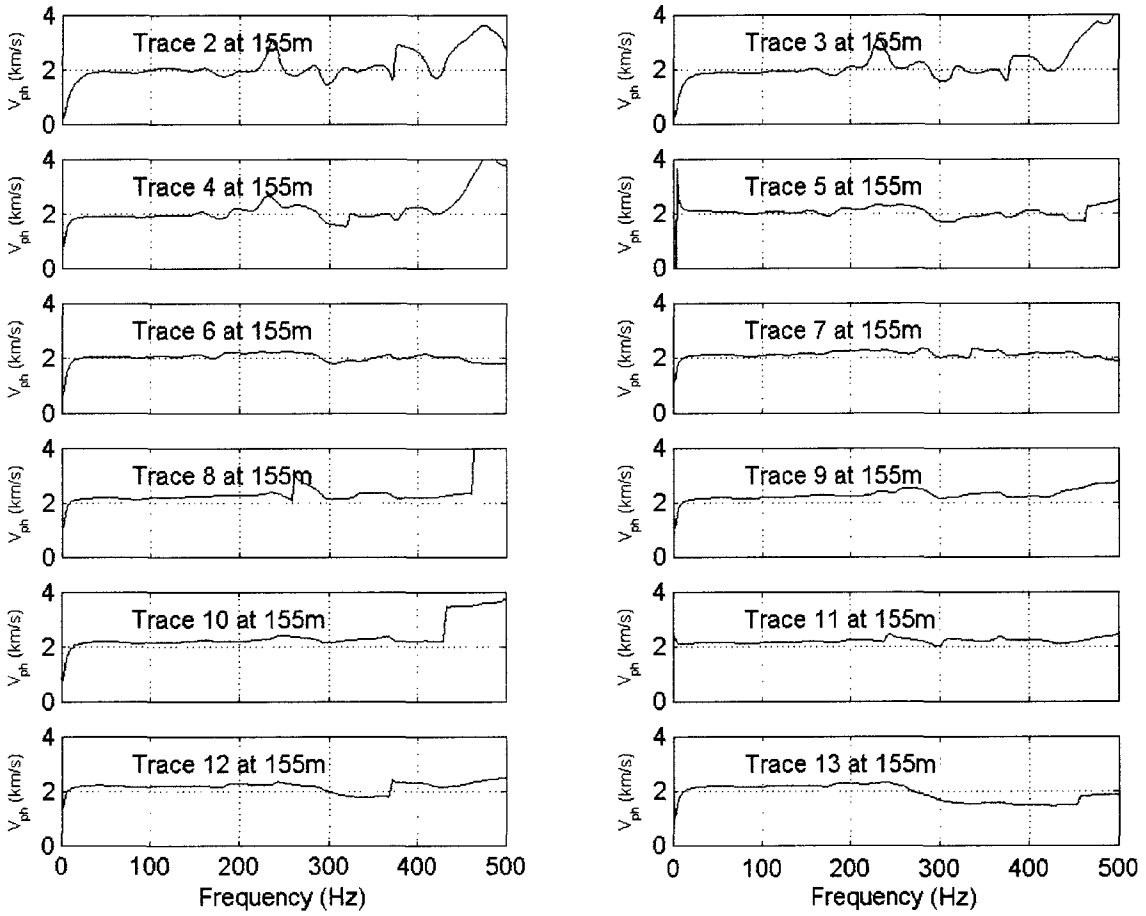

Figure 2.12: Phase velocity fixing trace at 125m compared with the other 12 traces

Type of velocity	m/s
Sonic average	2420 ± 140
VSP average	2260 ± 290
VSP phase	2194 ± 41

Table 2.2: Velocity comparison summary

study (25-120 Hz) and average to 2194 ± 41 m/s. Frequencies lower than 25 Hz are considered noisy as discussed before and the corresponding values are ignored. Table 2.2 summarizes the average VSP and sonic velocities.

For the spectral ratio plots, the logarithm of the amplitude ratio are plotted versus frequencies from 20Hz to 120Hz as in equation 2.5 or 2.6. Then the data is fitted to a straight line using a least squares approach. The quality of the linear fit is assessed by computing the Pearson's correlation coefficient[13]. Given two datasets x and y, this correlation coefficient r is given by:

$$r = \frac{C_{xy}}{\sqrt{\sigma_x^2 \, \sigma_y^2}}$$

where

$$C_{xy} = \frac{1}{N} \sum (x_i - m_x)(y_i - m_y)$$

$$\sigma_x^2 = \frac{1}{N} \sum (x_i - m_x)$$

$$\sigma_y^2 = \frac{1}{N} \sum (y_i - m_y)$$

Where m is the mean and N is the number of samples. If $r = 1$ x, is perfectly linearly related to y, and therefore the data is perfectly fit to the straight line. Alternately, if $r = 0$ there is no linear relationship between x and y; we do not expect a linear description to work. If $r = -1$ then the two are perfectly linearly related again but inversely. Next section shows the line fitting when the first trace at 125 m is fixed and compared with all other 12 deeper traces.

Spectral ratio for the fk filtered data

Figure 2.13 shows the plot of $\frac{v}{x} ln \frac{A(x\,,f)}{A(x_0\,,f)}$ vs frequency where the x_0 is the fixed trace at 125 m depth. This trace is then compared with the other 12 deeper traces. The average sonic velocity over the formation is used in this case. The Pearson's correlation coefficients range from 0.88 to 0.96 and indicate a high degree of linear fit. The quality factor Q is computed from the slope of this lines in the next section. The complete plot set for all other approaches using first beak times and phase and VSP average velocities is included in the Appendix 1.

Spectral ratio for the median filtered data

In figure 2.14 $\frac{v}{x} ln \frac{A(x\,,f)}{A(x_0\,,f)}$ is plotted vs frequency for the fixed trace 1 at 125m for the median filtered dataset. Aside from the first depth, the correlation coefficients are high and range from 0.83 to 0.97. For this dataset the average sonic velocity is used. The complete plot set for all other approaches using first beak times and phase and VSP average velocities is also included in Appendix 1.

A cycle character in the spectral ratio plots characterized by a kink at 80Hz is observed in the data. This effect cannot be explained by random noise or errors associated with the acquisition device since the errors associated with FFT [50] do no allow for such a smooth trend to be created by this noise. However, this can be explained by means of the interference of the downgoing tubewave with the downgoing pulse. As it is observed in figure 1.11, the downgoing tubewave (TW1) is recorded close to the first break for the area of interest (125 m to 160 m). Also, both events have very similar velocities which makes it difficult to be filtered without damaging the actual signal. As a result, noise may be included in the analysis when the first break is windowed. To investigate this effect, different fk filters where applied to the dataset.

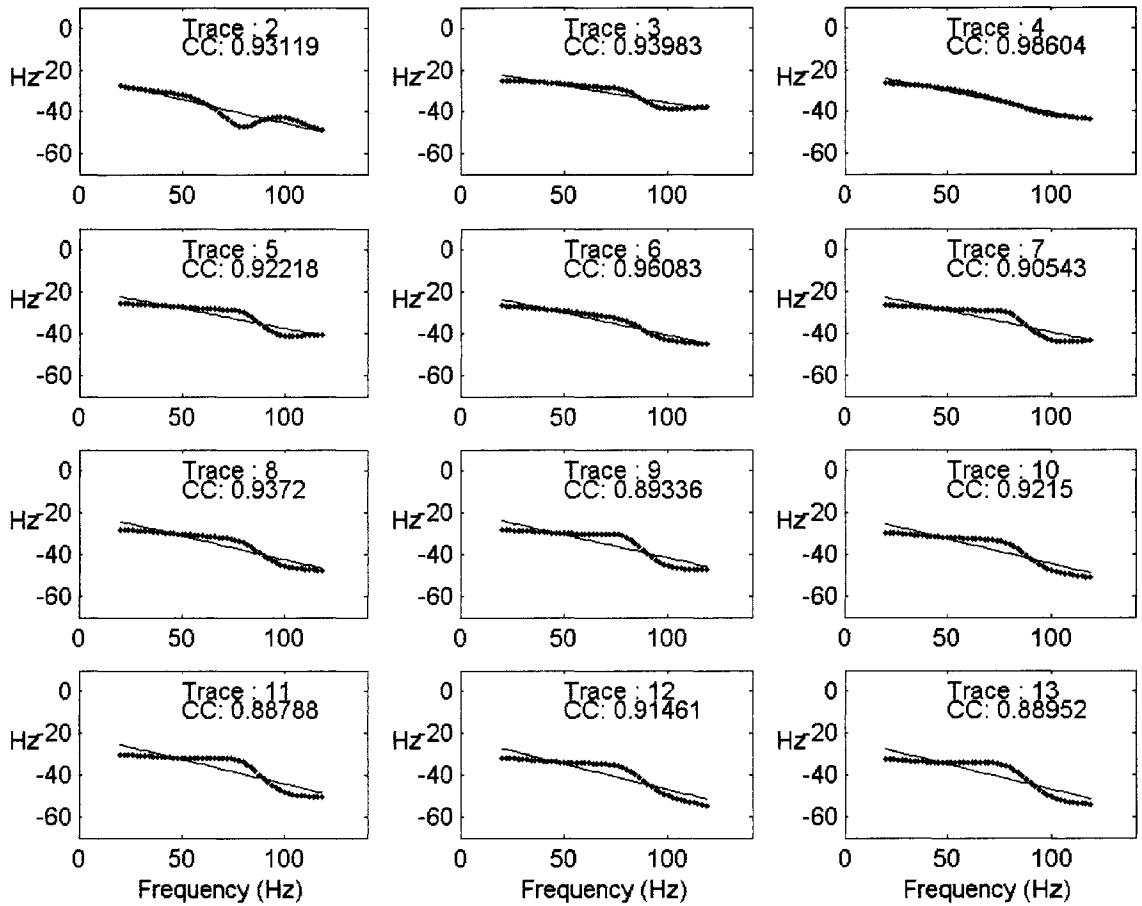

Figure 2.13: Spectral ratio plot using the average VSP velocity for the *fk* filtered dataset. Trace 1 is compared with the 12 other traces. cc denotes the correlation coeficient between the data and the straigth line

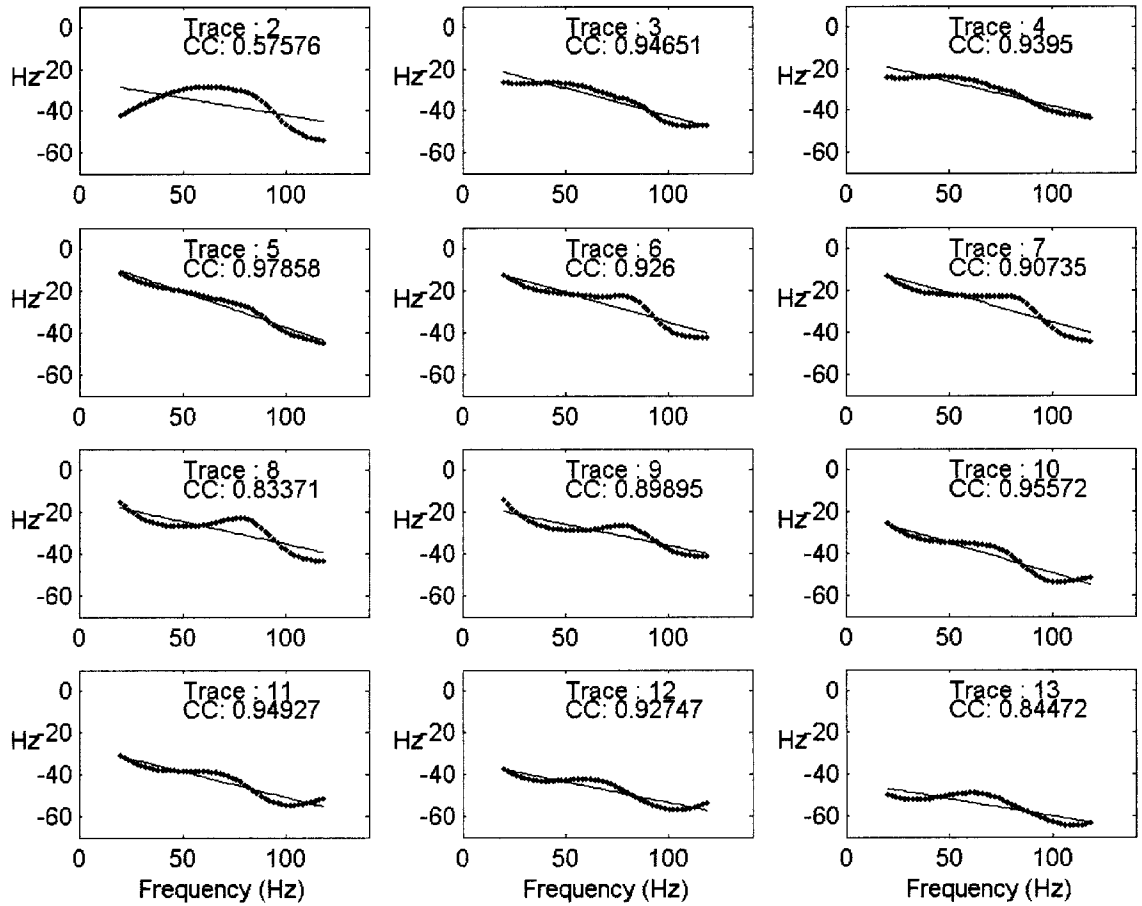

Figure 2.14: Spectral ratio plot using the average VSP velocity for the median filtered dataset. Trace 1 is compared with the 12 other traces. cc denotes the correlation coeficient between the data and the straigth line.

Different fk window widths were used to isolate the downgoing pulse from the noise. Figure 2.15 shows a comparison of the raw fk transform of the VSP data (panel a) and the spectra obtained using different windows used to isolate the downgoing wavefield. Panel b) shows the actual filter used throughout this study. To evaluate the effect of the tubewave, filter c) was applied to the data (which highly attenuated the tubewave). The results have shown that the more the window is narrowed (i.e the closer to the actual downgoing pulse) the more lineal the trend is in the spectral ratio plots.)

Figure 2.16 shows a comparison of the spectral ratio plots for the originally filtered fk dataset (figure 2.15b) and a dataset filtered with a the narrower window (figure 2.15c). It is observed that the linearity of the plot is increased as the window is narrowed. However, as mentioned before, the side effect of isolating the downgoing pulse with such a narrow window is a distortion of the actual signal since both signal are overlapped in the fk panel. To avoid this side effect the data is keep filtered with the first filter, but the kink character is explained.

2.4 Results

The quality factor Q is computed from the slope $m = -\frac{\pi}{Q}$ of each fit line shown in the last figures. The uncertainty in the slope is given by the maximum and minimum slope of the least squares fitting. Their uncertainty is propagated through the quality factor Q by the simple rules of error propagation. From the slope m, the uncertainty is propagated to Q as follows:

$$Q = -\frac{\pi}{m}$$

$$\delta Q = \frac{\pi \delta m}{m^2}$$

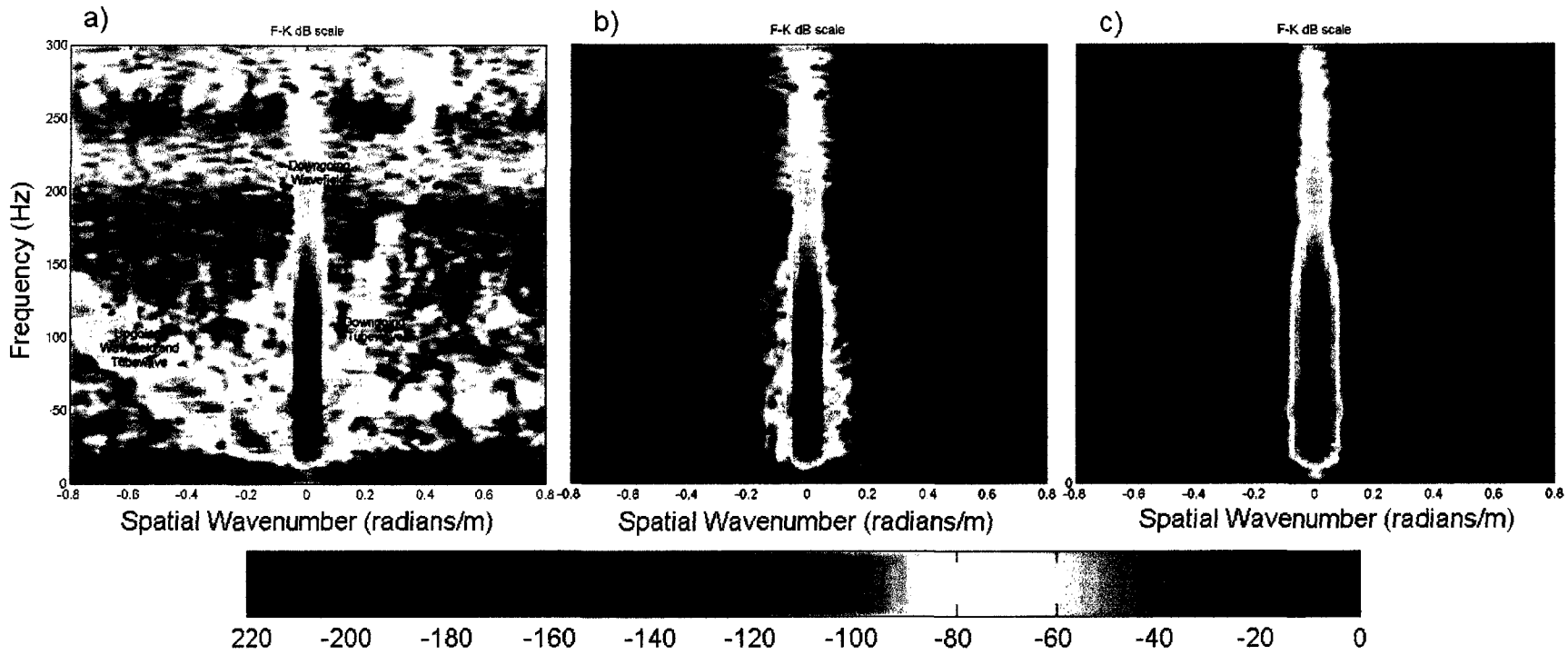

Figure 2.15: Different fk filters to isolate the downgoing wavefield. a) Flattened VSP data. b) *fk* filter used in this study. c) Narrow fk filter.

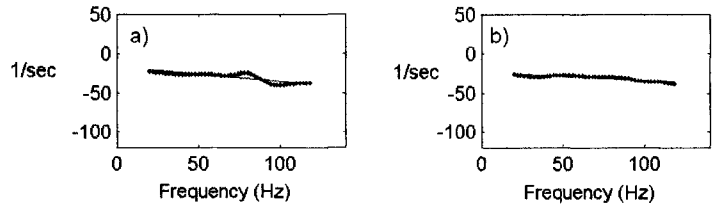

Figure 2.16: Effect of the tubewave to the spectral ratio plots. a) Using wide filter. b) Using narrow filter. Fixed trace at 125 m compared to trace at 140 m.

	Time	Sonic velocity	VSP velocity	Phase velocity
fk filter	17.4 ±1.2	14.7 ±1.0	15.7±1.1	16.8±1.2
median filter	15.8 ±1.2	13.5±1.1	14.5±1.4	15.6±1.2

Table 2.3: Q overall average for the different approaches used.

When trace 1 is made to be the reference, 12 values of Q may be obtained. Figure 2.17 and figure 2.18 show the results for the fk and median filtered data, respectively. Panel a) is using the first break time difference, panel b) using average sonic velocity, panel c) using average VSP velocity, and panel d) using the phase velocity. There are 12 Q estimates for each approach. It is useful to make a comparison of the values of Q determined by slightly differing methods. This is carried out as a consistency check.

Based on the Q values, an average quality factor over the 12 samples from 125m to 155m is computed. The average Q bounds are referred as the red dashed lines in figures 2.17 and 2.18. For the computation of those averages, only those fits having $r \geq 0.8$ were deemed acceptable and included in the final average. This average quality factors represent an overall estimate since it takes into account both "near" and "far" values of Q determined from receivers separated from 2.5 m to 30 m. For this first fixed trace at 125 m the Q values are summarized in the table 2.3.

When the time difference is used the quality factor averages to 17.4 ± 1.2 for the fk

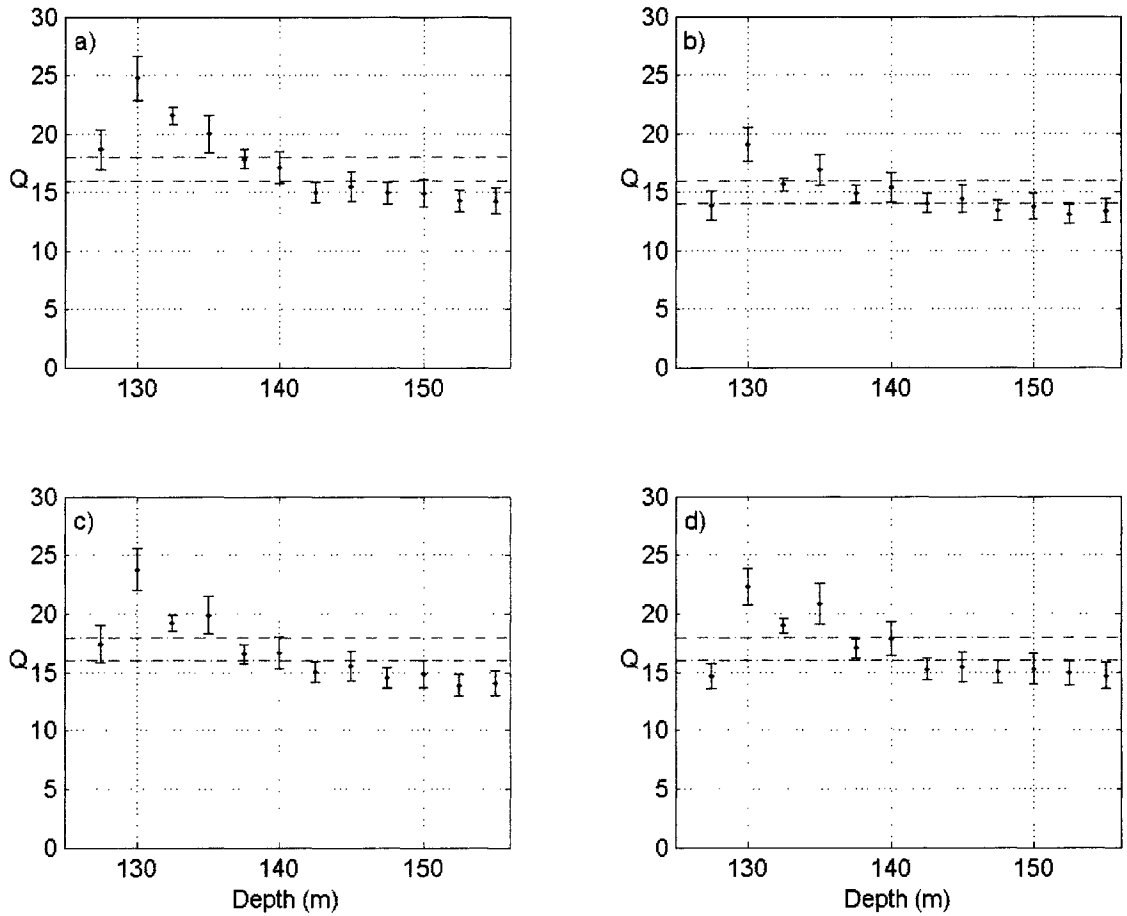

Figure 2.17: Q estimates fixing trace at 125m for *fk* filtered data. a) Using time differences. b) Using average sonic velocity. c) Using average VSP velocity. d) using phase velocities. Q Average bounds are shown by the red dashed lines

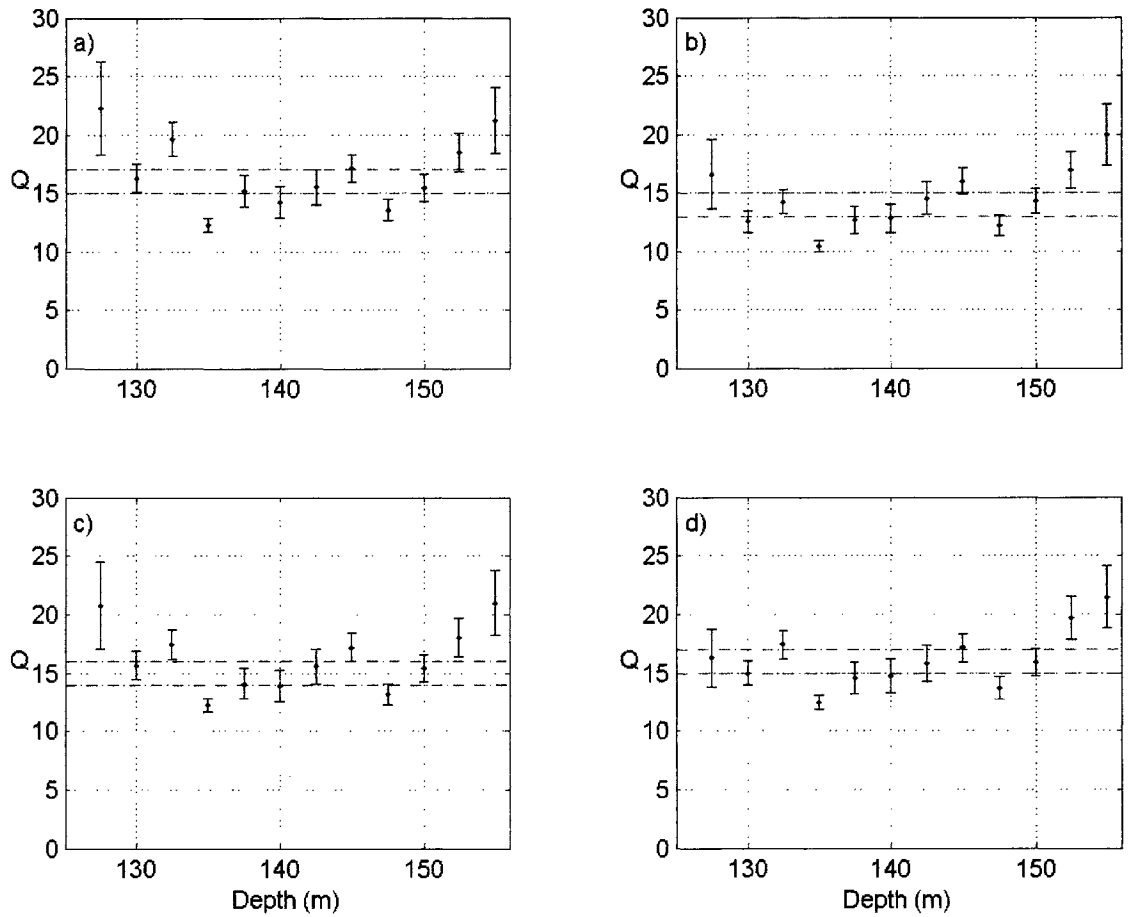

Figure 2.18: Q estimates fixing trace at 125m for the median filtered data. a) Using time diferences. b) Using average sonic velocity. c) Using average VSP velocity. d) Using phase velocities. Q Average bounds are shown by the red dashed lines

filtered dataset (figure 2.17a) while for the median filtered dataset it is 15.8 ± 1.2 (figure 2.18 a). If the average sonic velocity is used the quality factor averages to 14.7 ± 1.0 for the fk filtered data (figure 2.17b) while for the median filtered data it is 13.5 ± 1.1 (figure 2.18b). Using the average VSP velocity yields 15.7 ± 1.1 for the fk dataset while for the median filtered it yields 14.5 ± 1.4. Using the phase velocity yields an average quality factor of 16.8 ± 1.2 for the fk filtered data (figure 2.17d) while for the median filtered data it averages to 15.6 ± 1.2 (figure 2.18b). Overall, all Q values values are within the same range.

The fk filtered Q values (figure 2.17) show a smooth trend of decreasing values from top to bottom. Q does not follow this trend in the median filtered dataset (figure 2.18). For the fk filtered dataset, Q increases at the top half of the formation to to about 20 to 25 and in the bottom half of the formation, Q tends to be lower close to 15. The median dataset does not follow a trend.

As shown before in the average VSP velocity computation, the use of the first break times in determining interval velocities leads to unreal velocities. Even though the $Q's$ computed using the first break times are not far from those using the other approaches; they are less reliable than the values determined using the average sonic or phase velocity. Consequently, in the remainder of this discussion the results are based on average sonic and phase velocities.

The last results shown in figures 2.18 and 2.17 use a fixed trace 1 at 125 m compared to all other deeper traces. Next 2 figures show a summary of Q values for different fixed traces using the average sonic velocity (figure 2.19) and phase velocity (figure 2.20) for the fk filtered dataset. Each panel shows the fixed trace number as well as the bounds for the average Q value for the given fixed trace.

Overall, the average quality factor decreases weakly with depth. Using the average sonic velocity yields Q values from as high as 15.3 ± 0.4 when the first trace at 125 m is fixed to as low as 10.2 ± 0.9 when the trace 11 at 150 m is fixed (figure 2.19). This

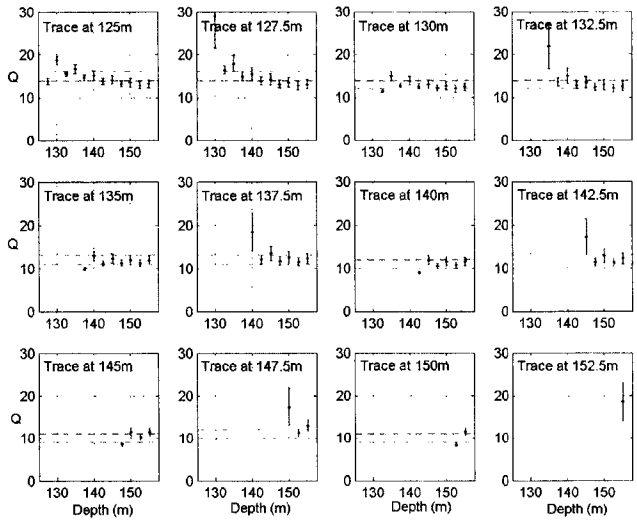

Figure 2.19: Q estimates using sonic average velocity for different fixed traces for the fk filtered dataset. Q Average bounds are shown by the red dashed lines

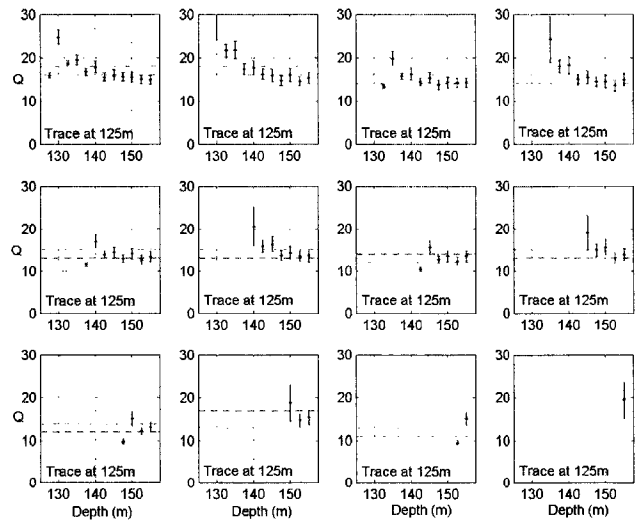

Figure 2.20: Q estimates using phase average velocity for different fixed traces for the *fk* filtered dataset. Q Average bounds are shown by the red dashed lines

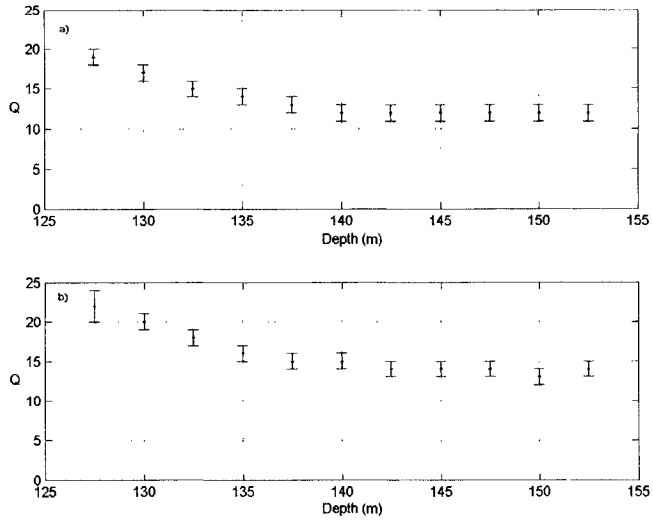

Figure 2.21: Q log for *fk* filtered dateset. a) Using sonic average velocity. b) Using the phase velocity.

decrease trend is also noted when the phase velocity is used (figure 2.20). However, when the average sonic velocity is used the Q values tend to be more aligned over the average than when the phase velocity is used.

Tables 2.4 and 2.5 summarize the obtained $Q's$ when each different trace is fixed for the fk filtered dataset. The first row shows the depth of the reference trace. The first column shows the depths at which the second traces are. The first Q column corresponds to the first fixed trace at 125 m. r shows the Pearson's correlation coefficient between the data and the fitted line as discussed before. The higher the r, the lower the error bars of Q. Table 2.4 shows the results for using the time difference in the top while the results using the average sonic velocity are in the bottom. Table 2.5 shows the results using the average VSP velocity in the top and the results using the phase velocity are in the bottom.

A Q profile over the McMurray Formation is built by comparing trace pairs separated by 5 m using the average sonic and phase velocities. In this way, the average Q value over this thickness is assigned to the midpoint within the two traces. Figure 2.21

ref ->	125.0 m			127.5 m			130 m			132.5 m			135.0 m			137.5 m			140.0 m			142.5 m			145.0 m			147.5 m			150.0 m			152.5 m		
m	Q	δQ	r	Q	δQ	r	Q	δQ	r	Q	δQ	r	Q	δQ	r	Q	δQ	r	Q	δQ	r	Q	δQ	r	Q	δQ	r	Q	δQ	r	Q	δQ	r	Q	δQ	r
127.5	19	2	0.94																																	
130.0	25	2	0.88	36	15	0.35																														
132.5	22	1	0.97	23	2	0.89	18	1	0.92																											
135.0	20	2	0.88	21	3	0.71	16	1	0.87	13	4	0.39																								
137.5	18	1	0.95	18	1	0.88	15	1	0.96	13	1	0.87	13	1	0.94																					
140.0	17	1	0.87	17	2	0.78	14	1	0.86	13	2	0.71	13	1	0.85	12	4	0.42																		
142.5	15	1	0.93	14	1	0.88	12	1	0.93	11	1	0.87	11	1	0.95	9	1	0.86	8	1	0.92															
145.0	15	1	0.87	15	2	0.81	13	1	0.86	12	1	0.78	12	1	0.85	12	2	0.72	12	1	0.85	19	6	0.43												
147.5	15	1	0.92	15	1	0.88	13	1	0.91	12	1	0.87	12	1	0.92	12	1	0.86	12	1	0.93	15	1	0.86	13	1	0.88									
150.0	15	1	0.88	14	1	0.83	13	1	0.86	13	1	0.81	12	1	0.86	12	1	0.79	12	1	0.85	15	2	0.73	13	1	0.85	14	4	0.44						
152.5	14	1	0.91	14	1	0.89	13	1	0.91	12	1	0.88	12	1	0.91	12	1	0.87	12	1	0.91	13	1	0.87	12	1	0.91	12	1	0.87	10	1	0.82			
155.0	14	1	0.88	14	1	0.85	13	1	0.87	12	1	0.84	12	1	0.86	12	1	0.82	12	1	0.86	13	1	0.80	12	1	0.86	12	2	0.75	11	1	0.86	13	4	0.43

ref ->	125.0 m			127.5 m			130 m			132.5 m			135.0 m			137.5 m			140.0 m			142.5 m			145.0 m			147.5 m			150.0 m			152.5 m		
m	Q	δQ	r	Q	δQ	r	Q	δQ	r	Q	δQ	r	Q	δQ	r	Q	δQ	r	Q	δQ	r	Q	δQ	r	Q	δQ	r	Q	δQ	r	Q	δQ	r	Q	δQ	r
127.5	14	1	0.84																																	
130.0	19	1	0.88	30	12	0.35																														
132.5	16	1	0.97	17	1	0.89	12	1	0.92																											
135.0	17	1	0.88	18	3	0.71	15	1	0.87	22	8	0.39																								
137.5	15	1	0.95	15	1	0.88	13	1	0.96	14	1	0.87	10	1	0.94																					
140.0	15	1	0.87	16	2	0.78	14	1	0.86	15	2	0.71	13	1	0.85	19	6	0.42																		
142.5	14	1	0.93	14	1	0.88	13	1	0.93	13	1	0.87	11	1	0.95	12	1	0.86	9	1	0.92															
145.0	14	1	0.87	14	1	0.81	13	1	0.86	14	2	0.78	13	1	0.85	14	2	0.72	12	1	0.85	18	5	0.43												
147.5	13	1	0.92	13	1	0.88	12	1	0.91	13	1	0.87	12	1	0.92	12	1	0.86	11	1	0.93	12	1	0.86	9	1	0.88									
150.0	14	1	0.88	14	1	0.83	13	1	0.86	13	1	0.81	12	1	0.86	13	1	0.79	12	1	0.85	13	2	0.73	12	1	0.85	18	5	0.44						
152.5	13	1	0.91	13	1	0.89	12	1	0.91	12	1	0.88	12	1	0.91	11	1	0.87	11	1	0.91	12	1	0.87	10	1	0.91	12	1	0.87	9	1	0.82			
155.0	13	1	0.88	13	1	0.85	13	1	0.87	13	1	0.84	12	1	0.86	12	1	0.82	12	1	0.86	13	1	0.8	12	1	0.86	13	2	0.75	12	1	0.86	18	5	0.43

Table 2.4: Q summary table for *fk* filtered dataset. Top: using time difference. Bottom: using average sonic velocity.

ref ->	125.0 m			127.5 m			130 m			132.5 m			135.0 m			137.5 m			140.0 m			142.5 m			145.0 m			147.5 m			150.0 m			152.5 m		
m	Q	δQ	r	Q	δQ	r	Q	δQ	r	Q	δQ	r	Q	δQ	r	Q	δQ	r	Q	δQ	r	Q	δQ	r	Q	δQ	r	Q	δQ	r	Q	δQ	r	Q	δQ	r
127.5	17	2	0.84																																	
130.0	24	2	0.88	38	15	0.35																														
132.5	19	1	0.97	21	2	0.89	14	1	0.92																											
135.0	20	2	0.88	22	3	0.71	19	2	0.87	28	9	0.39																								
137.5	17	1	0.95	18	1	0.88	16	1	0.96	17	1	0.87	13	1	0.94																					
140.0	17	1	0.87	18	2	0.78	17	1	0.86	19	3	0.71	16	1	0.85	24	7	0.42																		
142.5	15	1	0.93	15	1	0.88	14	1	0.93	15	1	0.87	14	1	0.95	15	1	0.86	12	1	0.92															
145.0	16	1	0.87	16	2	0.81	14	1	0.86	15	2	0.78	15	1	0.85	17	2	0.72	15	1	0.85	22	7	0.43												
147.5	15	1	0.92	14	1	0.88	13	1	0.91	14	1	0.87	13	1	0.92	14	1	0.86	13	1	0.93	15	1	0.86	11	1	0.88									
150.0	15	1	0.88	15	1	0.83	14	1	0.86	14	1	0.81	13	1	0.86	14	2	0.79	14	1	0.85	16	2	0.73	15	1	0.85	22	7	0.44						
152.5	14	1	0.91	14	1	0.89	13	1	0.91	13	1	0.88	12	1	0.91	13	1	0.87	12	1	0.91	14	1	0.87	13	1	0.91	13	1	0.88	9	1	0.86			
155.0	14	1	0.88	14	1	0.85	14	1	0.87	14	1	0.84	13	1	0.86	13	1	0.82	13	1	0.86	14	2	0.8	14	1	0.86	16	2	0.75	15	1	0.86	23	7	0.43

ref ->	125.0 m			127.5 m			130 m			132.5 m			135.0 m			137.5 m			140.0 m			142.5 m			145.0 m			147.5 m			150.0 m			152.5 m		
m	Q	δQ	r	Q	δQ	r	Q	δQ	r	Q	δQ	r	Q	δQ	r	Q	δQ	r	Q	δQ	r	Q	δQ	r	Q	δQ	r	Q	δQ	r	Q	δQ	r	Q	δQ	r
127.5	15	1	0.89																																	
130.0	22	2	0.91	30	9	0.42																														
132.5	19	1	0.97	20	1	0.91	12	1	0.94																											
135.0	21	2	0.86	22	3	0.73	18	1	0.88	23	6	0.46																								
137.5	17	1	0.95	19	2	0.87	16	1	0.96	16	1	0.89	11	1	0.95																					
140.0	18	1	0.87	18	2	0.79	17	2	0.84	18	3	0.73	15	1	0.87	19	5	0.49																		
142.5	15	1	0.92	16	1	0.87	15	1	0.93	16	1	0.85	14	1	0.94	15	1	0.87	10	1	0.93															
145.0	15	1	0.87	16	2	0.81	15	1	0.85	16	2	0.78	15	2	0.83	17	2	0.73	14	1	0.86	18	4	0.5												
147.5	15	1	0.91	14	1	0.88	13	1	0.9	15	1	0.86	13	1	0.91	15	1	0.84	13	1	0.92	14	1	0.87	9	1	0.9									
150.0	15	1	0.87	15	2	0.83	14	1	0.86	14	2	0.8	14	1	0.85	15	2	0.79	15	1	0.82	16	2	0.74	14	1	0.87	17	4	0.51						
152.5	15	1	0.90	14	1	0.88	14	1	0.9	13	1	0.87	13	1	0.89	14	1	0.86	13	1	0.9	14	1	0.83	13	1	0.91	13	1	0.88	9	1	0.86			
155.0	15	1	0.88	15	1	0.84	14	1	0.86	14	1	0.83	13	1	0.86	14	1	0.81	14	1	0.85	14	2	0.8	15	1	0.82	16	2	0.76	14	1	0.87	17	4	0.52

Table 2.5: Q summary table for the *fk* filtered dataset. Top: using average VSP velocity. Bottom: using phase velocity.

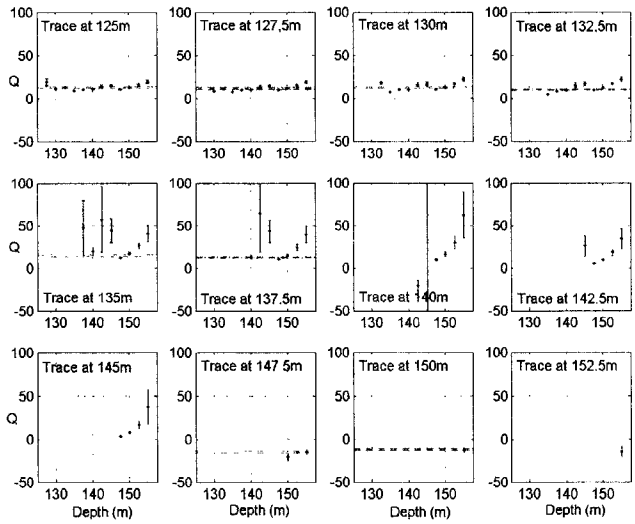

Figure 2.22: Q estimates using phase average velocity for different fixed traces for the median filtered dataset. Q Average bounds are shown by the red dashed lines

shows the Q profile using the sonic (panel a) and phase velocity (panel b) from 127.5 m to 150 m. A decrease of the quality factor with depth using both velocities is observed. This behavior is the same seen when comparing different fixed traces as shown above (2.17).

The Q estimates for the median filtered dataset are shown in figure 2.22. Reliable average quality factors can be estimated when the fixed trace is moved down until level 42 at 132.5 m. For the 3 first levels Q varies as 13.5 ± 1.1, 12.8 ± 0.9, 15.1 ± 1.29 and 12.1 ± 0.9. For reference traces deeper than 132.5 m the quality factors are much more uncertain. At these depths the $Q's$ show large error bars, this means poor linear fits to the equation 2.5, and sometimes even non-physical negatives values. At those levels it was shown previously (Processing section) that the upgoing reflection from the bottom of the formation distorts the downgoing first break pulse (figure 2.3). This behavior of Q on the median filtered dataset can be explained in terms of the median filter algorithm which does not perform as well as the fk algorithm in isolating the events. The median filter uses adjacent amplitudes and takes the

median of them which can still cause some mixing of amplitudes at different levels. On the other hand, the fk filter better attenuates the events with negative apparent velocity which are in a different panel than the downgoing events. However, the fk filter could also result in some degree of smoothing of the results between traces.

A comparison from the Q estimates from the fk filtered data in figure 2.19 and the median filtered data in figure 2.22 demonstrates that the the first better performs in isolating the downgoing pulse. The fact that the Q estimates are poor deeper then 132.5 m is due to the contamination of the upgoing reflection produced at 160 m that distort the downgoing amplitude pulse 7 levels up. While the fk technique filters this upgoing event, the median does not perform as well. As a result values that not correlate and even negative Q values are observed for those depths.

Tables 2.6 and 2.7 summarize the obtained $Q's$ when each different trace is fixed for the median filtered dataset. The first row shows the depth of the reference trace. The first column shows the depths at which the second traces are. The first Q column corresponds to the first fixed trace at 125 m. r shows the Pearson's correlation coefficient between the data and the fit line as discussed before. The higher the r, the lower the error bars of Q. Table 2.6 shows the results using the time difference in the top while the results using the average sonic velocity are in the bottom. Table 2.7 shows the results using the average VSP velocity in the top and the results using the phase velocity in the bottom.

2.5 Summary and Conclusions

The spectral ratio method has been proven to be a powerful technique to quantify wave attenuation using VSP data. Before the technique is applied, it is necessary to pre-process the VSP traces so that the distortion caused by the upgoing reflections to

ref ->	125.0 m			127.5 m			130 m			132.5 m			135.0 m			137.5 m			140.0 m			142.5 m			145.0 m			147.5 m			150.0 m			152.5 m		
m	Q	δQ	r	Q	δQ	r	Q	δQ	r	Q	δQ	r	Q	δQ	r	Q	δQ	r	Q	δQ	r	Q	δQ	r	Q	δQ	r	Q	δQ	r	Q	δQ	r	Q	δQ	r
127.5	22	4	0.63																																	
130.0	16	1	0.89	13	1	0.84																														
132.5	20	1	0.89	19	1	0.89	30	3	0.82																											
135.0	12	1	0.95	10	1	0.97	9	1	0.96	3	1	0.96																								
137.5	15	1	0.85	14	1	0.87	14	2	0.78	10	1	0.72	121	224	0.08																					
140.0	14	1	0.83	13	1	0.86	13	2	0.77	10	1	0.73	23	8	0.38	9	2	0.63																		
142.5	16	1	0.83	15	1	0.85	15	2	0.76	12	2	0.72	28	9	0.41	17	3	0.62	60	46	0.18															
145.0	17	1	0.90	16	1	0.92	18	1	0.87	15	1	0.85	33	6	0.65	25	3	0.74	59	35	0.23	58	50	0.16											
147.5	14	1	0.90	13	1	0.90	13	1	0.89	11	1	0.89	15	2	0.79	12	1	0.79	12	2	0.65	10	2	0.66	6	1	0.68								
150.0	15	1	0.89	15	1	0.89	15	1	0.87	14	1	0.86	19	3	0.73	16	2	0.71	18	4	0.54	15	3	0.54	11	2	0.56	-21	7	0.42					
152.5	19	2	0.85	18	2	0.85	19	2	0.82	18	2	0.8	28	5	0.61	24	5	0.59	30	9	0.43	27	9	0.41	23	8	0.39	-23	7	0.43	-24	9	0.38		
155.0	21	3	0.74	21	3	0.74	23	4	0.66	22	4	0.63	37	12	0.41	33	10	0.41	45	22	0.29	44	23	0.26	41	28	0.21	-20	8	0.34	-20	10	0.27	-16	12	0.18

ref ->	125.0 m			127.5 m			130 m			132.5 m			135.0 m			137.5 m			140.0 m			142.5 m			145.0 m			147.5 m			150.0 m			152.5 m		
m	Q	δQ	r	Q	δQ	r	Q	δQ	r	Q	δQ	r	Q	δQ	r	Q	δQ	r	Q	δQ	r	Q	δQ	r	Q	δQ	r	Q	δQ	r	Q	δQ	r	Q	δQ	r
127.5	17	3	0.63																																	
130.0	13	1	0.89	10	1	0.84																														
132.5	14	1	0.89	13	1	0.89	20	2	0.82																											
135.0	10	1	0.95	9	1	0.97	9	1	0.96	6	1	0.96																								
137.5	13	1	0.85	12	1	0.87	13	1	0.78	11	1	0.72	96	177	0.08																					
140.0	13	1	0.83	12	1	0.86	13	2	0.77	12	2	0.73	24	8	0.38	14	2	0.63																		
142.5	15	1	0.83	14	1	0.85	16	2	0.76	15	2	0.72	31	10	0.41	23	4	0.62	72	56	0.18															
145.0	16	1	0.90	16	1	0.92	18	1	0.87	17	2	0.85	35	6	0.65	29	4	0.74	61	37	0.23	53	45	0.16											
147.5	12	1	0.90	12	1	0.90	12	1	0.89	11	1	0.89	14	2	0.79	12	1	0.79	11	2	0.65	8	1	0.66	4	1	0.68								
150.0	14	1	0.89	14	1	0.89	15	1	0.87	14	1	0.86	19	3	0.73	16	2	0.71	17	4	0.54	14	3	0.54	10	2	0.56	-26	8	0.42					
152.5	17	2	0.85	17	2	0.85	18	2	0.82	18	2	0.8	26	5	0.61	24	5	0.59	27	8	0.43	24	8	0.41	20	7	0.39	-23	7	0.43	-20	7	0.38		
155.0	20	3	0.74	20	3	0.74	23	4	0.66	23	4	0.63	37	12	0.41	34	11	0.41	45	21	0.29	41	22	0.26	39	26	0.21	-22	9	0.34	-21	11	0.27	-21	16	0.18

Table 2.6: Q summary table for the median filtered dataset. Top: using time difference. Bottom: using average sonic velocity.

ref ->	125.0			m	127.5			m	130			m	132.5			m	135.0			m	137.5			m	140.0			m	142.5			m	145.0			m	147.5			m	150.0			m	152.5			m
m	Q	δQ	r		Q	δQ	r		Q	δQ	r		Q	δQ	r		Q	δQ	r		Q	δQ	r		Q	δQ	r		Q	δQ	r		Q	δQ	r		Q	δQ	r		Q	δQ	r		Q	δQ	r	
127.5	21	4	0.63																																												
130.0	16	1	0.89	13	1	0.84																																								
132.5	17	1	0.89	17	1	0.89	25	3	0.82																																						
135.0	12	1	0.95	11	1	0.97	11	1	0.96	7	1	0.96																																			
137.5	14	1	0.85	14	1	0.87	16	2	0.78	14	2	0.72	120	222	0.68																																
140.0	14	1	0.83	14	1	0.86	15	2	0.77	14	2	0.73	30	11	0.38	17	3	0.63																													
142.5	16	1	0.83	15	1	0.85	17	2	0.76	17	2	0.72	38	12	0.41	29	5	0.62	91	71	0.18																									
145.0	17	1	0.90	17	1	0.92	19	2	0.87	19	2	0.85	41	7	0.65	35	5	0.74	77	46	0.23	67	58	0.16																					
147.5	13	1	0.90	13	1	0.89	12	1	0.89	12	1	0.89	16	2	0.79	14	2	0.79	14	2	0.65	10	2	0.66	5	1	0.68																	
150.0	15	1	0.89	15	1	0.89	16	1	0.87	15	1	0.86	21	3	0.73	18	3	0.71	20	5	0.54	17	4	0.54	13	3	0.56	-33	10	0.42													
152.5	18	2	0.85	18	2	0.85	20	2	0.82	20	2	0.8	28	5	0.61	26	5	0.59	31	9	0.43	28	9	0.41	25	8	0.39	-28	9	0.43	-25	9	0.38									
155.0	21	3	0.74	22	3	0.74	24	4	0.66	25	4	0.63	40	13	0.41	36	11	0.41	48	23	0.29	46	25	0.26	46	31	0.21	-27	11	0.34	-26	13	0.27	-26	20	0.18					

ref ->	125.0			m	127.5			m	130			m	132.5			m	135.0			m	137.5			m	140.0			m	142.5			m	145.0			m	147.5			m	150.0			m	152.5			m
m	Q	δQ	r		Q	δQ	r		Q	δQ	r		Q	δQ	r		Q	δQ	r		Q	δQ	r		Q	δQ	r		Q	δQ	r		Q	δQ	r		Q	δQ	r		Q	δQ	r		Q	δQ	r	
127.5	16	2	0.69																																											
130.0	15	1	0.90	11	1	0.87																																							
132.5	17	1	0.90	16	1	0.91	21	2	0.85																																					
135.0	12	1	0.94	12	1	0.97	11	1	0.96	7	1	0.95																																		
137.5	15	1	0.84	14	1	0.86	16	2	0.78	13	2	0.73	54	47	0.16																															
140.0	15	1	0.82	14	1	0.85	16	2	0.75	14	2	0.73	27	8	0.42	14	2	0.66																												
142.5	16	2	0.82	16	2	0.84	18	2	0.76	18	3	0.69	36	11	0.43	26	4	0.66	42	15	0.37																									
145.0	17	1	0.90	17	1	0.91	20	2	0.86	20	2	0.85	46	10	0.57	33	4	0.77	58	25	0.32	43	23	0.26																					
147.5	14	1	0.91	13	1	0.91	13	1	0.9	13	1	0.89	16	2	0.81	15	2	0.8	13	2	0.69	9	1	0.71	4	1	0.76																	
150.0	16	1	0.89	16	1	0.90	16	1	0.88	16	1	0.87	22	3	0.74	19	2	0.75	23	5	0.54	16	3	0.59	11	2	0.64	-87	84	0.17													
152.5	20	2	0.84	19	2	0.86	21	2	0.82	19	2	0.82	28	5	0.64	28	5	0.61	30	8	0.48	36	13	0.36	22	7	0.45	-43	19	0.31	-84	101	0.12									
155.0	21	3	0.76	24	3	0.72	25	4	0.66	26	5	0.63	35	9	0.47	35	10	0.45	56	28	0.28	41	18	0.31	85	107	0.11	-35	18	0.27	-51	50	0.14	80	190	0.06					

Table 2.7: Q summary table for the median filtered dataset. Top: using average VSP velocity. Bottom: using phase velocity.

the downgoing pulse is minimized. This distortion is the result of the interference of the upgoing reflections with the downgoing pulse and causes a change in the amplitude and shape of the first break pulse which is to be analysed via the spectral ratio. This is achieved by a separation of the two wavefields (the downgoing and the upgoing) using a multichannel filter such as a median or an fk filter.

To separate the wavefields two different approaches were applied: an fk and a median filter. For the median filter, different window lengths of : 5, 7 and 9 samples were tested. For the fk filter the complete negative k quadrant was muted where the upgoing events are contained. It was done to minimize smearing as a result of the filtering. Figure 2.3 shows a comparison of the downgoing wavefields obtained after those filters were applied. Panel a) is the raw VSP data (i.e. downgoing and upgoing events), panel b) is the downgoing wavefield using the fk approach and panel c) is the downgoing wavefield obtained using a 7-sample median filter approach.

After the data was filtered, the first break was isolated using a window so that the information to be analysed in each trace corresponds to the first pulse traveling into the Earth. Figure 2.4 illustrates the data windowing. Once the first break is isolated, the data is ready to be analysed via the spectral ratio technique.

The wave velocity was computed through different approaches: using first break times from the actual VSP data, the average sonic velocity, average VSP velocity and using the phase velocity. Using the first break times to compute interval velocity resulted to be problematic (figure 2.9b). For example, within the McMurray Formation (120 m to 155 m), this interval velocity varies from 2000 m/s to 5000 m/s. This velocity is not expected since the layer has a roughly constant sonic velocity of 2420 ± 140 m/s. Indeed at deeper levels in the borehole this velocity is sometimes negative. This behavior of the velocity is not physical and may be the product of statistical fluctuation due to the sampling rate. Taking the two farthest traces withing the formation yields a velocity of 2260 ± 290 m/s. The phase velocity within the McMurray Formation

V sonic	V VSP	Porosity	Young's M.	Perm.	Q
2420 ±140 k/s	2260±290 k/s	>30 percent	0.5Gpa	10pa.s	21.9±2.1
			-10Gpa	-1000pa.s	-11.8±0.9

Table 2.8: Summary of petrophysical variables.

was computed using an FFT approach calculating phase differences between traces. Overall the phase velocity is constant and averages to 2194 ± 41 m/s for frequencies up to 200 Hz (figure 2.12).

The fk filtering approach performed better in isolating the wavefields. At depth levels strongly distorted by upgoing reflections, the Q estimates could not be computed for the median filtered dataset due to the poor linear fitting of the spectral ratio data. As a result, it was only possible to measure Q at levels with low distortion using the median filter approach. Alternately, it was able to measure Q for the fk filtered dataset at all depth levels with good confidence.

From top to the half of the McMurray Formation, a weak decreasing trend of the quality factor is observed when different reference traces are used. This behavior is the same seen when comparing different fixed traces separated 5 meters. This is illustrated in the Q log shown in figure 2.21. Using the average sonic velocity (panel a), the formation shows Q values in the top half (127.5 m to 137.5 m) that decrease from 19.3 ± 0.7, to 13 ± 0.9. The bottom half (140 m to 152.5 m) is characterized by a roughly constant 11.8 ± 0.9 quality factor. This decreasing trend is also noted when the phase velocity is used. In this case, Q decreases from 21.9 ± 2.1 to 15.1 ± 0.9; and the bottom half shows an average of 14.1 ± 0.9.

Table 2.8 summarizes some of the petrophysical properties for the McMurray Formation. This is characterized, as mentioned before, by a dispersive velocity from the sonic to the seismic frequencies. The porosity of the reservoir is higher than 30 percent due to the low compaction of the sediments. The bulk modulus varies from

0.5 Gpa to 10 Gpa while the viscosity of the heavy oil can vary from 10 to 1000 pa.s depending on the temperature of the reservoir. Overall, the quality factor measured in this study range from 21.9 ± 2.1 to the top half to 11.8 ± 0.9 in the bottom half. This values correspond to the seismic response prior to steam injection so that it is expected a change in the attenuation response after the injection began due to the change in the acoustic properties in the reservoir (i.e bulk modulus, permeability of the fluid, among others). Further studies may include a comparison of the values obtained in this study with values computed after started the gas injection into the reservoir..

There is some consensus in the literature that local flow or "squirt" mechanisms are the most important ones describing seismic wave attenuation in saturated porous rocks [25, 45]. At low frequency, the fluid in compliant cracks is squeezed into pores or cracks that are less compliant because of their shape or orientation. At high frequency, the fluid in the compliant cracks becomes isolated causing the rock to be stiffer [45]. As a result the higher the frequency the higher the phase velocity. The dispersion observed from the difference between the sonic and seismic velocities, if true, may be an indicator of these two different regimes, although it is not sure what mechanism governs the attenuation in this case.

To cover the complete frequency bandwidth necessary to model any attenuation mechanism, it would be necessary to measure attenuation in the lab using any technique mentioned before. This would provide attenuation data at ultrasonic frequencies (i.e. at the high frequency regime) necessary to fit any attenuation model. Sams*et al.* [45] used a complete spectra of attenuation measurements (VSP, crossswell, sonic and core) to fit a squirt flow model in sediments from the Imperial College test site. The data presented in this study represents the low frequency regime (up to 120 Hz) . If both high and low frequency regime data were measured, they would be used to constrain the attenuation mechanism that dominates in this case; such as local or squirt

flow, Biot model or any combination. Future work also includes the measurement in the lab of the seismic wave attenuation in pure heavy oil, as well as in fully saturated samples to try to determine the role of the crude in the attenuation.

Bibliography

[1] Aki, K., and Richards, P., 1980: Quantitative Seismology: Theory and practice, W.H. New York.

[2] Aostra UTF Site 1986 Reflection Seismic Study, 1986. Prepared for Alberta Oil Sands Technology and Reserarh Authority Edmonton, Alberta.

[3] Balch, A., Lee, M., Miller, J., and Ryder, R, 1982: The use of vertical seismic profiles in seismic investigations of the Earth. Geophysics, Vol. 47, p906-918.

[4] Bickel, S., and Natarajan, R., 1985: Plane-wave Q-deconvolution. Geophysics, Vol. 50, p1426-1439.

[5] Biot, M., 1956: Theory of propagation of elastic waves in a fluid-saturated porous solid. I. Low-frequency range. J Acousti. Soc Am. v28, p168-178.

[6] Biot, M., 1956: Theory of propagation of elastic waves in a fluid-saturated porous solid. II. High-frequency range. J Acousti. Soc Am. Vol.28, p179-191.

[7] Bourbie, T., Coussy, O., and Zinszner, B., 1987: Acoustic of porous media. Gulf Publishing.

[8] Bruce, C., 1984: Vertical seismic profiles: an introduction. First Break, November 1984, p9-19.

[9] Canada's Oil Sands and Heavy Oil. Petroleum Communication Foundation. April 2000.

[10] Caplan, M., 2002: Regional geology of the McMurray Formation, Athabasca bitumen accumulation region, Northeastern Alberta : A synthesis. CSPG annual meeting 2002.

[11] Chalaturnyk, R.J., 1996: Geomechanics of the steam as sited Gravity Drainage Process in Heavy Oil Reservoirs. Ph.D Thesis, University of Alberta.

[12] Data Analysis: Computer Based Measuring Techniques, 1999. University of Upsala website: http://www.fysik.uu.se/kurser/fy660/compendium/Lsqf/.

[13] Deutsch, C., 2002: Geostatistical Reservoir Modeling. Applied Geostatistical Series. Oxford University Press.

[14] Dila, A., and Eastwood, J., 1995: Spectral analysis applied to seismic monitoring for thermal recovery. The leading Edge, p1117-1122.

[15] Fitch, A., 1984: Interpretation of vertical seismic profiles. First Break, June 1984, p19-23.

[16] Ganley, D., and Kanasewich, E., 1980: Measurements of absorption and dispersion form chech shot surveys. Jour. of Geophys. Res., Vol 85, p5219-5226.

[17] Gordon, R., and Davis, L., 1968: Velocity and attenuation of seismic waves in imperfectly elastic rock. J. Geophys. Res. Vol.73 , p3917-3935.

[18] Grech, M., 1998: True Amplitude Processing in VSP's. Master of Science Thesis, University of Alberta.

[19] Hardage, B., 2000: Vertical Seismic Profiling, Third updated and revised edition. Handbook of Geophysical Exploration. Pergamon.

[20] Hargreaves, N., and Calvert, A., 1991: Inverse Q filtering by Fourier transform. Geophysics, Vol. 56, p519-527.

[21] Harris, F. J, 1978: On the Use of Windows for Harmonic Analysis with the Discrete Fourier Transform. Proceedings of the IEEE, Vol. 66, p. 51-84.

[22] Hauge, P.,1981: Measurements of attenuation from Vertical Seismic Profile. Geophysics, Vol. 46, p1548-1448. Hauge, P., 1981: Measurements of attenuation from vertical seismic profiles. Geophysics, Vol. 46, p1548-1558.

[23] Hinds, R., Anderson, N., and Kuzmiski, R., 2002: VSP interpretative Processing: Theory and Practice. SEG open file publications No.3.

[24] Hinds, R., and Kuzmiski, R., 2001: VSP for the interpreter/processor for 2001 and beyond: Part 1. CSEG Recorder, September 2001, p84-95.

[25] Jones, T., 1986: Pore fluids and frequency-dependent wave propagation. Geophysics, Vol. 51, p1939-1953.

[26] Klimentos, T., and McCann, C., 1990: Relationships among compressional wave attenuation, porosity, clay content and permeability in sandstones. Geophysics, Vol.55, p988-1014.

[27] Lay, T., and Wallace, T., 1995: Modern Global Seismology. Academic Press.

[28] Maresh, J., Hobbs, R., While, R., and Smallwood, J.,: 2003. Attenuation of Atlantic margin basalts using downhole VSP. 73rd Ann. Internat. Mtg.: SEG, 1310-1313.

[29] Martin, N., Azavache, A., and Donati, M., 1998: Indirect oil detection by using p-wave attenuation analysis in Eastern Venezuela Basin. 68th SEG Ann. Mtg, p914-917.

[30] Mavko, G., and Nur, A., 1975: Frictional attenuation: an inherent amplitude dependence. J. Geophys. Res., Vol.84, p4769-4776.

[31] Mitchel, J., 1996: Energy absorption analysis: a case study. 66th SEG Ann. Internat. Mtg: p1785-1788.

[32] Molyneux, J., and Schmitt, D., 2000: Compressional-wave velocities in attenuating media: A laboratory physical model study. Geophysics, Vol.65, p1162-1167.

[33] Newman, P., 1973: Divergency effects in a layered earth. Geophysics, Vol. 38, p481:488.

[34] Numata, K., Yamamoto, K., Ishimito, H., Otsuka, K, Kawabe, K., Ando., M and Tsubono K., 2004: Systematic measurement of the intrinsic losses in various kinds of bulk fused silica. Department of Physics, University of Tokio. From http:\\arxiv.org/pdf/gr-qc/0404027.

[35] O'Brian, P., and Lucas, L., 1971: Velocity dispersion of seismic waves. Geophysical Prospecting, Vol.19, p1-26.

[36] O'Doherty, R.F., and Anstey, N.A., 1971: Reflections on amplitudes. Geophysical Prospecting, Vol.19, p430-458.

[37] Peselnick, L., and Outerbridge, W., 1961: Internal friction in shear and shear modulus of Solohofen limestone over a frequency range of 10^7cycles per second. Geophys. Res., Vol. 66, p581-588.

[38] Peselnick, L., and Zietz, I., 1959: Internal friction of fine grained limestones at ultrasonic frequencies. Geophysics, Vol. 24, p285-296.

[39] Pujol J., 1985: Vertical Seismic Profiling: Data processing and interpretation, velocity determination and attenuation measurements: Ph.D. thesis. Univ. of Wyoming.

[40] Pujol, J., and Smithson S., 1991: Seismic wave attenuation in volcanic rocks from VSP experiments. Geophysics, Vol. 56, p1441-1455.

[41] Pujol, J., Pezeshk, S., Zhang Y., and Zhao, C., 2002: Unexpected values of Q_s in unconsolidated sediments of the Mississippian Embayment. Bulletin of the Seismological Society of America, vol 92, No 3, p1117-1128.

[42] Pujol, J., Luschen, E., and Hu, Y., 1998: Seismic wave attenuation in metamorphic rocks from VSP data recorded in Germany's continental super-deep borehole. Geophysics, Vol. 63, p354-365.

[43] Ranalli, G., 1987: Rheology of the Earth. Allen&Unwin Publications.

[44] Rapoport, M., and Ryjkov, V., 1994: Seismic waves velocity dispersion: an indicator of hydrocarbon. 64th SEG Ann. Internat. Mtg, p94-96.

[45] Sams, M., Neep, J., Worthington, M., and King, M., 1997: The measurement of velocity dispersion and frequency-dependent intrinsic attenuation in sedimentary rocks. Geophysics,Vol.82, p1456-1464.

[46] Schoenberger, M., and Levin, F., K., 1974: Apparent Attenuation due to Intrabed Multiples. Geophysics, Vol. 39, p278-291.

[47] Sheriff, R., and Gelpard, L., 1983: Exploration seismology: History, theory and data acquisition. Volume I. Cambridge University Press. NY

[48] Sheriff, R., 2002: Encyclopedic dictionary of applied geophysics. Fourth Edition. Geophysical References series 13.

[49] Stainsby, S., and Worthington, M., 1985. Q estimation from vertical seismic profile data and anomalous variations in the central North Sea. Geophysics, Vol. 50, p615-626.

[50] Thacker, N., 1998: Error propagation and the Fourier Transform. University of Manchester. Taken form http://www.niac.man.ac.uk/Tina/docs/cvmsc/docs/fourier.ps

[51] Tittmann, B, 1977: Internal friction measurements and their implications in seismic Q structure models of the crust. AGU Geophys. monogr., Vol.20, The Earth's crust, p197-213.

[52] Toksoz, N., and Johnston D., 1981: Seismic Wave Attenuation. SEG: Geophysics Reprints series NO. 2.

[53] Tonn, R., 1991: The determination of the seismic quality factor Q from VSP data: A comparison of different computational methods. Geophysical Prospecting. Vol. 39, p1-27.

[54] Walsh, J., 1966: Seismic wave attenuation in rock due to friction. J. Geophys. Res., Vol.71, p2591-2599.

[55] Walsh, J., 1968: Attenuation in partially melted material. J. Geophys. Res, Vol.73, p2209-2216.

[56] Wang, Y., 2002: A stable and efficient approach of inverse Q filtering. Geophysics, Vol. 67, p657-663.

[57] Wang, Y., 2003: Quantifying the effectiveness of stabilized inverse Q filtering. Geophysics, Vol. 68, p337-345.

[58] Wightman, D., Rottenfusser, B., Kramers, J., and Harrison, R., 1989: Geology of the Athabasca oil sands deposits. Inm Herpler, L.G., Hsi, C. (Eds.), AOSTRA Technical Handbook on oil sands, Bitumen and heavy oil. AOSTRA.

[59] Yilmaz, O., 2001: Seismic data analysis: Processing inversion and interpretation of seismic data. SEG Investigations in geophysics No 10.

Appendix A

Glossary of terms

- Anisotropy: Change in a property in a medium depending on a specific direction.
- AVO: Amplitude variation versus offset study. Usually used to discriminate between fluids contained in a reservoir.
- Deconvolution: Improvement of the vertical resolution of a surface seismic by deconvolving the traces with an operator inverse of that of the input signal to the Earth.
- First break time: Arrival time of the first energy burst.
- Flat spectra: Also called a white spectra. The bandwidth contains all possible frequencies.
- Migration: An inversion operation involving rearrangement of seismic information elements so that reflections and diffractions are plotted at their true location [48].
- Multiple event: Seismic energy that has been reflected more than once [48].
- Primary event: Seismic energy that has been reflected only once and hence is not a multiple [48].

- Reflector: Traditionally called to a contrast in acoustic impedance between two layers that causes a seismic reflection.
- Smearing: To mix data originally recorded by different geophones.
- Surface waves: Energy that travels close to the surface. Its amplitude usually decays exponentially with depth.
- Sweep: The signal of a vibroseis is increased during a sweep of usually 7 seconds. For example it can be increased from 20 to 100Hz.
- Vertical resolution: Ability to resolve vertical events in a seismic section.

Appendix B

Plots spectral ratio

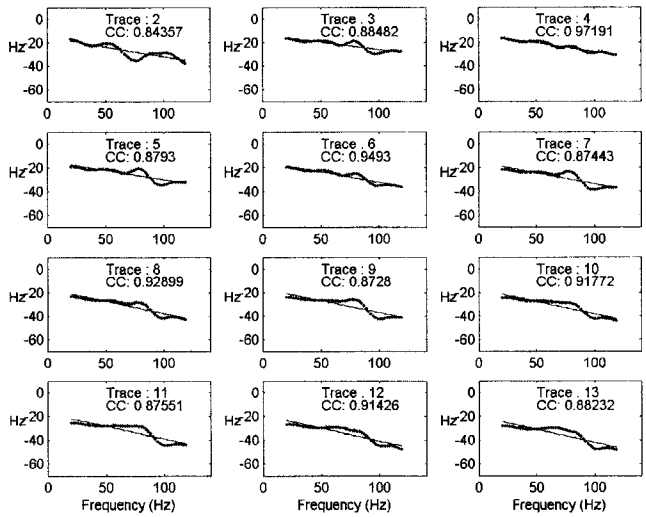

Figure B.1: Spectral ration plot for fk filtered data using time differences. Trace 1 at 125m is fixed compared to each deeper trace. CC denotes the correlation coeficient between the data and the fixed line.

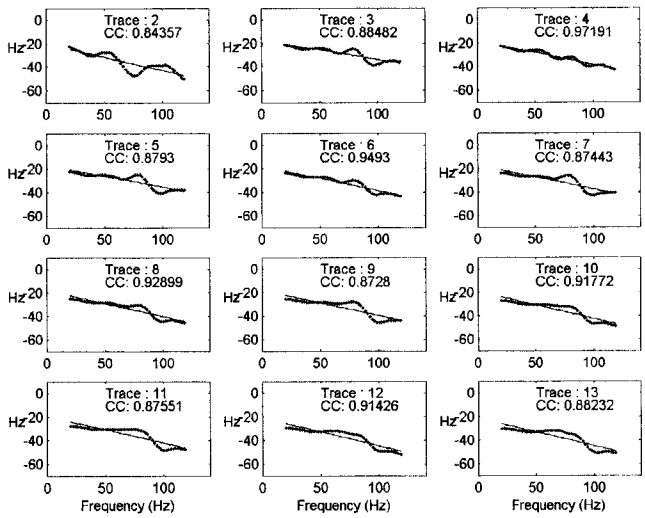

Figure B.2: Spectral ration plot for fk filtered data using the sonic velocity. Trace 1 at 125m is fixed compared to each deeper trace. CC denotes the correlation coeficient between the data and the fixed line.

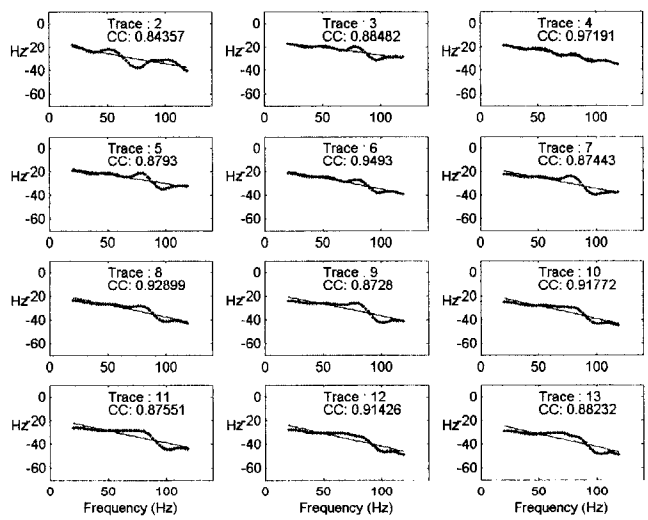

Figure B.3: Spectral ration plot for fk filtered data using the average VSP velocity. Trace 1 at 125m is fixed compared to each deeper trace. CC denotes the correlation coeficient between the data and the fixed line.

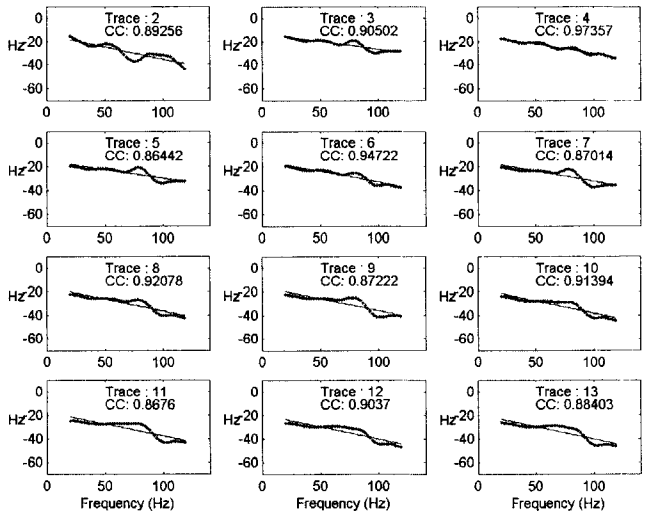

Figure B.4: Spectral ration plot for fk filtered data using the phase velocity. Trace 1 at 125m is fixed compared to each deeper trace. CC denotes the correlation coeficient between the data and the fixed line.

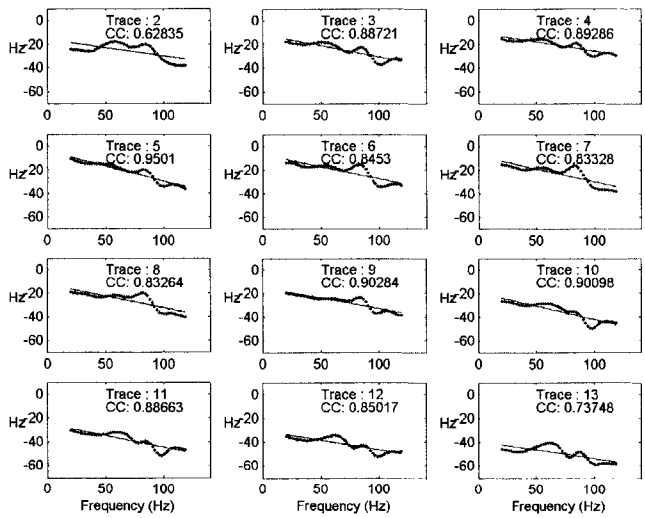

Figure B.5: Spectral ration plot for fk filtered data using time differences. Trace 1 at 125m is fixed compared to each deeper trace. CC denotes the correlation coeficient between the data and the fixed line.

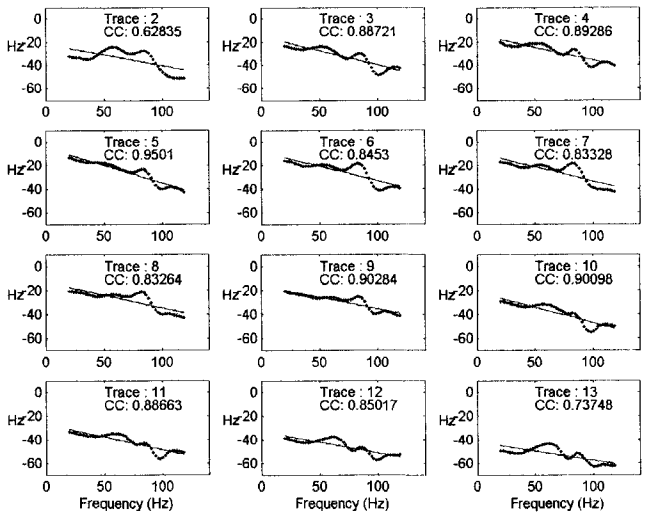

Figure B.6: Spectral ratio plot for the median filtered data using the average sonic velocity. Trace 1 at 125m is fixed compared to each deeper trace. CC denotes the correlation coeficient between the data and the fixed line.

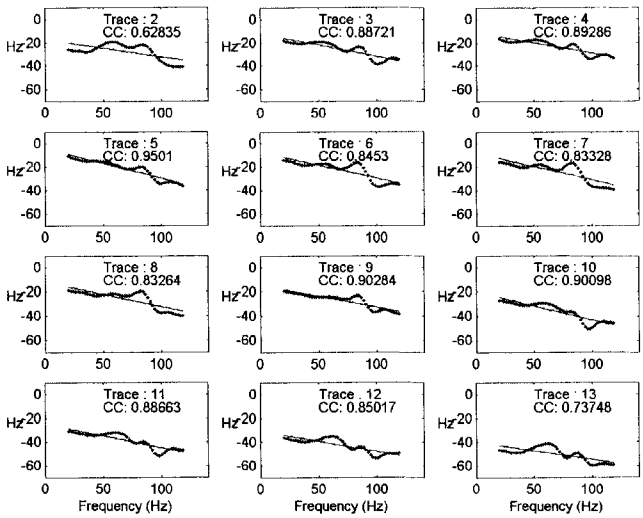

Figure B.7: Spectral ratio plot for the median filtered data using the average VSP velocity. Trace 1 at 125m is fixed compared to each deeper trace. CC denotes the correlation coeficient between the data and the fixed line.

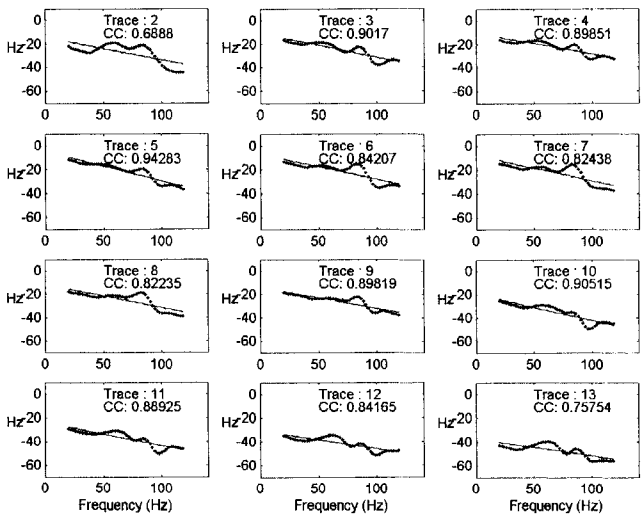

Figure B.8: Spectral ration plot for median filtered data using the phase velocity. Trace 1 at 125m is fixed compared to each deeper trace. CC denotes the correlation coeficient between the data and the fixed line.